IS-T- 901

The upper critical field in anisotropic superconductors

by

Daniel Wayne Youngner

Ph.D **Thesis submitted to Iowa State University**

Ames Laboratory, DOE

Iowa State University

Ames, Iowa 50011

Date Transmitted: August 1980

PREPARED FOR THE U.S. DEPARTMENT OF ENERGY
UNDER CONTRACT NO. W-7405-eng-82

DISCLAIMER

Printed in the United States of America

Available from
National Technical Information Service
U.S. Department of Commerce
5265 Port Royal Road
Springfield, VA 22161

The upper critical field in anisotropic superconductors

by

Daniel Wayne Youngner

A Dissertation Submitted to the

Graduate Faculty in Partial Fulfillment of the

Requirements for the Degree of

DOCTOR OF PHILOSOPHY

Department: Physics

Major: Solid State Physics

Approved:

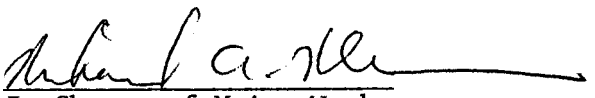

In Charge of Major Work

For the Major Department

For the Graduate College

Iowa State University
Ames, Iowa

1980

TABLE OF CONTENTS

The upper critical field in anisotropic superconductors

Daniel Wayne Youngner

Under the supervision of Richard A. Klemm
From the Department of Physics
Iowa State University

Theoretical descriptions of the upper critical fields in reentrant and anisotropic superconductors are presented. The theories are essentially microscopic in nature and incorporate many of the effects known to influence the behavior of superconducting electrons. In cases where adequate experimental data exist, the agreement between experiment and theory is found to be good.

I. INTRODUCTION

Superconductivity is a common low-temperature phenomenon known (1,2) to occur in more than forty elements and in several tens of thousands of alloys and compounds. The temperature at which a material becomes superconducting is called its transition temperature and is denoted by T_c. Materials in the superconducting state have no electrical resistance to direct currents, and will expel weak magnetic fields from their interiors. Sufficiently strong magnetic fields will penetrate samples and destroy the superconductivity, causing the sample to return to the normal (i.e., nonsuperconducting) state.

Superconductors can be classified as being of one of two types depending on how they respond to intermediate strength magnetic fields. Type I superconductors abruptly enter the normal state when the applied field reaches a temperature dependent critical value $H_c(T)$. In type II superconductors the magnetic field starts penetrating the material at $H_{c1}(T)$, but does not fully destroy the superconducting state until it reaches $H_{c2}(T)$ ($>H_{c1}(T)$). This thesis will be concerned exclusively with upper critical fields in type II superconductors.

Until recently (1960s), the upper critical field vs. temperature (H_{c2} vs. T) curves of virtually all known type II superconductors had the same general shape (3). As shown in Fig. 1, H_{c2} increased monotonically from zero at T_{c0} (the zero field transition temperature of the superconductor) to a maximum value at T = 0. The second derivative of this curve at T_{c0} and at all lower temperatures was negative. Known

a

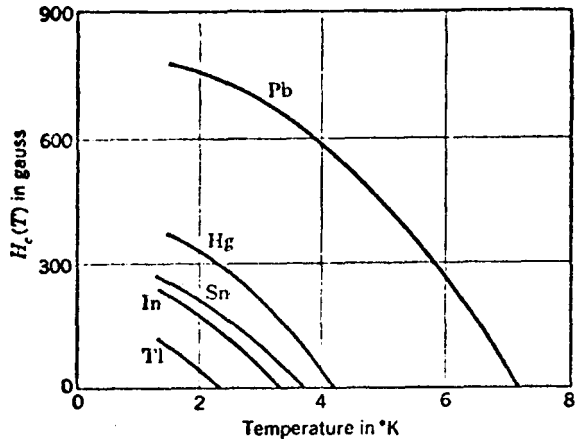

b

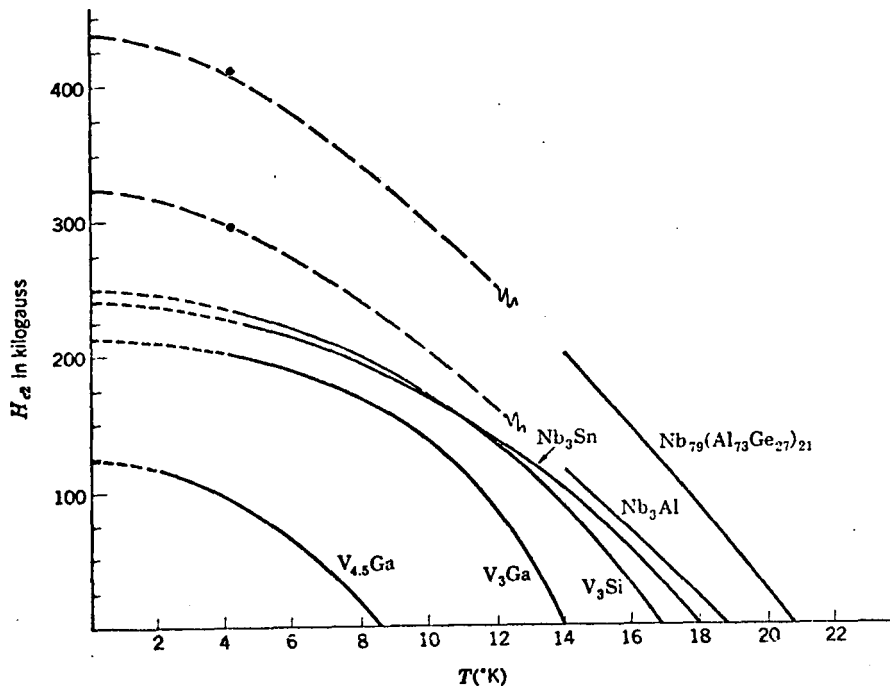

Figure 1. Critical field (1a) and upper critical field (1b) curves for type I and type II superconductors respectively (3). A specimen is normal above its curve and superconducting below

values of T_{c0} ranged from near zero to as high (4) as 21°K, and H_{c2} at T = 0 was typically less than, or at most slightly greater than, the paramagnetically limited (5) value of 18.6 T_{c0} k Gauss/Kelvin.

The upper critical fields of all of these materials could be explained by a well-known theory in which the Fermi surface is assumed to be spherically symmetric and the host lattice is assumed to be free of localized magnetic moments. Several important features of this theory will be discussed later in this chapter.

Recently several (6-23) new types of superconducting compounds with unusual upper critical field curves have been discovered. Two types of unusual superconductors will be discussed in this thesis. The first type (6-11) includes the ternary rare-earth alloys in which H_{c2} goes through a maximum and then returns to zero at a temperature $T_{c2} < T_{c0}$ (see Fig. 2). The second type (12-23) is the family of superconductors with highly anisotropic Fermi surfaces and pair states. Upward curvature in $H_{c2}(T)$ at T_{c0} and anomalously high values of $H_{c2}(T)$ at T = 0 have been seen in many anisotropic superconductors (see Fig. 3).

A. Ternary Rare-Earth Superconductors

There are two types of ternary rare-earth compounds which exhibit superconductivity and which display anomalous behavior in the temperature region below T_{c0}. The first is the Chevrel ternary molybdenum chalcogenides (6,7) with the formula $RE_yMO_6X_8$ (RE = Gd, Sm, Tb, Dy, Er; y = 1.0 or 1.2; X = Se or S). Several different types of experiments

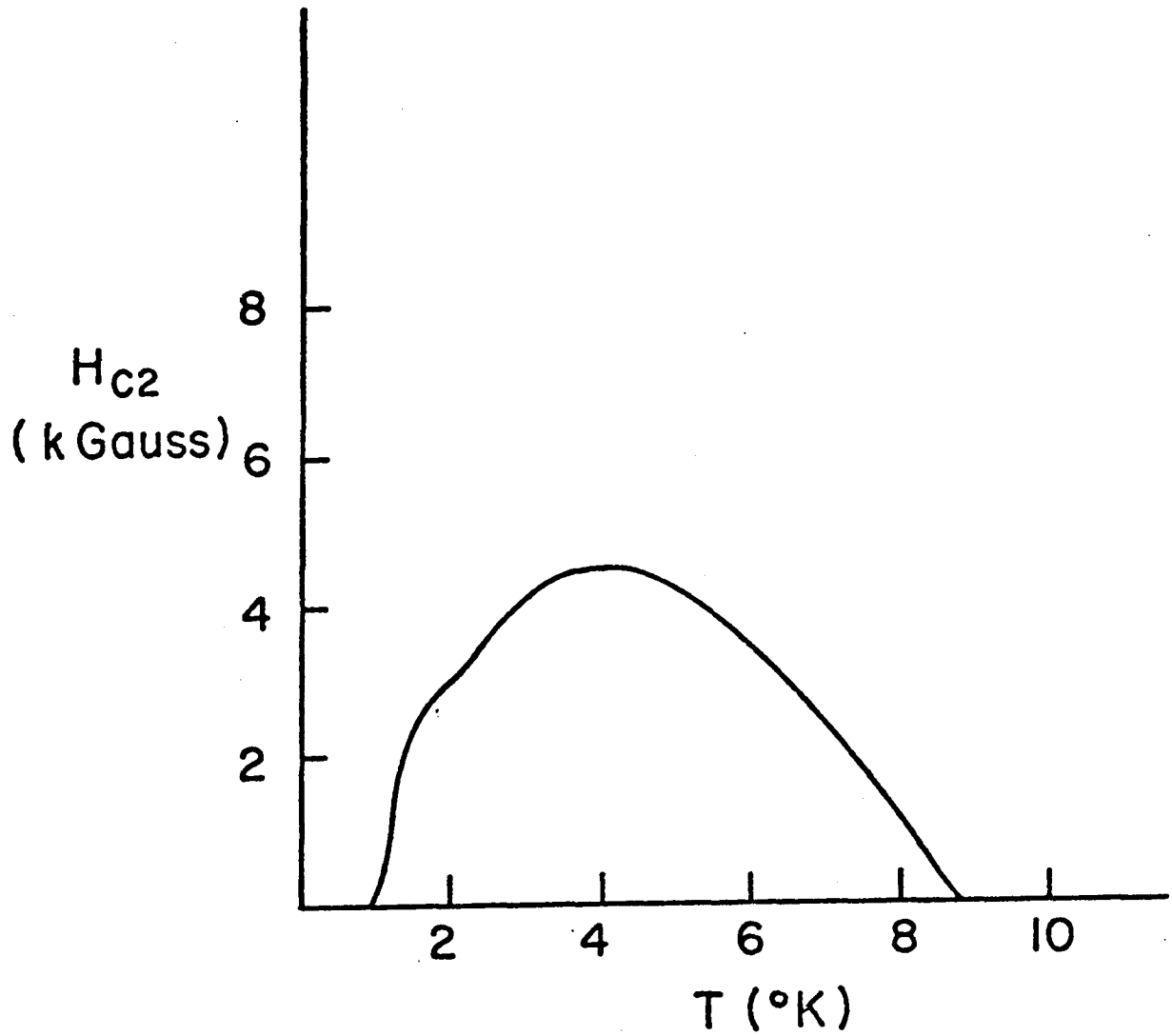

Figure 2. Upper critical field versus temperature of $ErRh_4B_4$ determined from ac electrical resistivity data (11). $H_{c2}(T)$ is the field required to reduce the resistivity to 50% of its normal state value

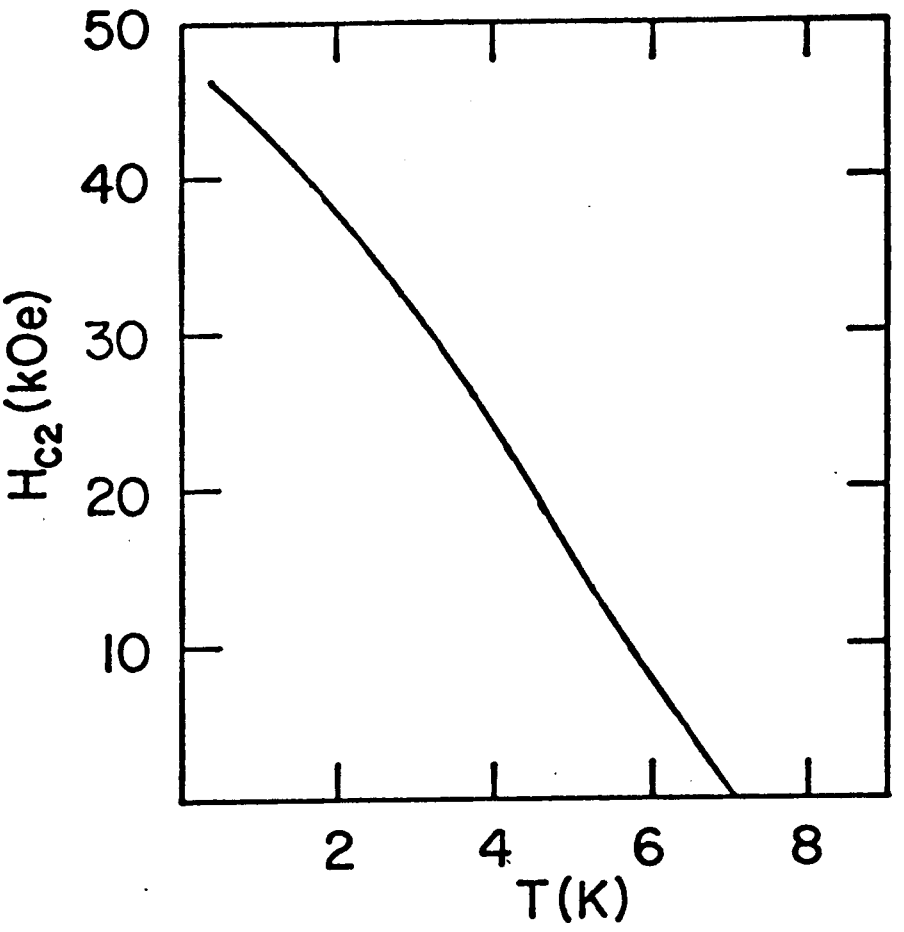

Figure 3. Experimental upper critical field data (13) on 2H-$NbSe_2$

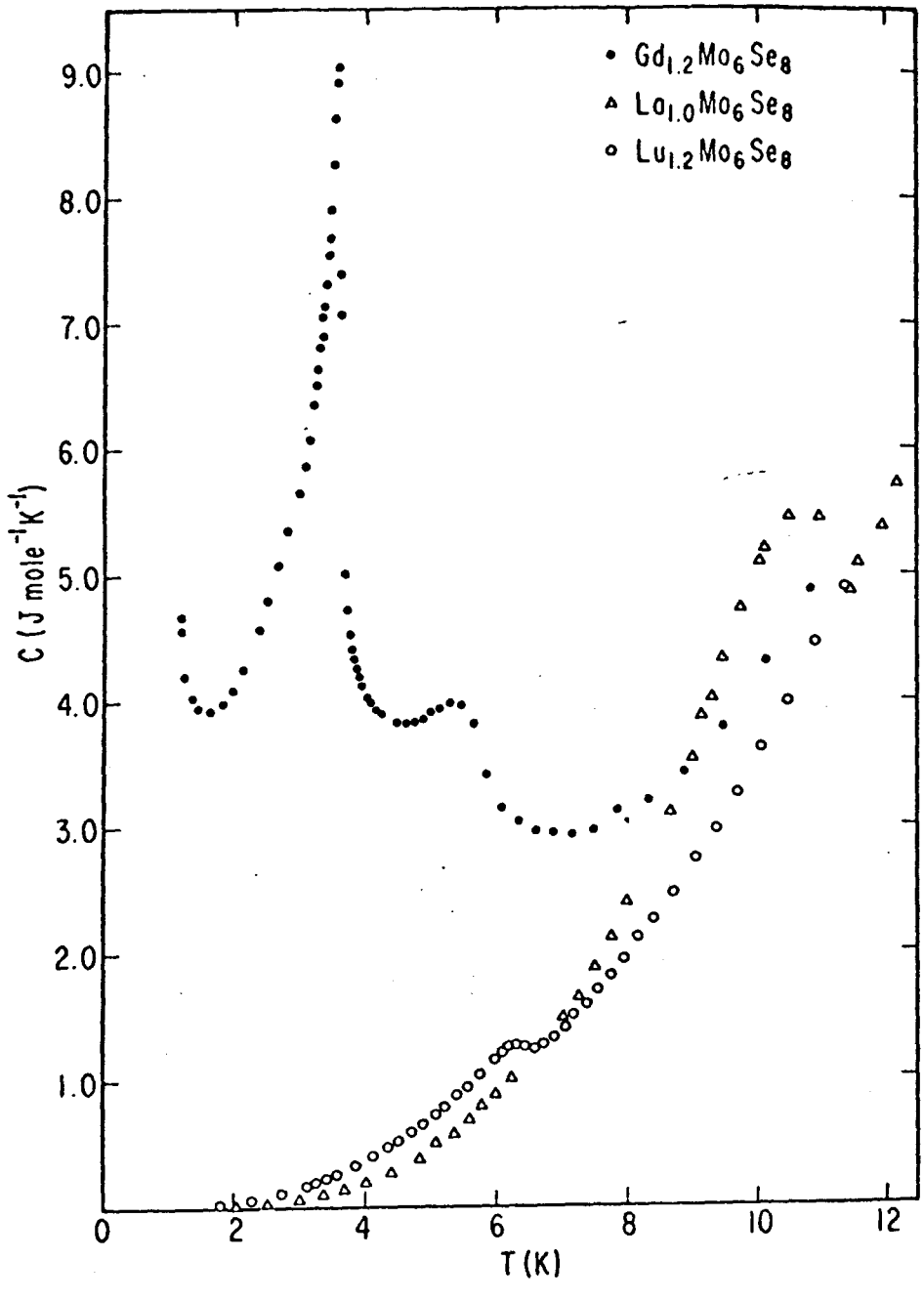

Figure 4. Specific heat versus temperature (7) for $Gd_{1.2}Mo_6Se_8$, $La_{1.0}Mo_6Se_8$ and $Lu_{1.2}Mo_6Se_8$

have been performed on these materials. Neutron scattering experiments (8) show that $HoMo_6S_8$, for example, undergoes a ferromagnetic transition below T_{c0}. Several Chevrel compounds have lamda-type anomalies in their specific heat curves below T_{c0}, indicative of the onset of long range magnetic order in them. In Fig. 4 we show specific heat data (7) on $Gd_{1.2}Mo_6Se_8$. The upper critical field curve (6) in $Gd_{1.2}Mo_6Se_8$ first increases as the temperature decreases, then reaches a maximum value at some finite temperature, and begins to decrease as the temperature is lowered further.

The second type (9) of ternary rare-earth alloy which exhibits superconductivity has the formula $RERh_4B_4$ where RE is a rare-earth element. As the temperature of these materials decreases, H_{c2} is often found to initially increase from 0 at T_{c1}, then reach a maximum value, decrease, and vanish at a temperature T_{c2} where $T_{c1} > T_{c2} > 0$. At T_{c2} the material reenters the normal state, and at temperatures just below T_{c2} the material becomes ferromagnetic. Experimental data taken by Maple *et al.* (9) on $ErRh_4B_4$ (Fig. 2) provide an example of this behavior. (The crystal structure of $ErRh_4B_4$ is shown in Fig. 5)

In the compounds mentioned above the 4f electrons of the rare-earth elements have localized magnetic moments which tend to order ferromagnetically. Simple theoretical considerations tell us that as the temperature of such a compound is lowered, the domains over which the local moments are ordered grow in size. When the radius ξ_m of the magnetic domains becomes comparable to the BCS coherence length ξ, the

individual Cooper pairs experience a magnetic field. This internally generated field tends to break the pairs, suppressing superconductivity in a manner analogous to an externally applied field acting on an ordinary superconductor. The external field required to destroy superconductivity in such a material is therefore diminished. At T_{c2} the internal field alone is strong enough to destroy superconductivity and cause the material to reenter the normal state. This simple theoretical argument will be quantified and developed more fully in Chapter II.

B. Anisotropic Superconductors

In many (12-18) materials with anisotropic Fermi surfaces and superconducting gaps the $H_{c2}(T)$ curve displays positive curvature near T_{c0} and unusually high values as T approaches zero. Recent experimental work by Orlando et al. (12), for example, shows upward curvature in the critical field curve of the A-15 materials Nb_3Sn, and perpendicular field measurements made by Dalrymple and Prober (13) on the hexagonally distorted material $NbSe_2$ (Fig. 3) show H_{c2} exceeding the predicted (24) value for spherically symmetric materials by $\sim$20% in the low-temperature regime. Several (16-18) other experimentalists have seen similar results.

Theoretical models attempting to describe these effects have included anisotropy in such things as the Fermi surface (25), the superconducting pair state (26), and the electron-electron coupling (27). These models, however, are either limited in validity to temperatures near to T_{c0}, or are plagued by other shortcomings which will be described more fully in Chapter III.

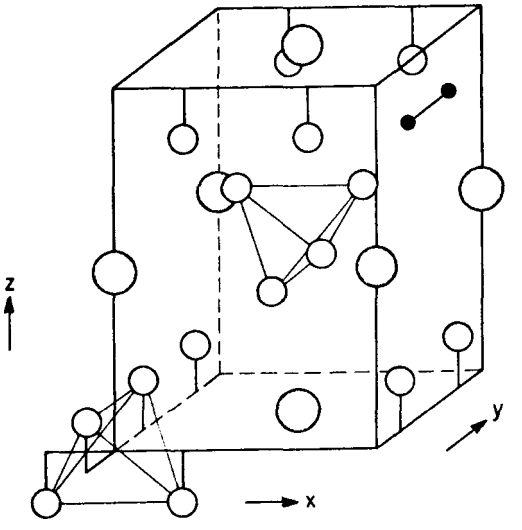

Figure 5. Crystal structure of $ErRh_4B_4$. The centers of the Rh_4 tetrahedra are located on the origin and center of the unit cell. Only one of the four B_2 pairs is indicated. ○, Er; ○, Rh; ●, B

In Chapter III a two-parameter model which incorporates Fermi surface and pair state anisotropy and which successfully describes $H_{c2}(T)$ over the entire temperature range will be presented.

C. Ginzburg Landau Theory

Thirty years ago Ginzburg and Landau (28) (GL) formulated a phenomenological theory which describes some of the properties of superconductors near their transition temperatures. The theory is conceptually simple and can be used to introduce some of the ideas encountered in the study of superconductivity.

Ginzburg and Landau assumed that the free energy of a superconductor could be written as

$$F_s = F_n + \int \left[\alpha|\psi|^2 + \frac{\beta}{2}|\psi|^4 + \frac{1}{2m^*}\left|\left(-i\hbar\nabla - \frac{e^*\vec{A}}{c}\right)\psi\right|^2 + \frac{h^2}{8\pi}\right] d\vec{r} \quad (1.1)$$

where F_n is the free energy in the normal state, ψ is the order parameter (or wave function) of the superconducting electrons, α is a parameter which is negative for $T < T_c$ and vanishes linearly at T_c, β is a positive constant parameter, $e^* = 2e$ and $m^* = 2m$ are the charge and mass respectively of a superconducting pair of electrons, and $\vec{h} = \nabla \times \vec{A}$ is the magnetic field. Minimizing the free energy with respect to variations in ψ^* and $\vec{A}$ leads to the coupled set of equations

$$\frac{1}{2m}\left[- i\hbar\nabla - \frac{2e\vec{A}}{c} \right]^2 \psi + \alpha\psi + \beta|\psi|^2\psi = 0 \quad , \tag{1.2}$$

$$\frac{\text{curl } \vec{h}}{4} = \frac{\vec{j}}{c} = \frac{e\hbar}{imc}(\psi^*\nabla\psi - \psi\nabla\psi^*) - \frac{4e^2}{mc^2}|\psi|^2\vec{A} \quad . \tag{1.3}$$

where $\vec{h} = \text{curl } \vec{A}$

Microscopic calculations (29-31) show that α and β are given by

$$\alpha = 1.83 \frac{\hbar^2}{2m} \frac{1}{\xi_0^2} \frac{T - T_c}{T_c} \quad , \tag{1.4}$$

$$\beta = 0.35 \frac{1}{N(0)} \left(\frac{\hbar^2}{2m} \frac{1}{\xi_0^2} \right)^2 \frac{1}{(k_B T_c)^2} \quad , \tag{1.5}$$

where ξ_0 is the coherence length at T = 0 and N(0) is the density of states at the Fermi level.

It follows (32,33) from GL theory that spatial correlations in the order parameter ψ exist over distances on the order of $\xi(T)$ where

$$-\frac{\hbar^2}{2m\alpha} = \xi^2(T) \tag{1.6}$$

and that magnetic fields penetrate into superconductors a distance $\lambda(T)$ where

$$\lambda(T) = \frac{1}{\sqrt{2}} \lambda_L(0) \left(\frac{T_c}{T_c - T} \right)^{1/2} \tag{1.7}$$

and $\lambda_L(0)$ is the field penetration depth at T = 0.

Near T_c where ψ is small, Eq. (1.2) can be written as

$$\frac{1}{2m}\left[-i\hbar\nabla - \frac{2e\vec{A}}{c} \right] \psi = - \alpha\psi \tag{1.8}$$

Eq. (1.8) is solved by equating $-\alpha$ with the lowest Eigenvalue of the differential operator on the left (see Appendix G for details). The solution gives:

$$H_{c2} = \frac{\phi_o}{2\pi\xi^2(T)} \tag{1.9a}$$

where $\phi_0 = c\hbar/4\pi e$ is the flux quantum. The essential feature of Eq. (1.8) is that near T_c, H_{c2} varies linearly with T:

$$H_{c2} \propto (T_c - T) \quad . \tag{1.9}$$

deGennes (33) and Saint-James, Thomas, and Sarma (32) provide very full accounts of GL theory.

D. The Microscopic Theory

Detailed descriptions of the theoretical techniques for dealing with systems containing large numbers of interacting fermions or bosons can be found in the literature (29,31). The description given here will be very sketchy. It is intended primarily to introduce ideas which will be developed more fully later and to quote results which will be used either as starting points for calculations to be performed later in this thesis or as reference points with which to compare results derived in this thesis.

Many body theory may be used to calculate the upper critical field of a superconductor. The procedure involves first finding an expression for the Green's function for interacting normal state electrons in a magnetic field, then correlating pairs of the normal state electrons by mathematically "turning on" the attractive BCS interaction. Seeking the conditions under which the normal state electrons are unstable with respect to the formation of superconducting pairs leads to a homogeneous integral equation, the solution of which gives $H_{c2}(T)$.

The procedure begins by defining the noninteracting single electron Green's function (29):

$$G(r_1, \tau_1, r_2, \tau_2) =$$

$$- \frac{\langle T_\tau(\psi(r_1, \tau_1,)\bar{\psi}(r_2, \tau_2)S)\rangle_o}{\langle S\rangle_o} \tag{1.10a}$$

where

$$\psi(r, \tau) = \exp[(H_o - \mu N)\tau]\psi(r) \exp[-(H_o - \mu N)\tau] \tag{1.10b}$$

$$\bar{\psi}(r, \tau) = \exp[(H_o - \mu N)\tau]\psi^+(r) \exp[-(H_o - \mu N)\tau] \tag{1.10c}$$

and ψ^+ and ψ are the usual Fermion creation and annihilation operators. Furthermore, $\langle \cdots \rangle_o = Sp\{\exp[(\Omega_o + \mu N - H_o)/T] \cdots\}$ (1.10d) where Sp (for "spur" $\equiv$ "trace") sums over all states in the grand cannonical ensemble, and

$$S(\tau) \equiv T_\tau \exp\{-\int_0^\tau H_{int}(\tau')d\tau'\}. \tag{1.10e}$$

In Eq. (1.10a), $S \equiv S(1/T)$. Throughout this thesis, units will be chosen such that $\hbar = k_B = c = 1$.

In cases where the Green's function depends on $\vec{r}_1$ and $\vec{r}_2$ only as $|\vec{r}_1-\vec{r}_2|$ and on τ_1 and τ_2 only as $\tau_1-\tau_2$, it proves convenient to define Fourier transforms

$$G^{(0)}(\vec{p},\omega) = \int d\vec{r} \exp(-i\vec{p}\cdot\vec{r}) \int d\tau \exp(i\omega\tau) G(\vec{r},\tau) \tag{1.10f}$$

Replacing the operators in $G^{(0)}(\vec{p},\omega)$ with their Eigenvalues leads to

$$G^{(0)}_{\alpha\beta}(\vec{p},\omega) = \frac{\delta_{\alpha\beta}}{i\omega - \xi(\vec{p})} \quad . \tag{1.10g}$$

Here, α and β are possible spin projections of the electron, $\vec{p}$ is the electron's momentum, $\omega = 2\pi T(\nu + 1/2)$ where T is the temperature of the material and ν is an integer, δ is the Kroeneker delta, and $\xi(\vec{p})$ is the electron's energy. Typically $\xi(\vec{p}) = \varepsilon_o(\vec{p}) - \mu = p^2/2m - \mu$ where m is the effective mass of an electron and μ is the chemical potential. The superscript (0) is used to indicate that the electron is in an unperturbed state.

Having eliminated all operators from the definition of the Green's function, we can Fourier transform the momentum variables in Eq. (1.10g) to obtain

$$G^{(0)}_{\alpha\beta}(\vec{r},\omega) = -\delta_{\alpha\beta} \frac{m}{2\pi r} \exp\left\{ i(\text{sgn }\omega)k_F r \frac{-|\omega|r}{v_F} \right\} \tag{1.11}$$

where k_F and v_F are the Fermi wavevector and the Fermi velocity respectively, $r = |\vec{r}|$, and $\text{sgn } x = x/|x|$.

By allowing the electron described by Eq. (1.10) or Eq. (1.11) to interact with other particles and fields, the electronic Green's function can be modified in a variety of ways. In an external magnetic field $\vec{H}(=\vec{B})$, for example, the real space Green's function becomes (34)

$$G^n_{\alpha\beta}(\vec{r},\omega) = -\delta_{\alpha\beta}\frac{m}{2\pi r}\exp\left\{\text{sgn }\omega\left[ik_F - \frac{\omega + i\mu_B\sigma H}{v_F}\right]r\right\}\exp\left(ie\int_0^r d\vec{s}\cdot\vec{A}(\vec{s})\right) \tag{1.12}$$

where μ_B is the Bohr magneton, $\sigma = \pm 1$ is the spin of the electron and $\vec{A}(\vec{s})$ is the magnetic vector potential. The factor $\exp(ie\int d\vec{s}\cdot\vec{A}(\vec{s}))$ comes from treating the magnetic field in a gauge invariant (35), semi-classical manner. We have assumed that the magnetic field affects only the relative phases of the electronic wavefunctions, and have neglected the effects of Landau quantization which become important only when $\mu_B H_{c2}/m \gtrsim \pi T + 1/\tau$.

If the electrons are allowed to scatter from randomly located non-magnetic impurities, the frequency ω in the Green's function is renormalized (29):

$$\omega \to \tilde{\omega} = \omega + \text{sgn }\omega/2\tau_1 \tag{1.13}$$

where τ_1 is the impurity scattering time. The procedure for treating impurity scattering is described in Appendix A and is shown diagrammatically in Fig. 6.

Figure 6. Diagrams showing impurity scattering. Each X indicates scattering from a single atom. X's joined by dotted lines indicate scattering from the same atom. The general integral equation is shown diagrammatically in Fig. 6a. As argued in Appendix A, diagrams like 6b serve only to renormalize the chemical potential and need not be considered. The contribution to G from diagrams with crossed impurity lines (i.e., Fig. 6f) are smaller than the contributions from diagrams with uncrossed lines (Figs. 6d and 6e) by a factor $(\varepsilon_F \tau)^{-1} << 1$, and may also be ignored. Diagrams like the ones in Figs. 6c, 6d, and 6e contribute significantly to the renormalization of G and must be retained. Figure 6g shows the integral equation which generates all of the significant contributions. See Appendix A for details

a 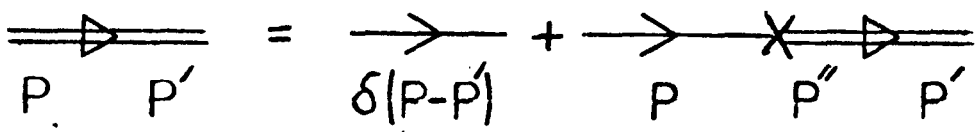

b 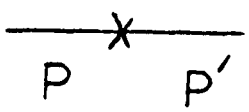

c 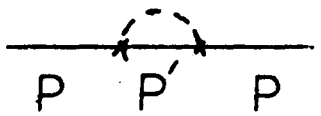

d 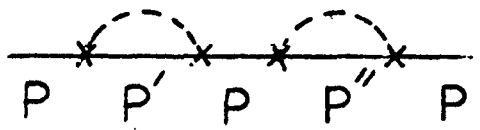

e 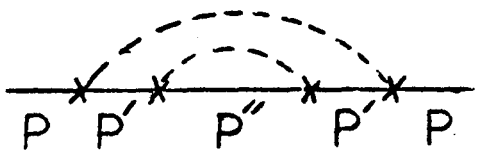

F 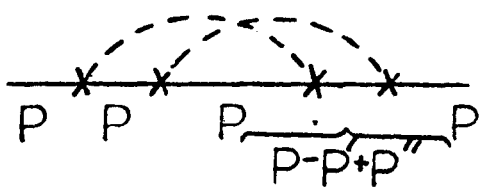

g 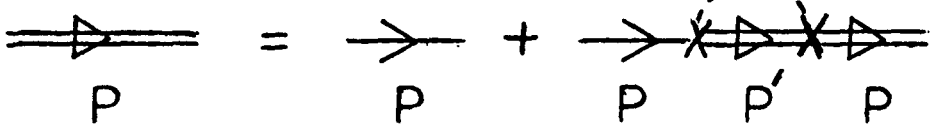

With the inclusion of spin-orbit scattering in our formalism, τ_1 gets replaced by the total impurity scattering time τ where (36) $1/\tau = 1/\tau_1 + 1/\tau_{so}$. A detailed description of the effects of spin-orbit scattering is given in Appendix B.

Numerous other modifications to the normal state electronic Green's function can be imagined. For an understanding of the topics to be discussed in this thesis, however, the three we've already mentioned -- interaction with a magnetic field, impurity scattering, and spin-orbit scattering -- are all that need to be considered.

Superconductivity is caused by an attractive, phonon mediated interaction between pairs of normal state electrons. The two particle propagator Δ for a pair of electrons in the presence of the interaction satisfies the integral equation (37)

$$\Delta(r_1,r_2,\Omega) = \sum_{\omega,\sigma} G_\sigma(r_1,r_2,\omega)G_{-\sigma}(r_1,r_2,\Omega-\omega) + VT \sum_{\omega,\sigma} \int d^3r\, G_\sigma(r_1,r,\omega)G_{-\sigma}(r_1,r,\Omega-\omega)\Delta(r_1,r_2,\Omega) \tag{1.14}$$

where V is the interaction strength (the BCS coupling constant). The Feynman diagram corresponding to Eq. (1.14) is shown in Fig. 7.

The existence of the superconducting state becomes infinitely more probable than the existence of the uncorrelated normal two-particle state only if Δ diverges relative to the uncorrelated product of Green's functions. When this happens, the homogeneous equation

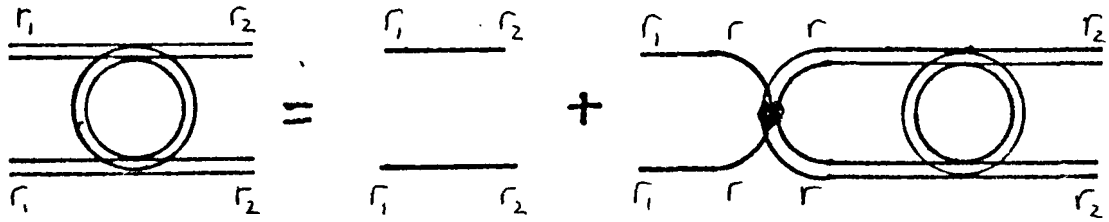

7a

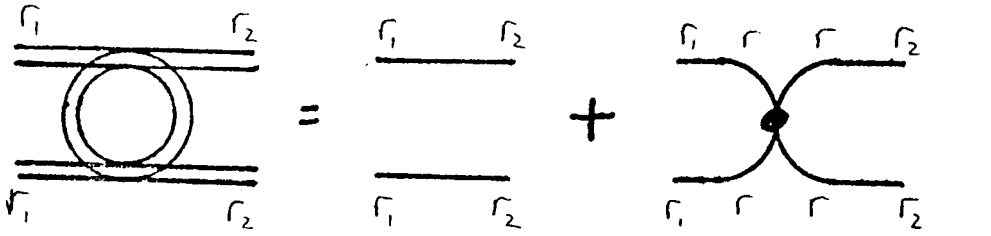

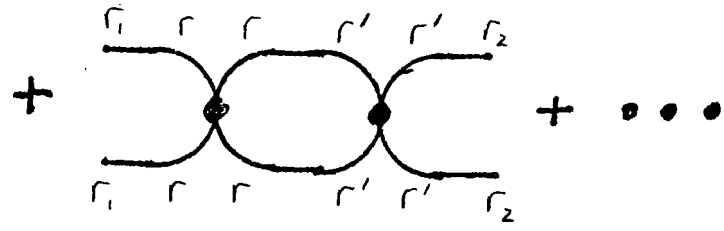

7b

Figure 7. Diagrammatic representation of Eq. (1.14). Δ, G, and V are represented by the quantity on the left of the = sign, a single line, and a dot, respectively. The integral equation shown in Fig. 7a generates the terms shown in Fig. 7b

$$\Delta(r) = VT \sum_{\omega,\sigma} \int d^3r' \, K_0(r,r',\omega)\Delta(r) \tag{1.15}$$

has a solution. Here,

$$K_0(r,r',\omega) = G_\sigma(r,r',\omega)G_{-\sigma}(r,r',-\omega) \tag{1.16}$$

is the kernel of the integral equation. We have made use of the fact that the superconducting state is most stable when $\Omega = 0$.

If, in addition to the BCS interaction, there are other mechanisms serving to enhance (or diminish) the correlation between paired superconducting electrons, the effects of the additional mechanisms should be incorporated into the kernel. Impurity scattering is one such mechanism. In the "ladder" approximation for impurity scattering shown schematically in Fig. 8 and discussed in Appendix F, the kernel changes from K_0 to K where K satisfies

$$K(r,r',\omega) = K_0(r,r',\omega) + \frac{1}{2\pi\tau N(0)} \int d^3r_1 \, K_0(r,r_1,\omega)K(r_1,r',\omega) \quad . \tag{1.17}$$

When impurity scattering is to be considered, it should enter the expressions for both the single particle propagator (Eq. (1.13)) and the two particle vertex (Eq. (1.17)). In Fig. 9 we show diagrams for some of the two particle propagators contributing to the superconducting state when both BCS coupling and impurity scattering are present.

If we include the effects of spin orbit scattering and spin paramagnetism on the superconducting state, it is necessary to generalize the formalism used to describe the state. The equations of motion for the different Green's functions in the superconductor depend on the spin

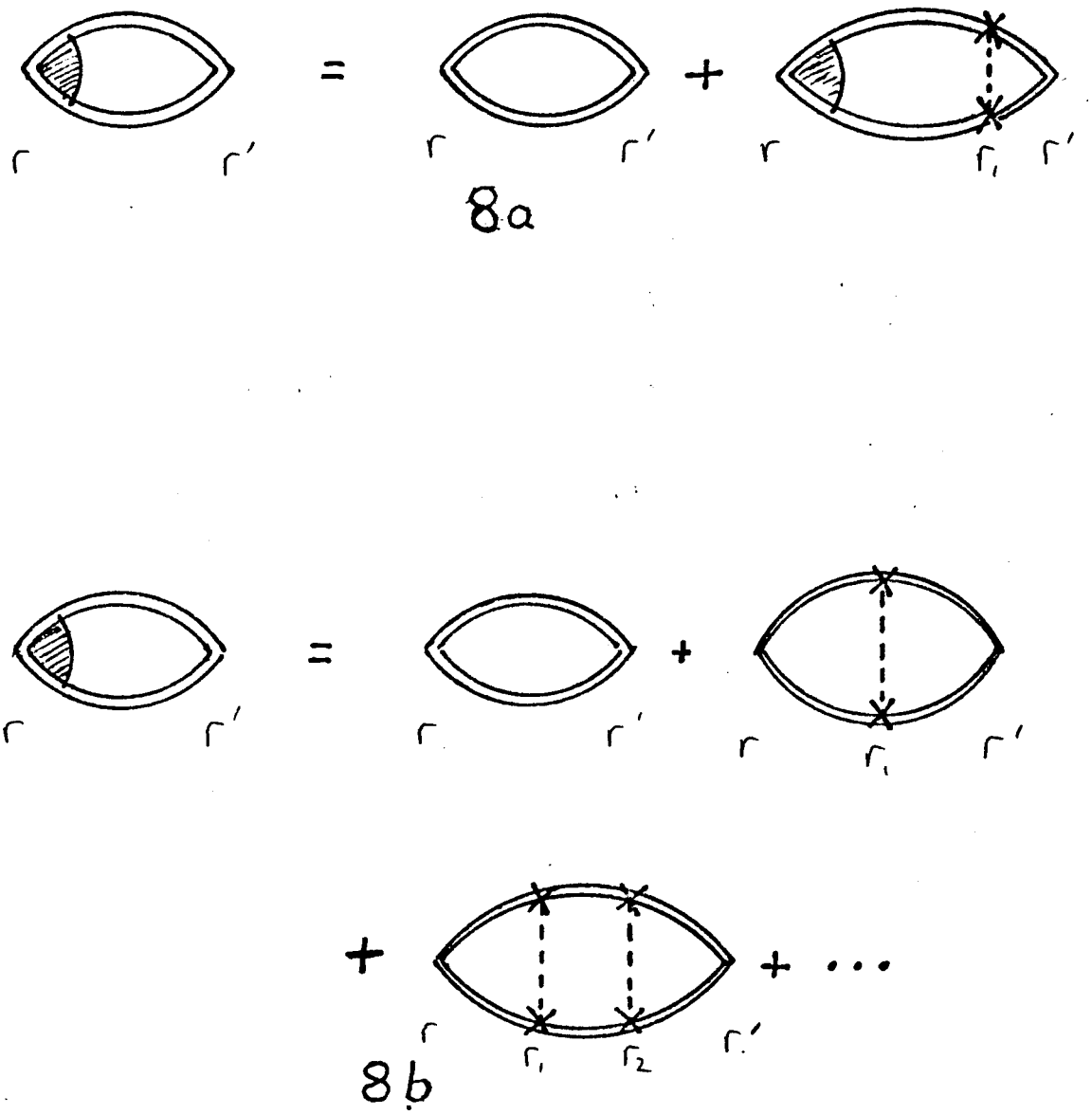

Figure 8. Diagrammatic depiction of how impurity scattering treated in the "ladder approximation" modifies the kernal. The integral equation (Eq. (1.17)) shown in Fig. 8a generates the terms shown in Fig. 8b

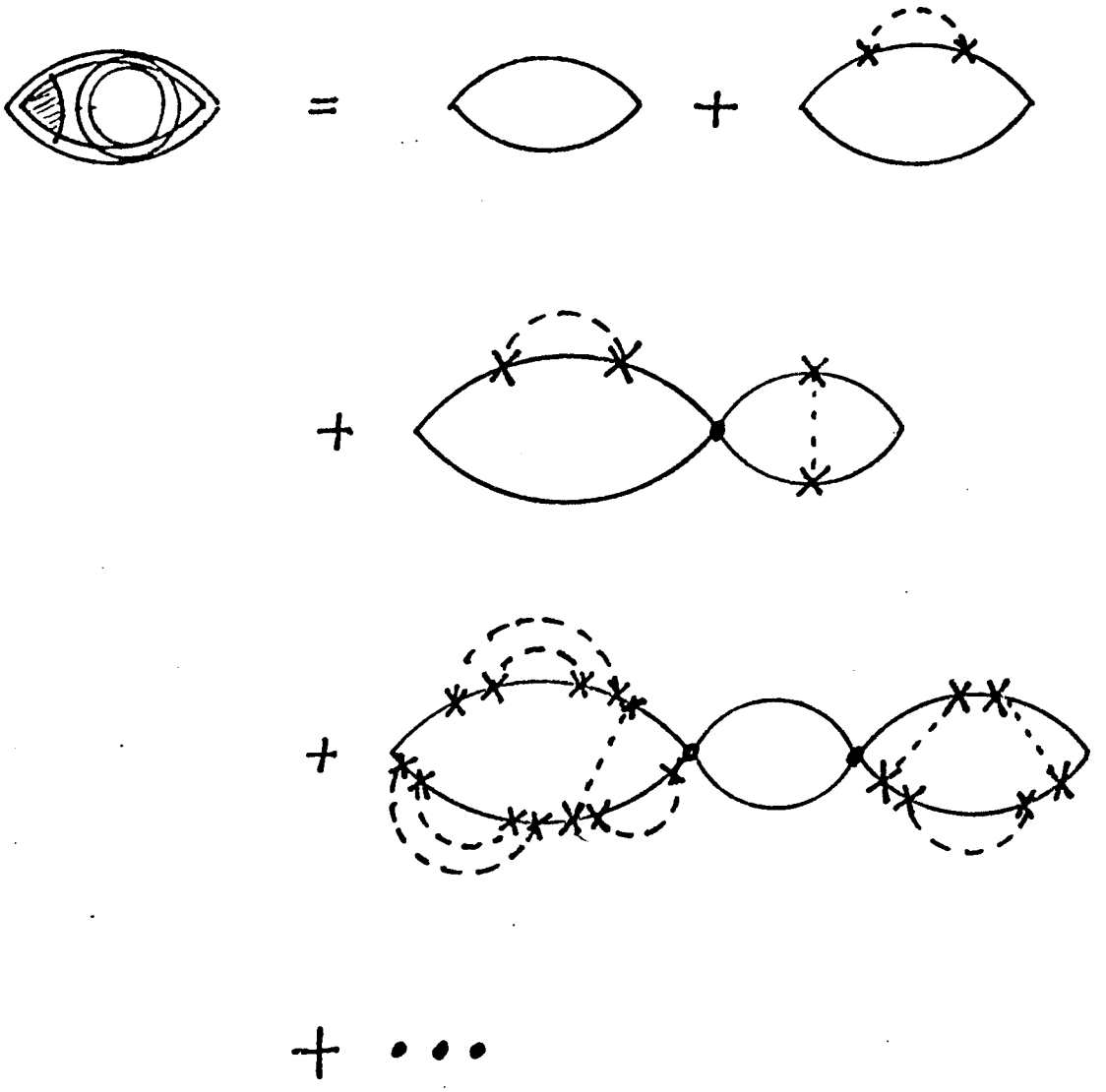

Figure 9. Some of the diagrams contributing to K when both the BCS force and impurity scattering are considered

indices of the Green's function and on whether it (the Green's function) is built from creation or annihilation operators. The various equations satisfied by the different Green's functions couple to one another in a manner conveniently expressed using the matrix notation of Werthamer, Helfand, and Hohenberg (36) (see Appendix B). With spin-orbit scattering, the normal state Green's function and the vertex renormalization equation are still formally described by Eqs. (1.12) and (1.14)-(1.17), but σ gets replaced by the Pauli spin matrices and G, K_0, and K become 2 x 2 matrices.

Once we've put all of the effects we're interested in (e.g., magnetic field, impurity scattering, spin-orbit scattering) into the kernal in Eqs. (1.15)-(1.17), the procedure for solving the equations is in principle straightforward. The solution gives T_c as a function of H, τ_1, τ_{so}, etc. When Δ is a slowly varying function of position (which is almost always the case in macroscopic samples), Eqs. (1.15)-(1.17) can be replaced by

$$1 = VT \sum_{\omega,\sigma} \int d^3r' \, K(r',\omega) \tag{1.18}$$

where $K(r',\omega)$ is the lowest eigenvalue of the kernal in Eqs. (1.15)-(1.17). In general, the mathematical core of the problem of finding $H_{c2}(T)$ lies in solving Eq. (1.18).

Several other theoretical research groups (24,25,36) have attempted to solve Eq. (1.18) under varying sets of conditions. Helfand and Werthamer (24) solved it in the absence of spin-orbit scattering. They found that Eq. (1.18) reduced to

$$\ln \frac{1}{t} = \sum_{\nu=-\infty}^{\infty} \left\{ \frac{1}{2\nu + 1} - \frac{(t/h^{1/2})J(\alpha_\omega)}{1 - (\lambda/h^{1/2})J(\alpha_\omega)} \right\} \tag{1.19}$$

where

$$J(\alpha_\omega) = 2 \int_0^\infty d\omega \, \exp(-\omega^2) \tan^{-1}(\alpha_\omega \, \omega) \tag{1.20}$$

$$= \sum_{n=0}^{\infty} (-1)^n \, \alpha_\omega^{2n+1} \, n!/(2n+1) \quad . \tag{1.21}$$

Here,

$$\alpha_\omega = h^{1/2}/(|2\nu + 1|t + \lambda) \tag{1.22}$$

$$h = 2e \, H_{c2}(v_F/2\pi T_{c0})^2 \tag{1.23}$$

$$\lambda = 1/2\pi T_{c0}\tau_1 \tag{1.24}$$

$$t = T/T_{c0} \quad . \tag{1.25}$$

Solutions to Eq. (1.19) are shown in Fig. 10.

Hohenberg and Werthamer (25) wrote the solution to Eq. (1.18) using a formalism that facilitates the inclusion of Fermi surface and pair state anisotropy. They showed that $H_{c2}(T)$ is determined by

$$1 = VT \sum_{\nu} [\, S_\omega^{-1} - 1/2\pi T_{c0}\tau \,]^{-1} \tag{1.26}$$

where

$$S_\omega = \frac{\pi}{|\tilde{\omega}|} \int d\hat{q} \, N(\hat{q}) \sum_{n=0}^{\infty} -1^n \left\langle S \left| \left(\frac{\vec{v}(\hat{q}) \cdot \vec{\pi}}{2\tilde{\omega}} \right)^{2n} \right| S \right\rangle \quad . \tag{1.27}$$

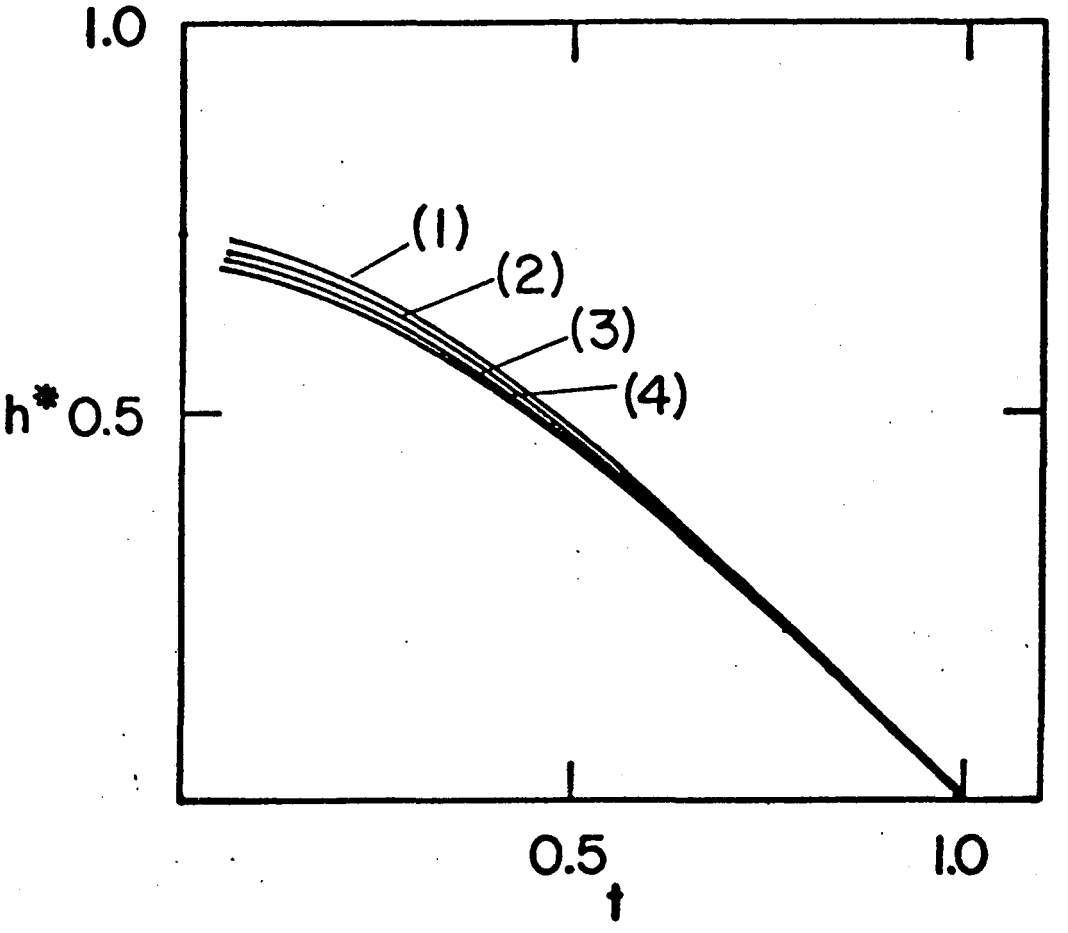

Figure 10. Upper critical fields for spherically symmetric materials. λ = (1) 0.0; (2) 0.5; (3) 5.0; (4) 50.0. These results may be obtained using either Eq. (1.19) or Eqs. (3.2) and (3.3)

Here, $\vec{\pi} = -i\nabla_r - 2e\vec{A}(\vec{r})$ is the gauge invariant momentum operator acting on the pair state $|S\rangle$. (More will be said about this model in Chapter III.) Hohenberg and Werthamer were only able to evaluate the first few terms in the sum over n in Eq. (1.27), and thus obtained results valid only near $T = T_{c0}$. Furthermore, although their formalism could handle anisotropy in the pair state $|S\rangle$, they did not consider its effects on $H_{c2}(T)$.

Werthamer, Helfand, and Hohenberg (36) showed that with spin-orbit scattering, $H_{c2}(T)$ is given by the solution of

$$\ln\frac{1}{t} = \sum_{\nu} \frac{1}{2\nu+1} - \{[\mathrm{Re}(I_\omega^{-1} - (\tau^{-1} - \tfrac{4}{3}\tau_{so}^{-1})/2\pi T)^{-1}]^{-1} - \tfrac{4}{3}(2\pi T\tau_{so})^{-1}\}^{-1} \tag{1.28}$$

where

$$I_\omega = [2\pi T/v_F(2eH)^{1/2}]J_1(\alpha_\omega) \tag{1.29}$$

$$J_1(z) = 2\int_0^\infty d\omega\, \exp(-\omega^2)\,\frac{1}{2i}\ln\left(\frac{1+iz\omega}{1-iz\omega}\right) \tag{1.30}$$

$$\alpha_\omega = v_F(2eH)^{1/2}(2|\omega| + \tau^{-1} + 2i\mu H)^{-1} \quad . \tag{1.31}$$

In the "dirty limit" ($l \ll \xi_o$), which is a limit frequently satisfied by materials in which spin-orbit scattering plays a significant role, Eqs. (1.28)- (1.31) become

$$\ln\frac{1}{t} = \left(\frac{1}{2} + \frac{i\lambda_{so}}{4\gamma}\right)\psi\left(\frac{1}{2} + \frac{\bar{h} + \frac{1}{2}\lambda_{so} + i\gamma}{2t}\right) + \left(\frac{1}{2} - \frac{i\lambda_{so}}{4\gamma}\right)\psi\left(\frac{1}{2} + \frac{\bar{h} + \frac{1}{2}\lambda_{so} - i\gamma}{2t}\right) - \psi\left(\frac{1}{2}\right) \tag{1.32}$$

where

$$\bar{h} = 2eH_{c2}(v_F^2\tau/6\pi T_{c0}) \tag{1.33}$$

$$\gamma = [(\alpha\bar{h}) - (\tfrac{1}{2}\lambda_{so})^2]^{1/2} \tag{1.34}$$

and ψ is the digamma function. The solution to Eq. (1.22) is plotted in Fig. 11. We observe that spin-orbit scattering reduces the limiting effect of Pauli paramagnetism thereby allowing for larger upper critical fields.

Most of the formulae quoted in the introduction will be used in some manner in the latter chapters of this thesis. We will use the spin-orbit formalism (Eqs. (1.32) and (1.33)) of WHH (36) in our calculation of $H_{c2}(T)$ in rare-earth compounds (Chapter II). In Chapter III we extend the scope of Eqs. (1.26) and (1.27) derived by Hohenberg and Werthamer (25) by showing how Fermi surface and pair state anisotropy affect $H_{c2}(T)$ in the range $0 < T \leq T_{c0}$. We find that our results reduce to those of Helfand and Werthamer (24) (Eqs. (1.19)-(1.25)) in the isotropic limit.

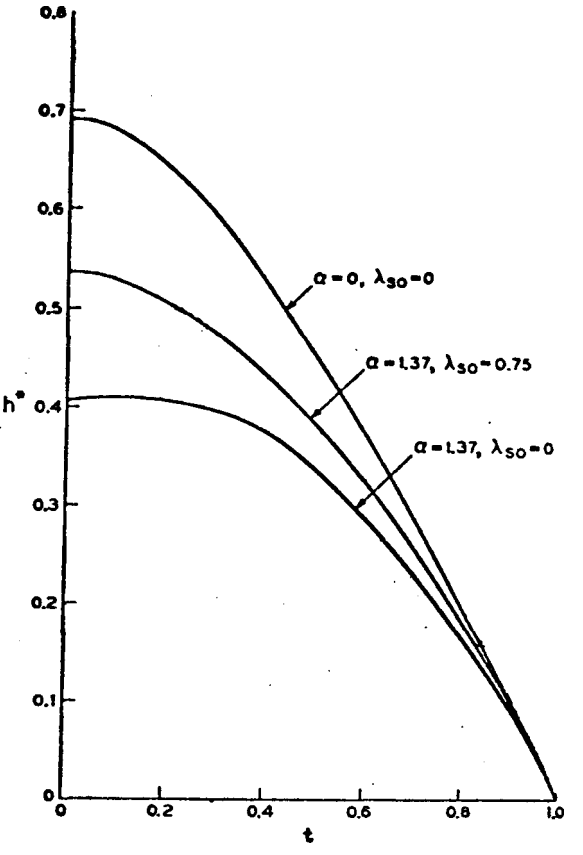

Figure 11. Upper critical fields with spin-orbit scattering (36)

II. TERNARY RARE-EARTH SUPERCONDUCTORS

A. Introduction

The ternary rare-earth compounds form an interesting and unique family of materials. In these compounds the competing effects of superconductivity and long-range ferromagnetic order each tries to dominate the behavior of the electrons at low temperatures. There are some rare-earth compounds which, because of this competition, initially enter the superconducting state at a temperature T_{c1}, then reenter the normal (i.e., nonsuperconducting), paramagnetic state at $T_{c2} < T_{c1}$, and finally ferromagnetically order at $T_M < T_{c2}$. $ErRh_4B_4$ is one such compound. Experimentally obtained upper critical field data (11) on $ErRh_4B_4$ is shown in Fig. 2.

All known ternary rare-earth compounds which exhibit superconductivity have either the formula $RERh_4B_4$ or the formula $RE_yMo_6X_8$ (RE = Gd, Sm, Tb, Dy, Er; y = 1.0 or 1.2, X = Se or S). Schematic diagrams of the crystal structure (38) of these compounds are shown in Fig. 5. When these compounds are cooled to low temperatures the conduction electrons, which are primarily the 4d electrons of Mo or Rh, would like to condense into the superconducting phase, but the localized magnetic moments, which come primarily from the 4f electrons of the rare-earth elements, would like to align themselves spatially with one another thereby making the compound ferromagnetic.

Our model treats the conduction electrons and the localized moments as two separate groups. This approximation is also used in the band

structure calculation (39) done for $ErRh_4B_4$ (see Fig. 12), and is consistent with the fact that in the compounds $REMo_6S_8$ and $REMo_6Se_8$ the variation of transition temperature with rare-earth elements can be described (40) by the Abrikosov-Gor'kov (AG) theory (41) with the deGennes factor (except when RE = Ce or Er). In our model the conduction electrons interact weakly with the local moments via an exchange integral I. The short-range interaction between local moments has strength $\mathcal{J}$ and is responsible for magnetic ordering at low temperatures. We treat I and $\mathcal{J}$ as independent parameters. Maekawa and Tachiki (42) used the same model as we to calculate thermodynamic properties and upper critical fields. Their theory, however, does not reduce to the AG theory as I goes to zero.

B. Formulation of the Theory

The model we use is essentially microscopic, but some simplifying, semi-phenomenological approximations are made in some of the formulae. We begin with the following model Hamiltonian, $\mathcal{H}$:

$$\mathcal{H} = \mathcal{H}_{BCS} + \mathcal{H}_{cf} + \mathcal{H}_{ff} \quad . \tag{2.1}$$

$\mathcal{H}_{BCS}$ describes the energy of the conduction electrons modified by the presence of a superconducting gap, and is given by

$$\mathcal{H}_{BCS} = \sum_{k\sigma} \varepsilon_k \, C^+_{k\sigma} \, C_{k\sigma} - \Delta \sum_k (C^+_{k\uparrow} \, C^+_{-k\downarrow} + \text{h.c.}) \quad . \tag{2.2}$$

In Eq. (2.2), ε_k is the normal energy of an electron with wavenumber k, and Δ is the spatially averaged condensation energy of the superconducting

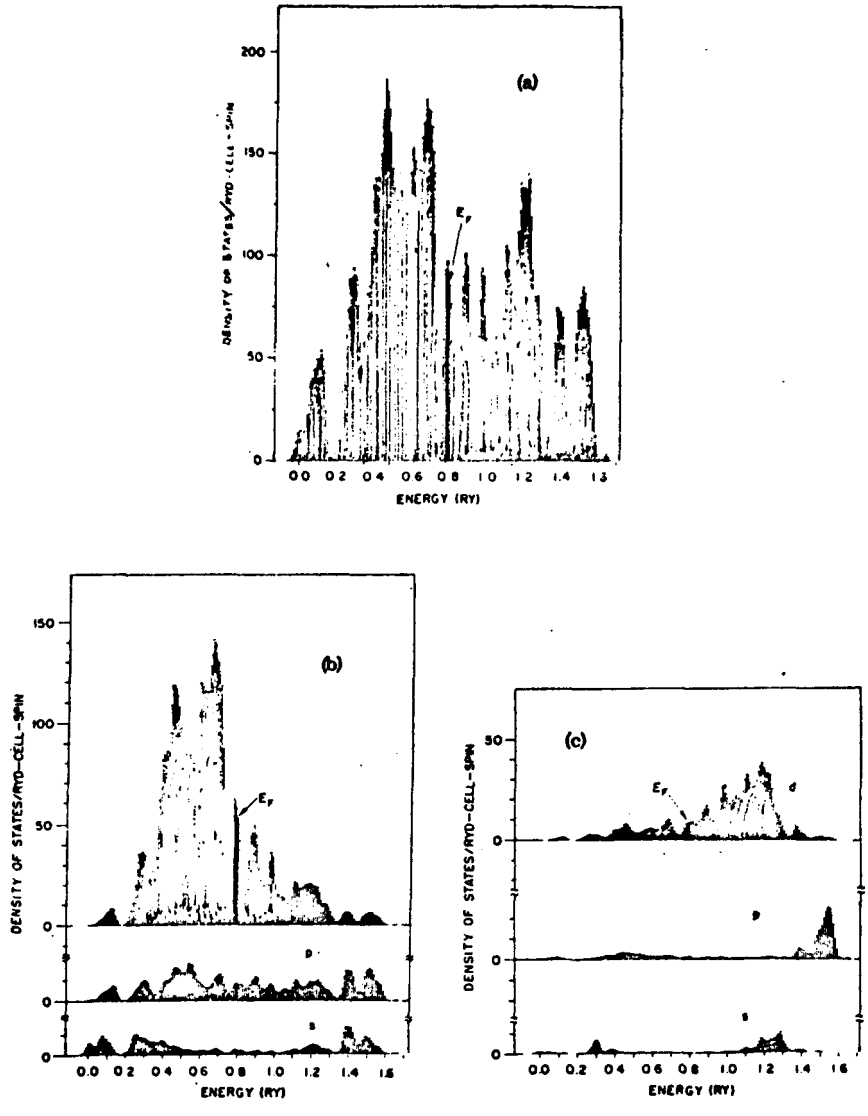

Figure 12. The calculated (a) total DOS and l-decomposed partial DOS for (b) Rh and (c) Er sites in $ErRh_4B_4$. The d electrons from Rh are seen to have a high density of states at the Fermi level. The magnetic 4f electrons of Er (not shown) are in spatially localized core states

electrons. We treat Δ as a free parameter. The creation and annihilation operators for electrons with wavenumber k and spin σ are denoted by $C^{+}_{k\sigma}$ and $C_{k\sigma}$ respectively, and satisfy the usual anticommutation relations

$$\{C_{\vec{k}\sigma}, C^{+}_{\vec{k}',\sigma'}\} = \delta_{\sigma\sigma'}\,\delta(k - k') \tag{2.3}$$

$$\{C_{\vec{k}\sigma}, C_{\vec{k}',\sigma'}\} = \{C^{+}_{\vec{k}\sigma}, C^{+}_{\vec{k}',\sigma'}\} = 0 \quad . \tag{2.4}$$

The abbreviation h.c. in Eq. (2.2) stands for hermitian conjugate.

The second term in the Hamiltonian describes the interaction between the conduction electrons and the local moments and is given by

$$\mathcal{H}_{cf} = -\frac{I}{2N}(g_J - 1)\sum \vec{J}_i \cdot \vec{\sigma}_{\mu\nu}\, C^{+}_{k\mu}\, C_{k'\nu}\, e^{i(k-k')R_i} \tag{2.5}$$

where I is the interaction strength between the conduction electrons and the local moments, N is the number of local spins per unit volume, g_J is the Landé g factor, and $\vec{\sigma}$ is the Pauli spin matrix. The total angular momentum at lattice site R_i is J_i.

The final term in the Hamiltonian shows how local magnetic moments interact with one another.

$$\mathcal{H}_{ff} = -\frac{1}{2}\sum_{ij} \mathcal{J}(R_i - R_j)\vec{J}_i \cdot \vec{J}_j \quad . \tag{2.6}$$

Here, $\mathcal{J}(R_i - R_j)$ is the interaction strength between pairs of spins separated by $R_i - R_j$.

We treat the exchange interaction I between the conduction electrons and the local moments within the Born approximation, and treat the spin-

spin interaction phenomenologically. Our model is similar to the model used in the AG theory except that in ours, translational symmetry of the spins is built in from the beginning.

The superconducting transition temperature is found by solving the linearized gap equation discussed in Chapter I. The procedure we will use for solving it is similar to the procedure used by Matsuura, Ichinose, and Nagaoka (43).

$$\Delta = V\, Q(T)\Delta \tag{2.7}$$

$$Q(T) = \int_0^{1/T} d\tau' \int dr' \langle T_\tau \{C_\uparrow(r\tau)C_\downarrow(r\tau)C_\downarrow^+(r'\tau')C_\uparrow^+(r'\tau')\}\rangle \tag{2.8}$$

where V is the BCS coupling strength, Δ is the spatially averaged pair state wavefunction, $C_\uparrow^+(r\tau)$ is the Heisenberg operator, and τ is the imaginary time. Note the similarity between Eqs. (2.7) - (2.8), and Eqs. (1.15) - (1.16). After applying space and time Fourier transformations, Eq. (2.8) becomes

$$Q(T) = T \sum_\omega \sum_k \gamma(\omega) G_k(\omega) G_{-k}(-\omega) \tag{2.9}$$

$$G_k^{-1}(\omega) = i\omega - \xi_k - \Sigma(\omega) \tag{2.10}$$

where $\omega = (2\nu + 1)\pi T$. The vertex correction $\gamma(\omega)$ and the self-energy correction $\Sigma(\omega)$ have been introduced. Although the expressions for γ and Σ will generally depend on both momentum k and energy ω, the expressions we will use are independent of k. Assuming electron-hole symmetry [$\Sigma(-\omega) = -\Sigma(\omega)$, $\gamma(-\omega) = \gamma(\omega)$] and performing the momentum integration

leads to

$$Q(T) = \pi N(0)\, T \sum_{\omega} \frac{\gamma(\omega)}{|\omega| + |\Sigma(\omega)|} \tag{2.11}$$

where N(0) is the density of states at the Fermi level. The Dyson equation for the vertex part (shown diagrammatically in Fig. 13) is

$$\gamma(\omega) = 1 + T \sum_{\omega'} \sum_{k'} \Gamma_{\uparrow\downarrow}(k\omega,k'\omega')\, G_{k'}(\omega')G_{-k'}(-\omega')\gamma(\omega') \tag{2.12}$$

where $\Gamma_{\uparrow\downarrow}(k\omega,k'\omega')$ is the irreducible four-point vertex which expresses the effective interaction between the conduction electrons. We have used the same notation for $\Sigma(\omega)$, $\gamma(\omega)$, and $\Gamma_{\uparrow\downarrow}(k\omega,k'\omega')$ as Ref. (43). Equations (2.7)-(2.12) are quite general and are formally similar to equations found in standard textbooks. To obtain results uniquely applicable to the rare-earth alloys we must derive expressions for Σ, γ, and Γ.

1. The self-energy

The self-energy $\Sigma(\omega)$ shown diagrammatically in Fig. 14 is given by

$$\Sigma(\omega) = \left(\frac{I}{2}\right)^2 T \sum_{\omega'} \sum_{k'} G_{k'}(\omega)\chi(k - k',\omega - \omega') \tag{2.13}$$

where the spin fluctuation propagator $\chi(q,\omega)$ is the dynamical susceptibility of the localized spin system. $\Sigma(\omega)$ is the self-energy associated with the second order process in the exchange interaction I in which an electron emits, then reabsorbs a spin fluctuation (or paramagnon). After some manipulations (Appendix C) Eq. (2.13) reduces to

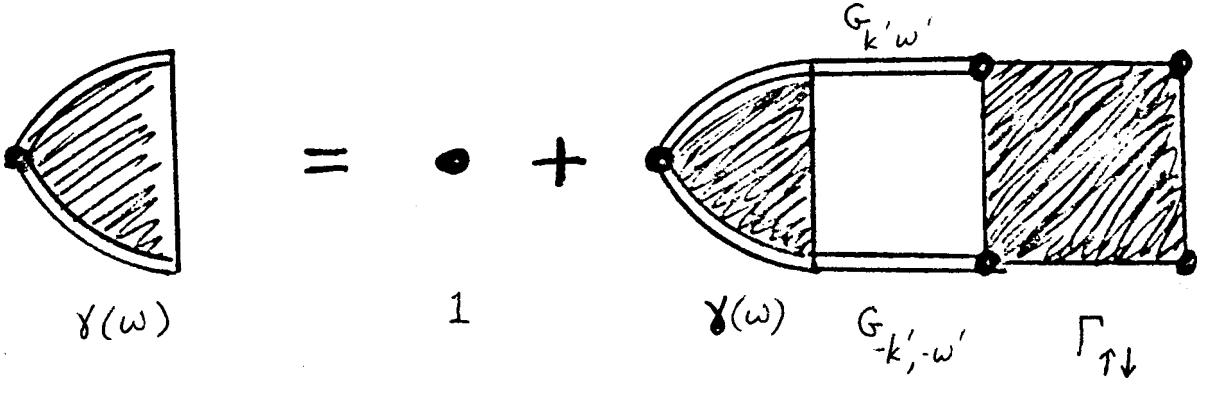

Figure 13. Diagrammatic representation of Eq. (2.12). The quantity on the left is the full two-electron vertex. The square on the far right depicts the four-point vertex which will be discussed later

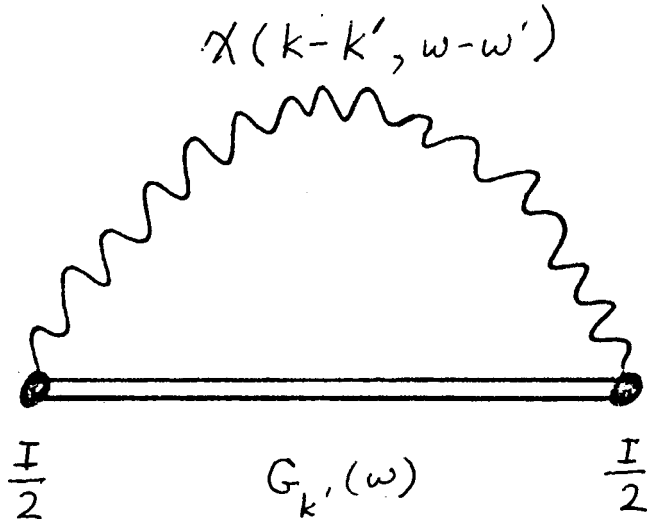

Figure 14. Self energy involving paramagnon exchange. The squiggly line represents a paramagnon propagator and the dots represent the coupling constant I

$$\Sigma(\omega) = -iN(0)\left(\frac{I}{2}\right)^2 \omega \sum_{\omega''} \frac{\theta(|\omega| - |\omega''|)\pi T}{|\omega|} \bar{\chi}(|k_F - k|,\omega'') \qquad (2.14)$$

$$\bar{\chi}(q,\omega'') = \int \frac{d\Omega_q}{4\pi} \chi(q,\omega'') \qquad (2.15)$$

where $\omega'' \equiv 2\pi T\nu$, k_F is the Fermi wave vector and $\theta(x)$ is the step function. We have neglected the real part of $\Sigma(\omega)$.

2. The vertex part

The four point vertex shown schematically in Fig. 15 is given by

$$\Gamma_{\uparrow\downarrow}(k\omega,k'\omega') = -\left(\frac{I}{2}\right)^2 \chi(k - k',\omega - \omega') \quad . \qquad (2.16)$$

The effective interaction between conduction electrons described by this expression is attractive, second order in the exchange integral I, and mediated by spin fluctuations. This interaction is similar to the phonon mediated interaction that induces the attractive force between conduction electrons responsible for superconductivity. In what follows we call the contribution from $\omega = \omega'$ in Eqs. (2.13) and (2.16) the elastic channel, and from $\omega \neq \omega'$ the inelastic channel. Much of our attention in this chapter will be focused on the elastic channel.

3. The dynamical susceptibility

The model we use to describe the dynamics of the spin system starts with the assumption that the static spin susceptibility (44) of the sample is of the Curie-Weiss form:

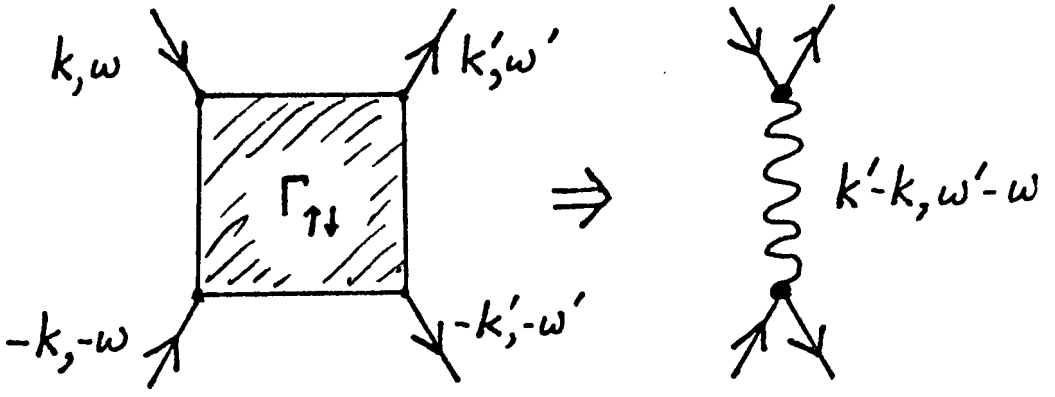

Figure 15. The four point vertex is replaced by simple paramagnon exchange. External Green's function lines have been included in this diagram to show how they couple to the vertex and to the paramagnon propagator

$$\chi = \langle \vec{S}_i \cdot \vec{S}_i \rangle = \frac{S(S+1)\lambda}{T - T_M} \tag{2.17}$$

where λ is a proportionality constant with units of energy, and T_M is the magnetic transition temperature. When strains are present in the spin system it is further assumed that the free energy functional acquires the form:

$$F = \lambda \int d^3\vec{r} \left(\frac{1}{2} Q \vec{S}^2(\vec{r}) + \frac{1}{2} A[\vec{\nabla}\vec{S}(\vec{r})]^2 \right) \quad . \tag{2.18}$$

Stability requires that Q and A be positive above T_M. In order that $S = \chi H$ when H is uniform, Q must be described by

$$Q = 1/\chi \quad . \tag{2.19}$$

A is a parameter measuring the stiffness of the spin system. We will ignore the possible dependence of A on T, λ, and S, and neglect terms higher order in S.

It proves useful to define Fourier transforms of the magnetization $\vec{S}$:

$$\vec{S}(\vec{r}) = \frac{1}{V} \sum_q \vec{S}(\vec{q}) \exp(-i\vec{q} \cdot \vec{r}) \quad . \tag{2.20}$$

The free energy can then be written as

$$F = \frac{\lambda}{V} \sum_q \frac{1}{2} (Q + Aq^2) \vec{S}(\vec{q}) \cdot \vec{S}(-\vec{q}) \quad . \tag{2.21}$$

We can find the thermal expectation value of particular magnetization-magnetization correlation functions by knowing that classically each q degree of freedom contributes $\frac{1}{2}(k_B)T$ to the total free energy.

$$F = \sum_{q} \frac{1}{2} T \tag{2.22}$$

but

$$F = \frac{\lambda}{V} \sum_{q} \frac{1}{2} (Q + Aq^2) \langle \vec{S}(\vec{q}) \cdot \vec{S}(-\vec{q}) \rangle \quad . \tag{2.23}$$

Therefore

$$\chi(q) = \langle \vec{S}(\vec{q}) \cdot \vec{S}(-\vec{q}) \rangle = \frac{VT}{\lambda(Q + Aq^2)} \tag{2.24a}$$

$$= \frac{S(S + 1)T}{T - T_M + \frac{S(S + 1)T\lambda}{V} Aq^2} \tag{2.24b}$$

$$= \frac{S(S + 1)T}{T - T_M + (aq)^2} \tag{2.24c}$$

where

$$a^2 = \frac{S(S + 1)T\lambda A}{V} \quad . \tag{2.25}$$

We insert dynamical effects into our expression for the spin-spin correlation function by assuming that the self-correlation relaxes exponentially in time as described by deGennes (45,46):

$$\langle \vec{S}(\vec{q},0) \cdot \vec{S}(-q,t) \rangle = \langle S(\vec{q}) \cdot S(-q) \rangle \exp(-\Lambda q^2 t) \quad . \tag{2.26}$$

The diffusion coefficient Λ is in general a function of the spin-spin coupling constants (46,47). We choose to treat it as an independent parameter. Fourier transforming Eq. (2.26) leaves us with

$$\int \frac{dt}{2\pi} \exp(-i\omega t)\langle \vec{S}(\vec{q},0)\cdot\vec{S}(-\vec{q},t)\rangle \equiv \chi(\vec{q},\omega) = \langle \vec{S}(\vec{q})\cdot\vec{S}(-\vec{q})\rangle \frac{\Lambda q^2}{\pi(\omega^2+\Lambda^2 q^4)} . \quad (2.27)$$

In principle we'd expect T_M, a, and Λ to be functions of $\mathcal{J}$, but in practice we take them to be free phenomenological parameters.

4. The phase diagram

An AG type of expression for the superconducting transition temperature can be derived provided the characteristic frequencies of the spin system described in Eq. (2.27) are much smaller than T_c (e.g., $\Lambda q^2 << |\omega|$). If the characteristic frequencies of the spin system are small, all scattering processes from the spins should be essentially elastic. In Appendix D we show that if we neglect the inelastic scattering channel in Eq. (2.13) we can derive the following expression for the self energy:

$$\Sigma(\omega) = \frac{-i}{2\tau(T)} \operatorname{sgn} \omega \quad (2.28)$$

where

$$\frac{1}{\tau(T)} = \frac{Tf(T)}{\tau_{AG}} \quad (2.29)$$

$$\frac{1}{\tau_{AG}} = 2\pi N(0) \left(\frac{I}{2}\right)^2 S(S+1) \quad (2.30)$$

and

$$f(T) = \frac{1}{(2ak_F)^2} \ln\left[\frac{T - T_M + (2ak_F)^2}{T - T_M}\right] \quad (2.31)$$

where a^2 is given by Eq. (2.25).

We comment that $(2ak_F)^2$ has units of energy. Our theory differs from the AG theory (41) in that in our theory the relaxation time (i.e., the pair-breaking parameter) is temperature dependent whereas in the AG theory it is constant.

If we neglect the inelastic scattering channel from the self-energy, we must also neglect it from the vertex correction in Eq. (2.16). We then have

$$\Gamma_{\uparrow\downarrow}(k\omega,k'\omega') = -\left(\frac{I}{2}\right)^2 \chi(k-k',\omega-\omega')\delta_{\omega,\omega'} \quad . \tag{2.32}$$

Substituting Eqs. (2.10), (2.11), (2.28), and (2.32) into Eq. (2.12) leads to (see Appendix K):

$$\frac{1}{gN(0)} = \sum_{\nu\geq 0} \frac{1}{\nu + \frac{1}{2} + \rho_c} \quad . \tag{2.33}$$

Sums like the one in Eq. (2.33) are formally divergent, but can be made convergent by properly introducing a cutoff at $\omega_\nu = \omega_D$. In Appendix E we show that Eq. (2.33) can be written as

$$-\ln\frac{T_c}{T_{c0}} = \psi\left(\frac{1}{2} + \rho_c\right) - \psi\left(\frac{1}{2}\right) \tag{2.34}$$

where $T_{c0} = 1.13\ \omega_D \exp(-1/gN(0))$ is the critical tempertaure when $I = 0$, ψ is the digamma function, and $\rho_c = 1/(2\pi T_c \tau(T_c))$. We will encounter formally divergent sums like the one in Eq. (2.33) several more times in this thesis. In each case the cutoff procedure described in Appendix E must be used.

There are two temperatures which give solutions to Eq. (2.34): an upper critical temperature, T_{c1}, and a lower one, T_{c2}. When $\rho_{c1} \equiv 1/(2\pi T_{c1}\tau(T_{c1})) << 1$ and $T_{c0} - T_{c1} << T_{c0}$, T_{c1} is explicitly given by

$$T_{c1} - T_{c0} = -\frac{\pi}{4} \frac{1}{\tau(T_{c0})} \quad . \tag{2.35}$$

If $T_M << T_{c0}$, we may rewrite Eq. (2.35) as

$$\frac{T_{c1}}{T_{c0}} = 1 - \frac{\pi}{4} \cdot \frac{1}{\tau_{AG}(2ak_f)^2} \ln\left[\frac{T_{c0} + (2ak_f)^2}{T_{c0}}\right] - \frac{\pi}{4} \cdot \frac{1}{\tau_{AG}[T_{c0} + (2ak_f)^2]} \cdot \left(\frac{T_M}{T_{c0}}\right) \quad . \tag{2.36}$$

The second solution of Eq. (2.34), T_{c2}, is typically very near T_M, and cannot in general be specified analytically. The phase diagram showing T_{c1} and T_{c2} versus T_M for different values of the coupling constant I is depicted in Fig. 16. We observe that there always exists a narrow region between the superconducting state and the magnetically ordered state in which the system is normal and paramagnetic. In other words the system always exhibits a reentrance phenomenon. There is no region where the two long-range orders coexist.

C. The Upper Critical Field

The starting point in a calculation of the upper critical field is the field dependent nonlocal linearized Gor'kov equation (34) described in Chapter I:

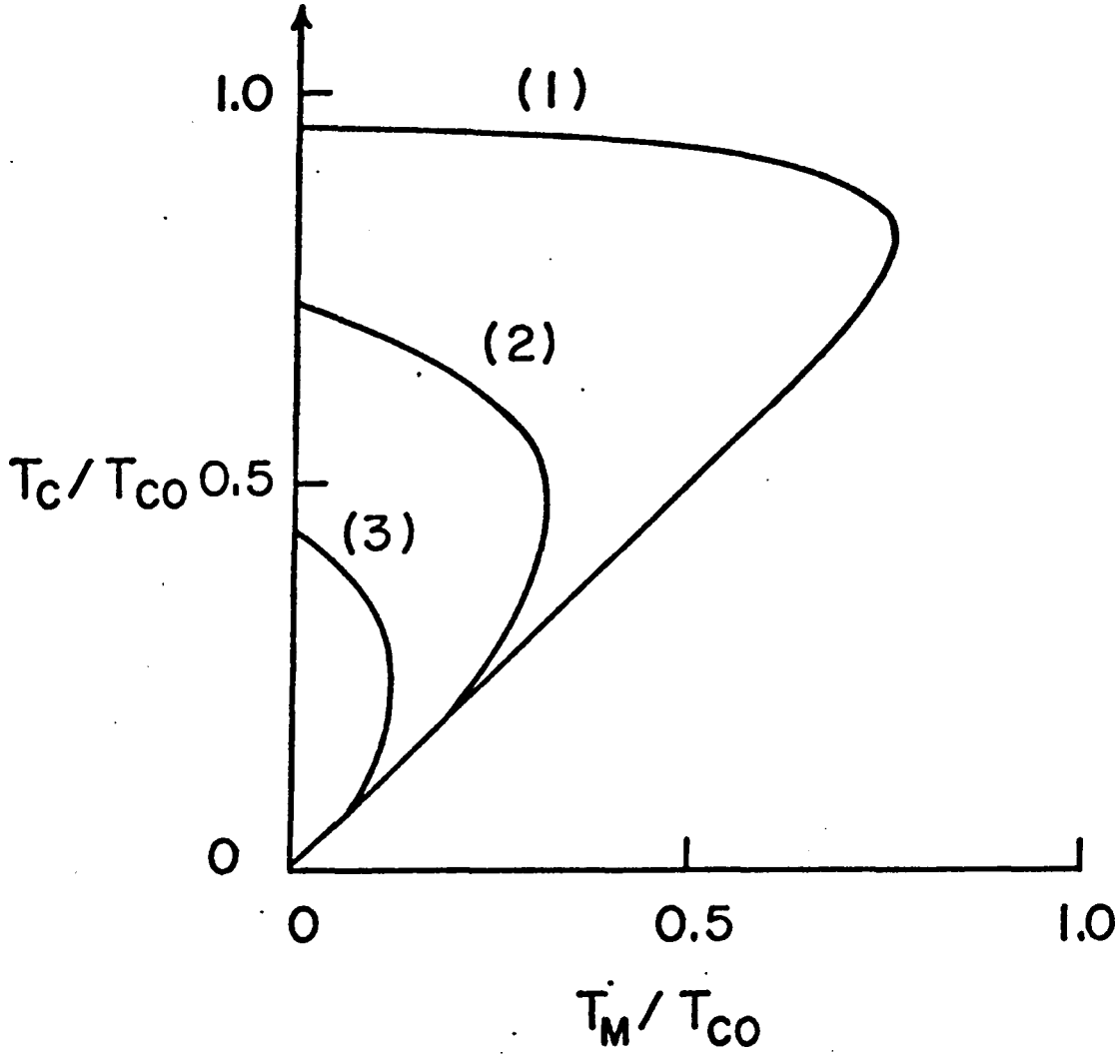

Figure 16. Phase diagram. $(2ak_f)^2/T_{c0} = 0.5$ (1) $N(0)(\frac{I}{2})^2(g_J-1)^2 \frac{1}{3} \cdot J(J+1)/T_{c0} = 0.01$; (2) 0.07; (3) 0.15. A sample is superconducting inside of (to the left of) its curve

$$\Delta(x) = gT \sum_{\nu} \int dx_1 Q_{\uparrow\downarrow}(x_1 - x;\omega_\nu)\, e^{2ie \int_x^{x_1} dsA(s)}\, \Delta(x_1) \tag{2.37}$$

$$Q_{\uparrow\downarrow}(x,\omega_\nu) = \langle G^n_{\downarrow}(x,\omega_\nu) G^n_{\uparrow}(x,-\omega_\nu)\rangle_{imp} \tag{2.38}$$

The expectation value $\langle \ldots \rangle_{imp}$ is an average over impurities (see Appendix A), and $G^n_\sigma(x,\omega_\nu)$ is the normal state Green's function:

$$G^n_\sigma(x,\omega_\nu) = -\frac{m}{2\pi|x|} \exp\left\{ ik^\sigma_F |x| \operatorname{sgn}\, \omega_\nu - \frac{|\tilde{\omega}_\nu|}{v^\sigma_F}\,|x| \right\} \tag{2.39}$$

$$\tilde{\omega}_\nu = \omega_\nu + \frac{1}{2}\left(\frac{1}{\tau(T)} + \frac{1}{\tau_0} \right) \operatorname{sgn}\, \omega_\nu \tag{2.40}$$

$$\frac{1}{\tau_0} = 2\pi N(0)\, n|U|^2 \tag{2.41}$$

$$k^\sigma_F = k_F - \frac{\sigma h}{v^\sigma_F} \quad . \tag{2.42}$$

Here, m is the electron mass, τ_0 is the relaxation time associated with scattering from nonmagnetic impurities, n is the concentration of nonmagnetic impurities, U is the scattering potential, and v^σ_f is the Fermi velocity of the up or down spin band. The internal molecular field h, acting on the conduction electrons, consists of a term expressing the interaction of the conduction electrons with the local moments and the Pauli paramagnetic term:

$$h = \frac{1}{N_0 g_J \mu_B} I\, \chi_0(T) H + \mu_B B \tag{2.43}$$

where $\chi_0(T)$ is the uniform bulk susceptibility given by $\chi_0(T) = (g_J\mu_B)^2 N_0/T \left\langle \vec{J}_q \cdot \vec{J}_{-q} \right\rangle\Big|_{q=0}$, and N_0 is the number of local spins per unit volume. We have adopted the semiclassical phase approximation for the orbital motion of the conduction electrons in an external magnetic field $\vec{H}$ ($\vec{A}$ is the vector potential) and have continued to neglect the inelastic scattering channel.

By applying the ladder approximation (Appendix F) to the vertex in $Q_{\uparrow\downarrow}(x,\omega_\nu)$ and by considering the dirty limit ($1/\tau_0 >> T_c$), we obtain the standard (48) pair-breaking equation from which we can determine H_{c2}:

$$\ln \frac{T}{T_{c0}} + \mathrm{Re}\ \psi\left(\frac{1}{2} + \frac{1}{2\pi T\tau(T)} + \frac{ih}{2\pi T} + \frac{DeB}{2\pi T} \right) - \psi\left(\frac{1}{2} \right) = 0 \quad . \qquad (2.44)$$

The diffusion constant $D \equiv \frac{1}{3}\tau_0 v_f^2$ is a measure of the dirtiness of samples. It is easy to check that in the limit $H_{c2} \to 0$ Eq. (2.44) reduces to Eq. (2.34). Notice that because the induced magnetization in the molecular field is linear in I, H_{c2} depends on the sign of I.

We consider two limiting cases. Near T_{c1} the upper critical field and the spin susceptibility are small so we may expand Eq. (2.44) in terms of H_{c2}. We obtain

$$H_{c2} = \frac{2\pi T_{c1}}{De\psi^{(1)}(\frac{1}{2} + \rho_{c1})}\left[1 - \frac{T_{c1}|f'(T_{c1})|}{2\pi\tau_{AG}}\psi^{(1)}(\tfrac{1}{2} + \rho_{c1}) \right](1 - \frac{T}{T_{c1}}) \ . \qquad (2.45)$$

If $T_{c2} << T_{c0}$, we can use the asymptotic expansion for large arguments of the digamma function. The result is

$$H_{c2} = \frac{(T - T_{c2})2\pi T_{c0}}{|I|g_J\mu_B J(J+1)/3} \cdot \sqrt{\left(\frac{1}{4e^\gamma}\right)^2 - \left(\frac{1}{2\pi T_{c0}\tau(T_{c2})}\right)^2} \qquad (2.46)$$

where γ is Euler's constant. Note that H_{c2} is proportional to $|I|^{-1}$ near T_{c2}. Numerical results for all temperatures are shown in Figs. 17-19.

It is not hard to include the effect of spin-orbit scattering which becomes important in high field type II superconductors (36). We define the relaxation time τ_{so} due to the spin-orbit scattering by (48)

$$\frac{1}{\tau_{so}} = \frac{1}{6} n_{so} N(0) \int d\Omega |v_{so}|^2 \sin^2\theta \tag{2.47}$$

where v_{so} is the interaction strength and n_{so} is the concentration of scattering centers. The resulting equation which determines H_{c2} is nearly identical to Eq. (1.32) derived by WHH (36), and is given by

$$\ln \frac{T}{T_{c0}} + \frac{1}{2}\left[\left(1 + \frac{b}{\sqrt{b^2 - h^2}}\right)\psi(\tfrac{1}{2} + \rho_-) + \left(1 - \frac{b}{\sqrt{b^2 - h^2}}\right)\psi(\tfrac{1}{2} + \rho_+)\right] - \psi(\tfrac{1}{2}) = 0 \tag{2.48}$$

where $b = 1/\tau_{so}$, and

$$\rho_\pm = \frac{1}{2\pi T}\left(\frac{1}{\tau(T)} + \frac{1}{\tau so} + DeB \pm \sqrt{b^2 - h^2}\right) . \tag{2.49}$$

Numerical results are shown in Fig. 20.

In the strong spin-orbit scattering case Eq. (2.48) reduces to

$$\ln \frac{T}{T_{c0}} + \psi(\tfrac{1}{2} + \rho(T) + \frac{DeB}{2\pi T} + \frac{h^2}{4\pi T \tau_{so}}) - \psi(\tfrac{1}{2}) = 0 \tag{2.50}$$

where $\rho(T) = 1/(2\pi T\tau(T))$.

It should be noted that the molecular field acting on the conduction electrons is linear in I. If the exchange integral is negative, the spin

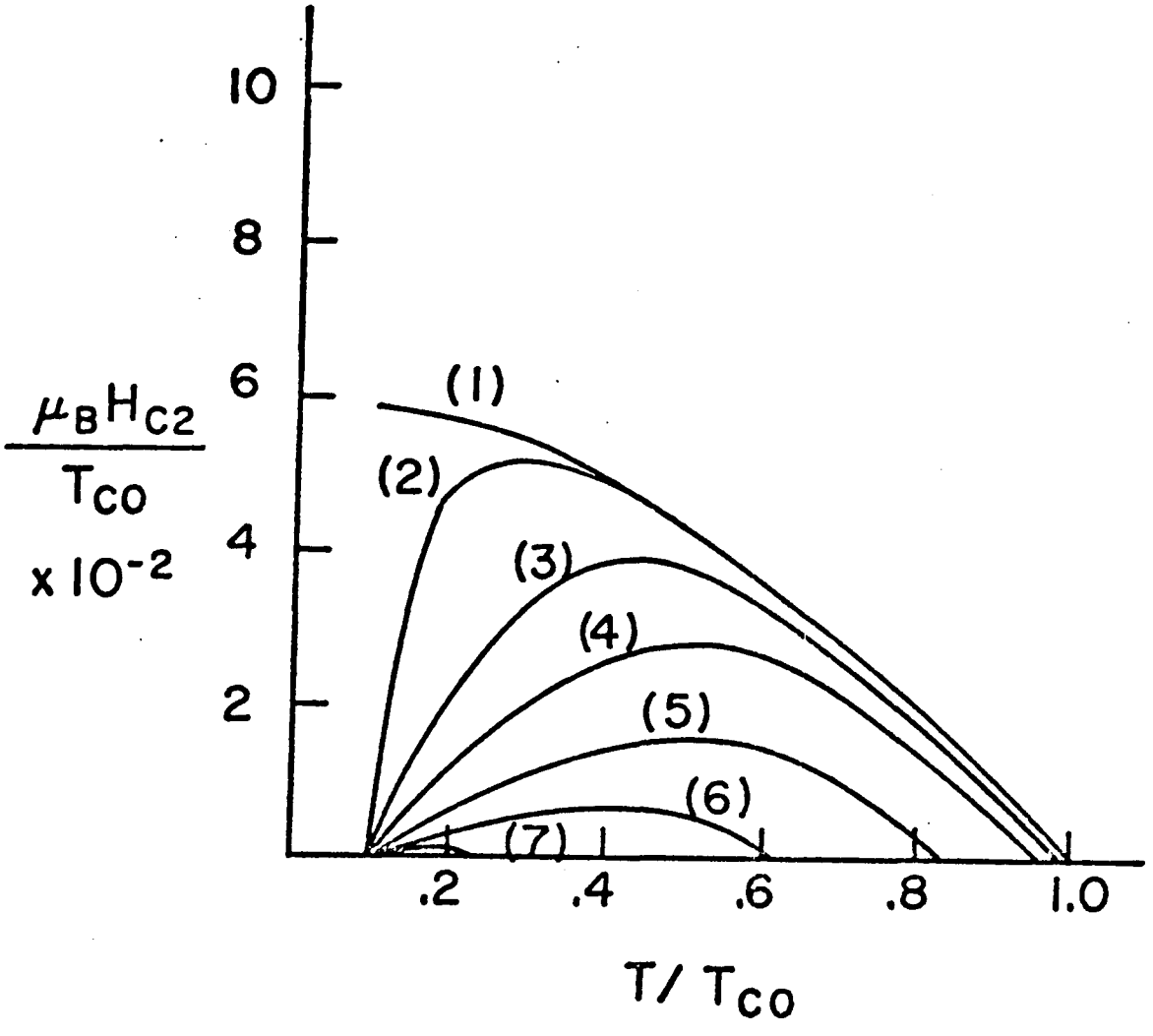

Figure 17. Upper critical field. Unless otherwise stated, the following parameters are used in Figs. 17-20. $I/T_{c0} = 0.5$, $T_M/T_{c0} = 0.1$, $De/2\pi\mu_B = 2.0$, $(2ak_F)^2/T_{c0} = 0.3$, $g_J = 2.0$, $J = 3.0$, $N_0 = 2 \times 10^{21}$ spins/cm^3, $N(0) = 1(eV)^{-1}$, $1/(6\pi\tau_{so}T_{c0}) = 0$. In Fig. 17 only, I/T_{c0} = (1) 0.0, (2) 0.1, (3) 0.5, (4) 1.0, (5) 2.0, (6) 3.0, (7) 4.0

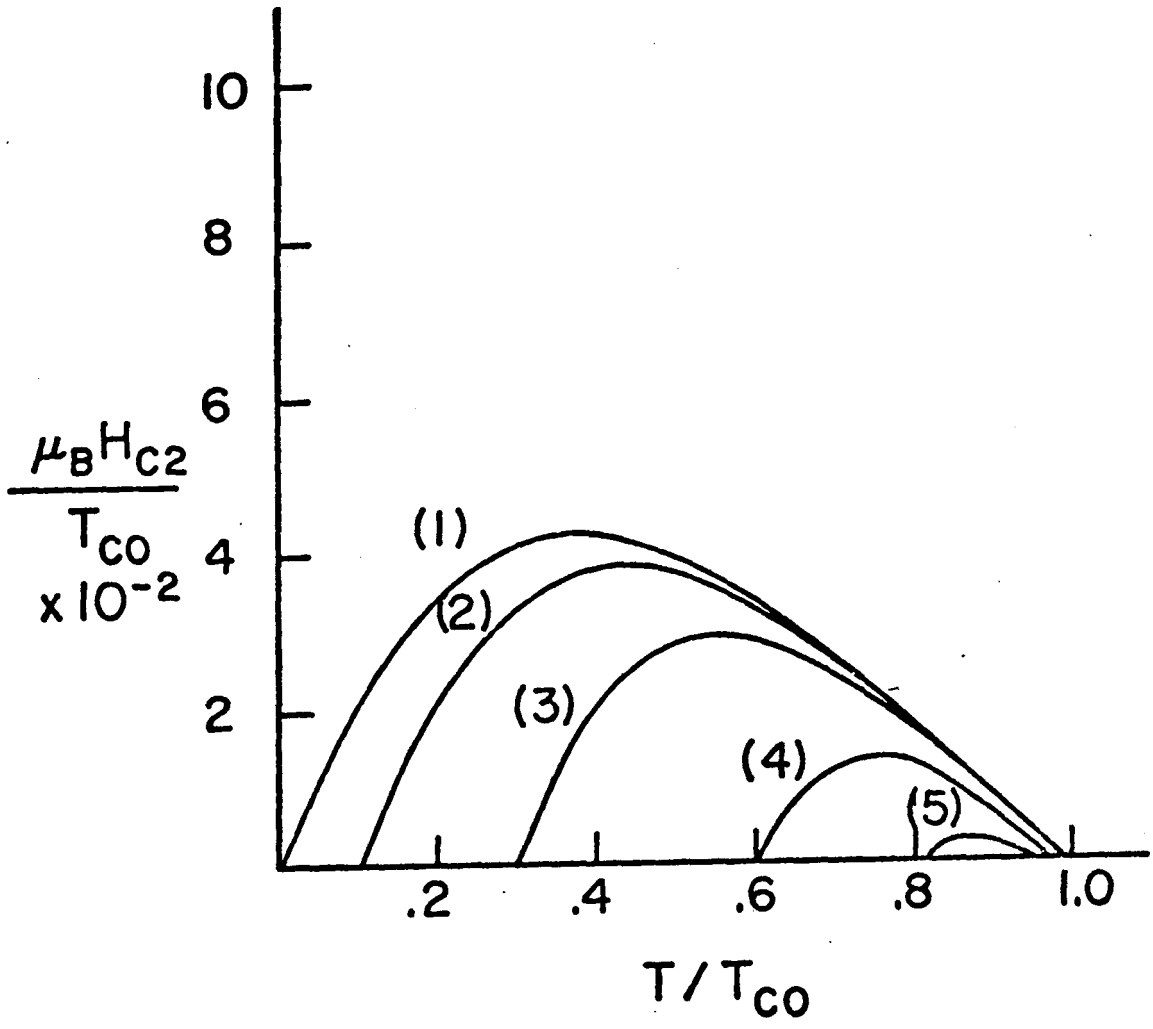

Figure 18. Upper critical field. The same parameters are used here as were used in Fig. 17 except: T_M/T_{c0} = (1) 0.0, (2) 0.1, (3) 0.3, (4) 0.6, (5) 0.8

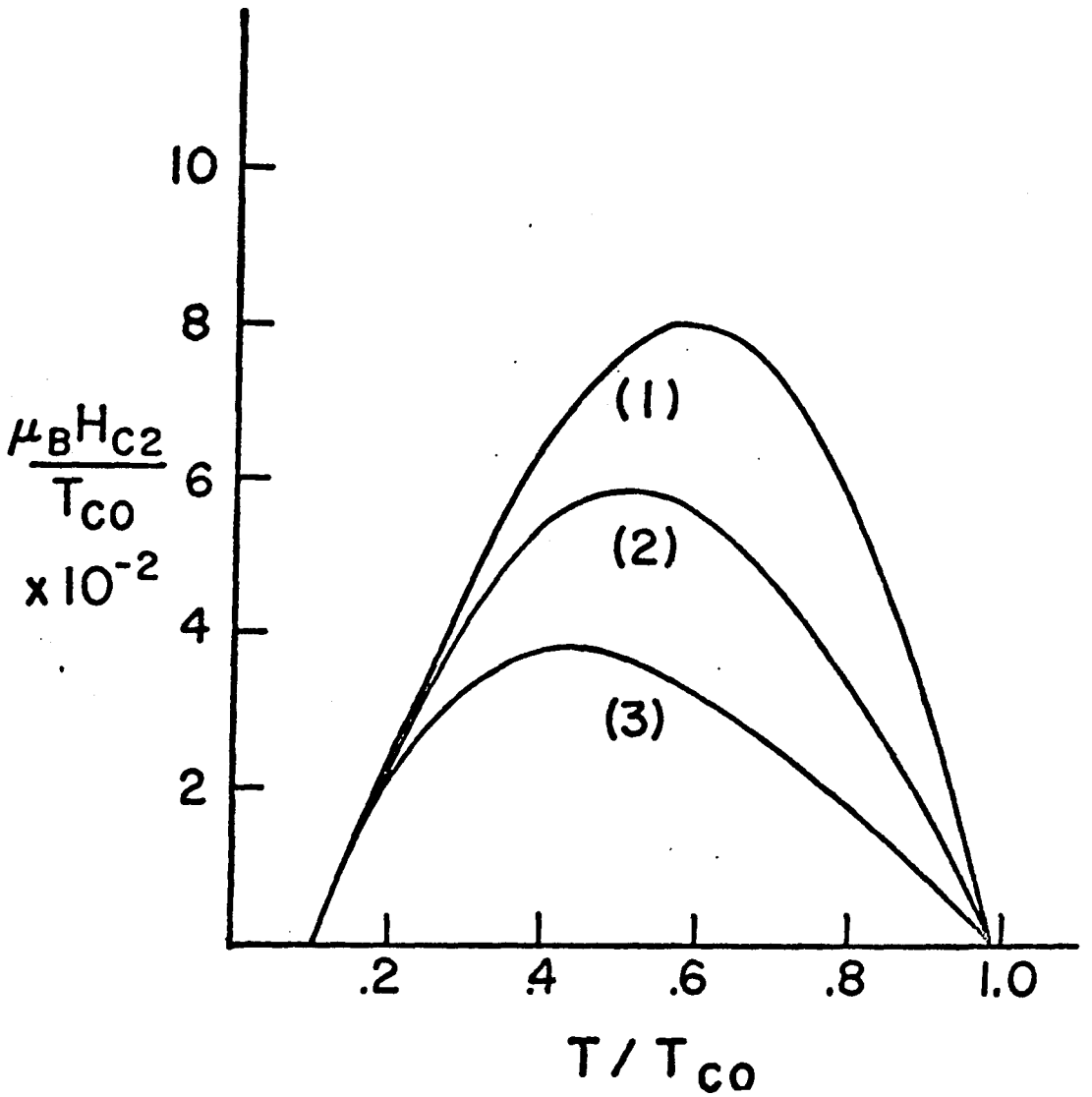

Figure 19. Upper critical field. The same parameters are used here as were used in Fig. 17 except: $De/2\pi\mu_B$ = (1) 0.5, (2) 1.0, (3) 2.0

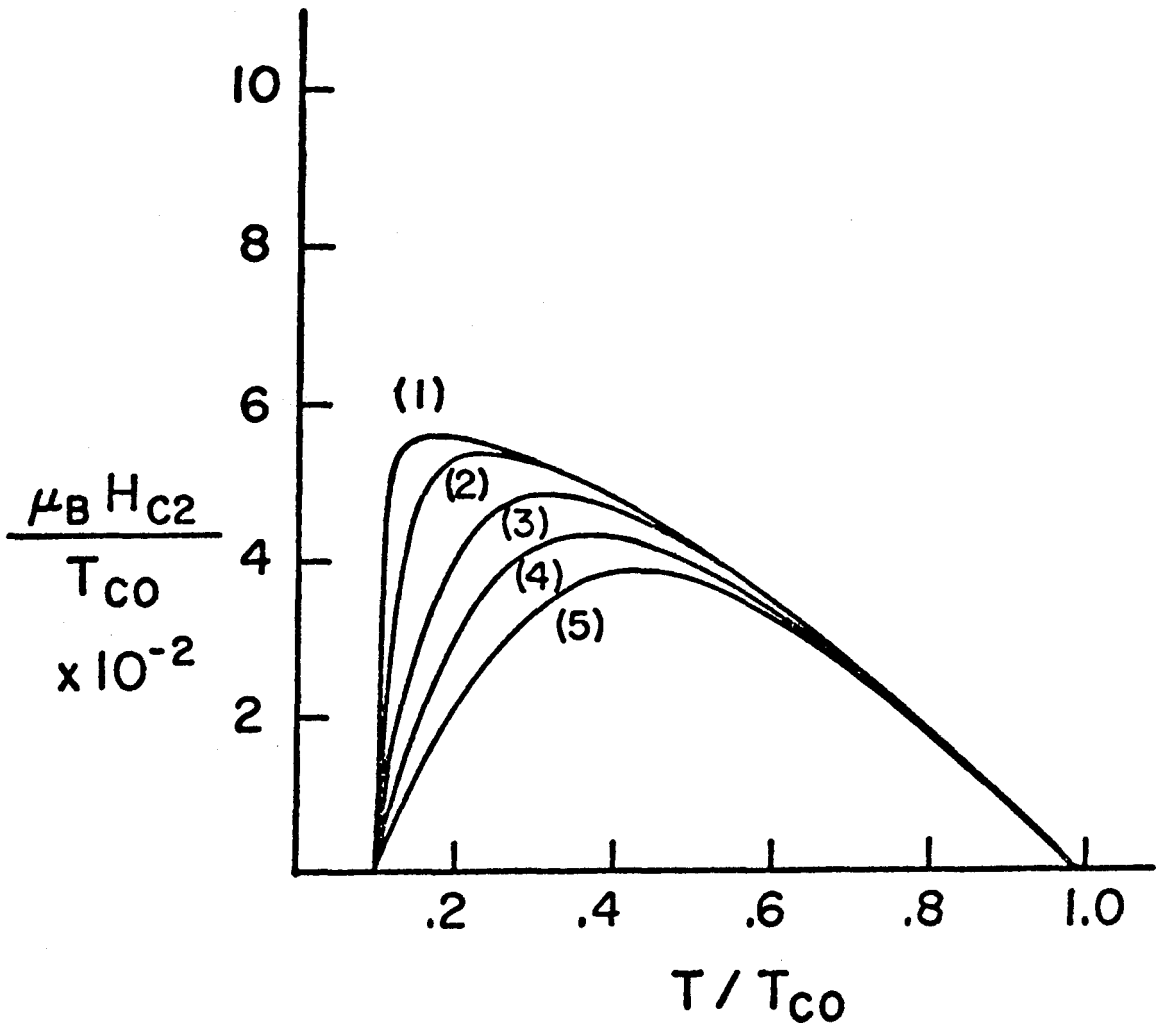

Figure 20. Upper critical field. The same parameters are used here as were used in Fig. 17 except: $1/(6\pi\tau_{so}T_{c0})$ = (1) 100, (2) 10, (3) 1.0, (4) 0.2, (5) 0.0

polarization counteracts the effect of Pauli paramagnetism thereby increasing the upper critical field. This is the Jaccarino-Peter effect (49). On the other hand, the pair-breaking parameter $\rho(T)$ is proportional to $I^2N(0)$ and therefore tends to suppress superconductivity regardless of the sign of I.

The results shown in Figs. 17-20 enable us to make several observations. We note (Fig. 17) that as the coupling I between the local moments and the conduction electrons increases, T_{c1} decreases, T_{c2} increases, and $H_{c2}(T)$ at all intermediate temperatures decreases. In short, the conduction electron-local moment interaction suppresses superconductivity. From Fig. 18 we see that as T_M approaches T_{c0}, the gaps between T_M and T_{c2} and between T_{c1} and T_{c0} grow in size, and $H_{c2}(T)$ between T_{c2} and T_{c1} becomes smaller. Figure 19 reveals that increasing the impurity scattering rate (i.e., making the samples dirtier) increases $H_{c2}(T)$ especially near T_{c1}, but doesn't affect either T_{c2} or T_{c1}. Figure 20 shows that increasing the spin-orbit scattering rate increases $H_{c2}(T)$ especially near T_{c2}, but doesn't cause shifts in either T_{c2} or T_{c1}.

D. Pseudo-Ternary Rare-Earth Compounds

Upper critical fields have been measured on the pseudo-ternary rare-earth rhodium borides $Lu_{1-x}Ho_xRh_4B_4$ (50), $Y_{1-x}Gd_xRh_4B_4$ (51), $Er_{1-x}Gd_xRh_4B_4$ (51), and $Er_{1-x}Ho_xRh_4B_4$ (52). The results of these measurements are qualitatively similar to the results of measurements made on pure ternary compounds. Because of the abundance of materials that can

be made by varying x in the range $0 \leq x \leq 1$, a great deal of information can be gathered, and a great deal can be learned about the nature of the electron-local moment interactions in these materials.

Our theory can be extended to treat (53a) the pseudo-ternary compounds $A_{1-x}B_xRh_4B_4$ (A,B = rare-earth elements) by assuming the scattering from A and B atoms is independent. The relaxation time defined in Eq. (2.29) becomes:

$$\frac{1}{\tau_{tot}(T)} = \left(\frac{1-x}{\tau_A} + \frac{x}{\tau_B} \right) T f_x(T) = \frac{1}{\tau_A} \left\{ 1 - x \left(1 - \frac{\tau_A}{\tau_B} \right) \right\} T f_x(T) \qquad (2.51)$$

where

$$\frac{1}{\tau_i} = 2\pi N(0) \left(\frac{I_i}{2} \right)^2 (g_J^i - 1)^2 J_i(J_i + 1) \quad , \quad (i = A \text{ or } B) \qquad (2.52)$$

$$f_x(T) = \frac{1}{(2ak_f)^2} \ln \left[\frac{T - T_M(x) + (2ak_f)^2}{T - T_M(x)} \right] \quad . \qquad (2.53)$$

The total angular momentum and the Landé g-factor for the A(B) atom are $J_A(J_B)$ and $g_J^A(g_J^B)$ respectively. The ferromagnetic transition temperature is now a function of x. The total relaxation time $\tau_{tot}(T)$ consists of two terms, τ_A and τ_B, multiplied by an enhancement factor $f_x(T)$. We note that J_A or J_B may vanish when the respective A or B atom is nonmagnetic, such as is the case for Y (with no 4f electrons) and Lu (with a closed 4f shell).

In the case in which a nonmagnetic atom A is replaced by a rare-earth magnetic atom B, the initial depression of the transition

temperature near x = 0 is given by

$$\frac{1}{T_c}\left(\frac{dT_c}{dx}\right)_{x=0} = -\frac{\pi^2}{8} N(0) I_B^2 (g_J^B - 1)^2 J_B(J_B + 1) f_0(T_{c0}) \quad . \tag{2.54}$$

When both A and B are magnetic rare-earth atoms the change in the upper critical temperature T_{c1} near x = 0 is given by

$$\frac{1}{T_{c1}}\left(\frac{dT_{c1}}{dx}\right)_{x=0} = \frac{\pi^2}{8} N(0) I_A^2 (g_J^A - 1)^2 J_A(J_A + 1) f_0(T_{c1})\left(1 - \frac{\tau_A}{\tau_B}\right) \quad . \tag{2.55}$$

If I is the same for both rare-earth atoms, which is plausible since rare-earth atoms are considered to have similar physical and chemical properties (53b), Eq. (2.55) reduces to

$$\frac{1}{T_{c1}}\left(\frac{dT_{c1}}{dx}\right)_{x=0} = \frac{\pi^2}{8} N(0) I^2 (g_J^A - 1) J_A(J_A + 1) f_0(T_{c1}) \cdot \left(1 - \frac{(g_J^B - 1)^2 J_B(J_B + 1)}{(g_J^A - 1)^2 J_A(J_A + 1)}\right) \quad . \tag{2.56}$$

This equation shows that the sign of the initial change of T_{c1} with dilution is determined solely by the relative magnitude of the two deGennes factors, $(g_J - 1)^2 J(J + 1)$.

Consider for example $(Lu_{1-x}Ho_x)Rh_4B_4$ and $(Y_{1-x}Gd_x)Rh_4B_4$. If we use free-ion values for the deGennes factors, we obtain from Eq. (2.54):

$$\frac{-\frac{1}{T_{c0}}\left(\frac{dT_c}{dx}\right)_{x=0}^{(Y-Gd)}}{-\frac{1}{T_{c0}}\left(\frac{dT_c}{dx}\right)_{x=0}^{(Lu-Ho)}} = \frac{(g_J^{Gd}-1)^2 J_{Gd}(J_{Gd}+1)}{(g_J^{Ho}-1)^2 J_{Ho}(J_{Ho}+1)} = \frac{15.75}{4.50} \approx 3.5 \quad . \tag{2.57}$$

This agrees well with the experimental value (50,51) of 3.4 - 5.1. Similarly, for $(Er_{1-x}Gd_x)Rh_4B_4$ and $(Er_{1-x}Ho_x)Rh_4B_4$ we obtain

$$\frac{-\frac{1}{T_{c1}}\left(\frac{dT_{c1}}{dx}\right)_{x=0}^{(Er-Gd)}}{-\frac{1}{T_{c1}}\left(\frac{dT_{c1}}{dx}\right)_{x=0}^{(Er-Ho)}} = \frac{1-\frac{(g_J^{Gd}-1)^2 J_{Gd}(J_{Gd}+1)}{(g_J^{Er}-1)^2 J_{Er}(J_{Er}+1)}}{1-\frac{(g_J^{Ho}-1)^2 J_{Ho}(J_{Ho}+1)}{(g_J^{Er}-1)^2 J_{Er}(J_{Er}+1)}} \simeq 6.77 \quad , \tag{2.58}$$

which is of the same order as the experimental value (51,52) ($\sim$10). Other evidence supporting the conclusion that the rare-earth atoms in these compounds behave magnetically like free ions includes measurements made on the magnetic susceptibility (11) and the Mössbauer effect (54) of $ErRh_4B_4$. Neutron diffraction data (55), however, gives smaller values for the magnetic moments than are expected from free-ion theory.

We have fit experimental phase diagram data on four pseudo-ternary compounds: $(Lu_{1-x}Ho_x)$-, $(Er_{1-x}Ho_x)$-, $(Er_{1-x}Gd_x)$-, and $(Y_{1-x}Gd_x)$-Rh_4B_4 using the following assumptions: (1) The deGennes factor is given by its free-ion value. (2) The hypothetical transition temperature T_{c0} is 11.5°K for all compounds. (This value is used because $LuRh_4B_4$, which is a compound in which I = 0 (Lu has no magnetic moment), has T_c = 11.5°K.) (3) The exchange integral I and the density of states, N(0) (taken to

be 0.5/eV), are the same for all four compounds and remain constant under alloying. (4) The ferromagnetic transition temperature $T_M(x)$ is taken from the experimental data to be a linear function (56) of x.

With these assumptions, the only remaining parameters are I and $(2ak_F)^2$. We have taken $(2ak_F)^2/T_{c0} = 10.0$ for all phase diagrams, and determined I using Eq. (2.34) to fit the upper transition temperature of $ErRh_4B_4$ at 8.55°K. This gives $I \approx 318$°K. The upper transition temperature of $TmRh_4B_4$ can then be calculated using $(g_J^{Tm} - 1)^2 J_{Tm}(J_{Tm} + 1) = 1.17$. The predicted value of ∿10.05°K compares well with the experimental value (57) of ∿9.80°K. Results are shown in Figs. 21-24. Overall fitting is quite good. If we allow I for Gd to vary slightly with its environment we can obtain a better fit for $(Er_{1-x}Gd_x)Rh_4B_4$ and $(Y_{1-x}Gd_x)Rh_4B_4$ as shown in Figs. 21-24. This indicates that simple free-ion theory does not work as well for compounds which contain Gd.

1. The upper critical field

The upper critical field for pseudo-ternary compounds can be obtained by modifying the temperature dependent scattering time (i.e., Eq. (2.29) becomes Eq. (2.51)) and the internal molecular field defined in Eq. (2.43). The modified molecular field h is given by

$$h = \{(1 - x)\, g_J^A J_A(J_A + 1) + x\, g_J^B J_B(J_B + 1)\} \frac{IH}{T - T_M(x)} + \mu_B B \quad . \quad (2.59)$$

Each constituent moment, J_A and J_B, exerts a molecular field proportional to its concentration on the conduction electrons. In the strong spin-orbit scattering limit Eq. (2.48) reduces to

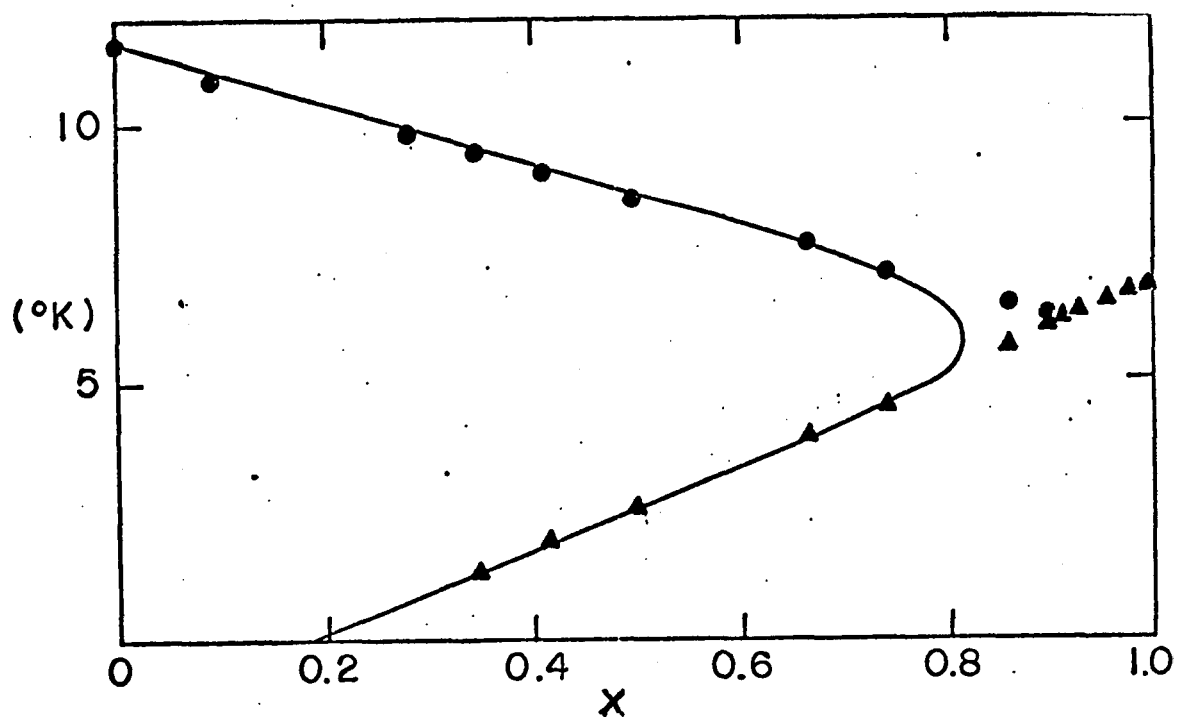

Figure 21. Phase diagram for $(Lu_{1-x}Ho_x)Rh_4B_4$. Unless otherwise stated, the following parameters will be used in Figs. 21-24: T_{c0} = 11.5°K, $(2ak_F)^2/T_{c0}$ = 10.0, $N(0)I^2/4T_{c0}$ = 0.094. The deGennes factors, $(g_J-1)^2J(J+1)$ =, Gd: 15.75, Ho: 4.60, Er: 2.55, Tm: 1.17, and Lu: 0. The experimentally determined upper critical temperatures and magnetic transition temperatures are labeled by circles and triangles respectively.

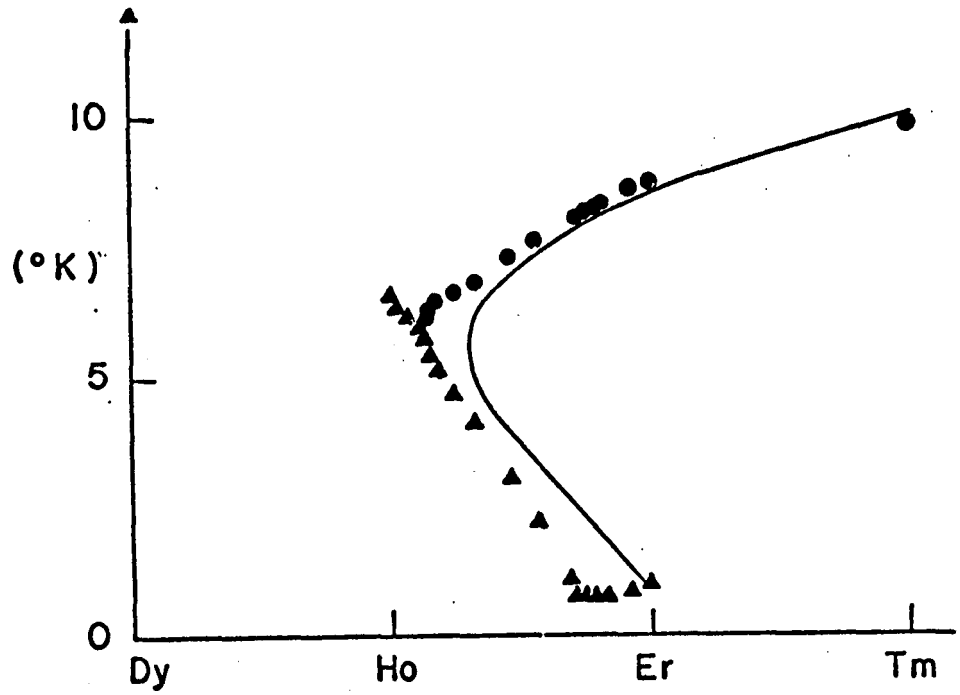

Figure 22. Phase diagram for $(Er_{1-x}Ho_x)Rh_4B_4$ and $(Er_{1-y}Tm_y)Rh_4B_4$

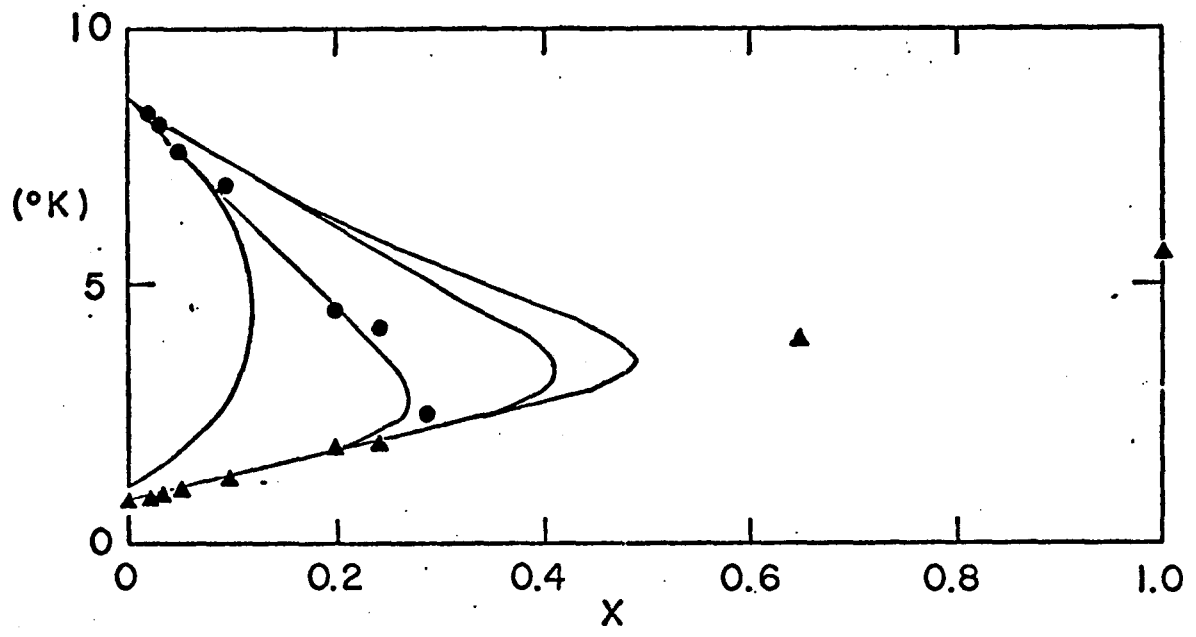

Figure 23. Phase diagram for $(Er_{1-x}Gd_x)Rh_4B_4$. $(2ak_F)^2/T_{c0}$ are respectively: (1) 100.0, 0.5222; (2) 10.0, 0.94; (3) 2.0, 0.038; (4) 0.01, 0.0176. The values of $N(0)I^2/4T_{c0}$ have been chosen to fix T_{c1} of pure $ErRh_4B_4$ at 8.55°K

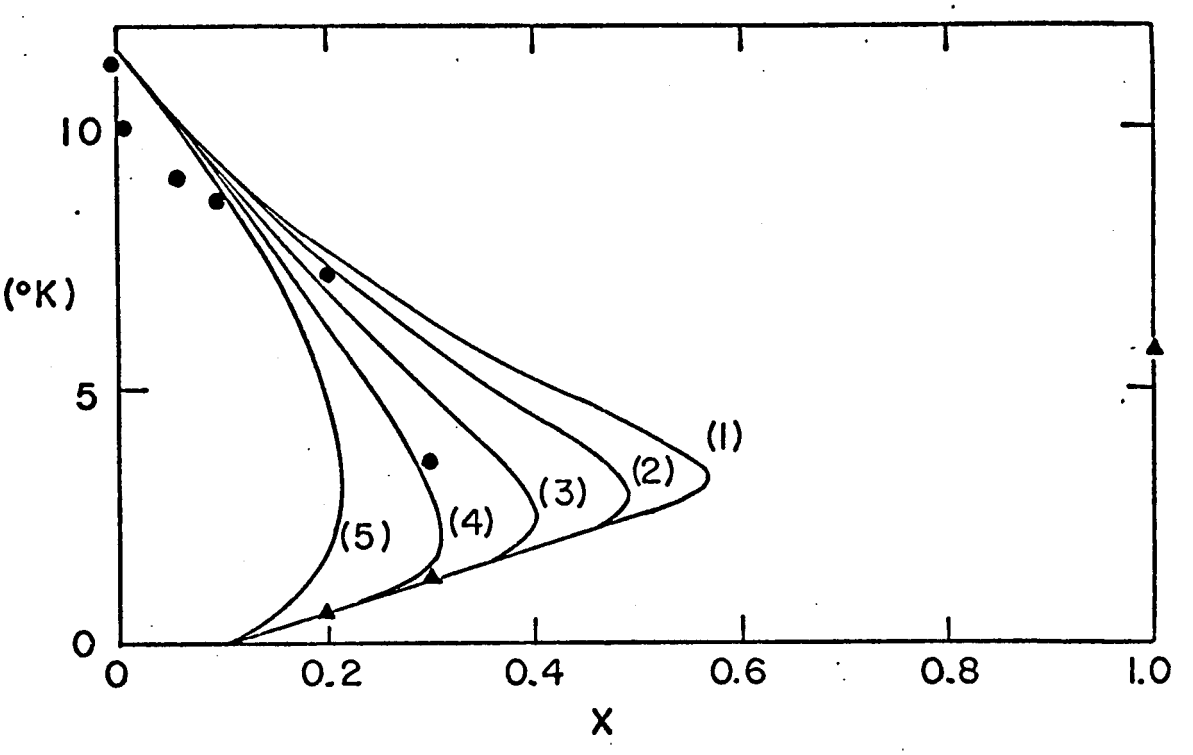

Figure 24. Phase diagram for $(Y_{1-x}Gd_x)Rh_4B_4$. Values of $(2ak_F)^2/T_{c0}$ and $N(0)I^2/4T_{c0}$ are respectively: (1) 100.0, 0.59; (2) 10.0, 0.115; (3) 2.0, 0.051; (4) 0.5, 0.035; (5) 0.01, 0.029. The values of $N(0)I^2/4T_{c0}$ have been chosen to fix the slope of T_{c1} vs. X at 25°K

$$\ln \frac{T}{T_{c0}} + \psi\left(\frac{1}{2} + \rho(T) + \frac{DeB}{2\pi T} + \frac{h^2}{4\pi T \tau_{so}}\right) - \psi\left(\frac{1}{2}\right) = 0 \quad . \tag{2.60}$$

where h is given by Eq. (2.59) and $\rho(T) = 1/(2\pi T\tau(T))$ with $\tau(T)$ given by Eq. (2.51). The spin-orbit scattering time τ_{so} is expected to be quite short for these rare-earth compounds. The diffusion constant D depends delicately on sample preparation and is related to the residual resistivity of the samples.

We have used Eq. (2.60) and the same set of parameters as in Fig. 23 to fit experimental data (51) on $Er_{1-x}Gd_xRh_4B_4$. The two additional parameters λ_{so} and D have been adjusted freely to give the best fits. We find $D \simeq 1.5$ and $1/2\pi\tau_{so}T_{c0} \simeq 1000$. Numerical results are shown in Figs. 25 and 26. While it is quite likely that D varies from sample to sample by $\sim$50% (to date, crystals of $Er_{1-x}Gd_xRh_4B_4$ are so small that resistivity ratios cannot be determined to better than 50%), we are unable to explain the extremely short spin-orbit scattering times and the large variations in τ_{so} from sample to sample.

Two major conclusions can be drawn from the results of this section. The first is that the rare-earth atoms in ternary and pseudo-ternary rare-earth compounds behave magnetically like free 3^+ ions. The second is that the coupling between rare-earth ions and the conduction electrons is weak and nearly independent of the atomic number of the ion. We also note that all rare-earth alloys made so far (i.e., the ones mentioned in this thesis) seem to be quite dirty and have very short spin-orbit scattering times.

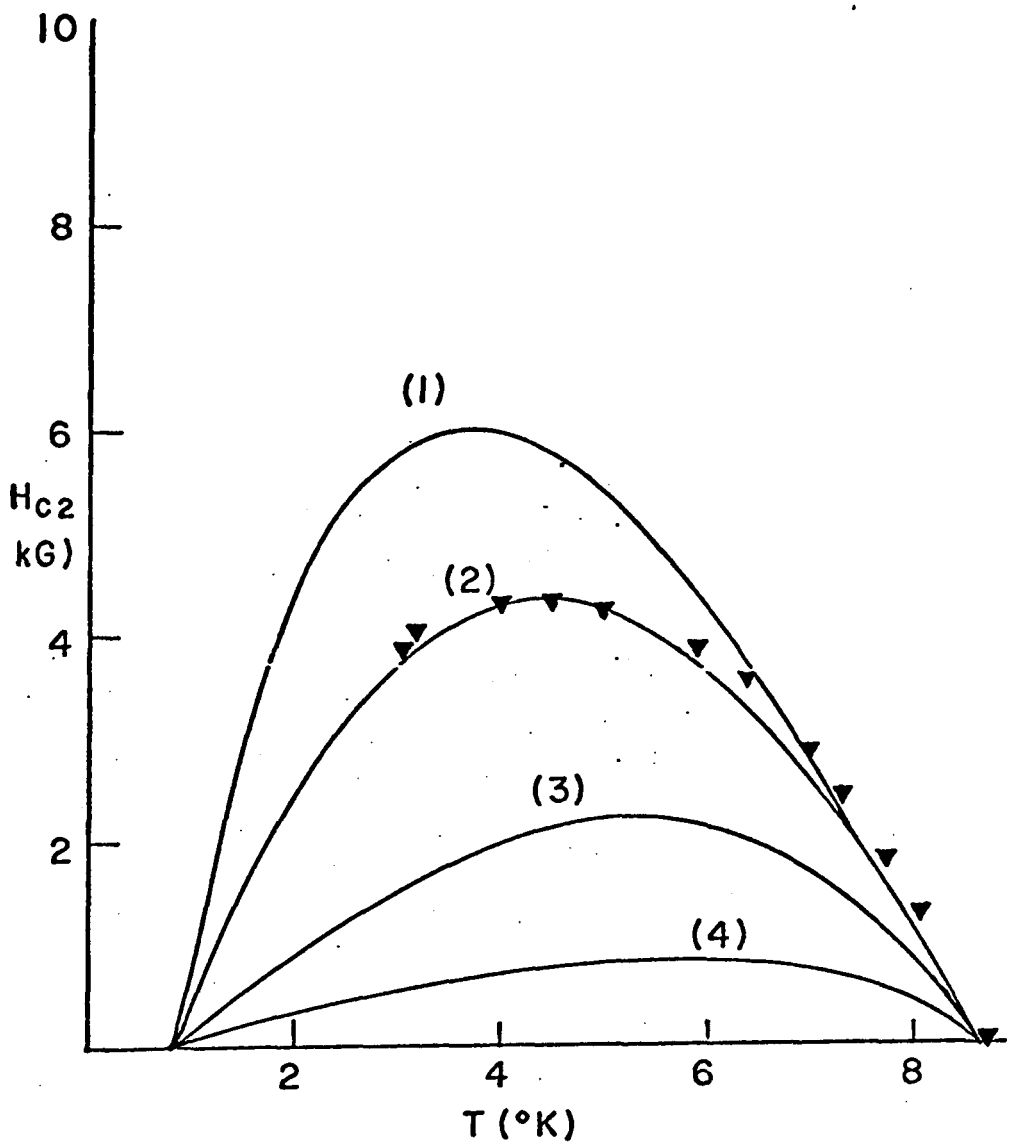

Figure 25. Upper critical field vs. temperature. The same parameters as used in Fig. 23 will be used in Figs. 25-26. The values of additional parameters used are: D = 1.35, $1/(2\pi T_{c0}\tau_{so})$ = (1) 10,000.0, (2) 1,000.0, (3) 100.0, (4) 10.0

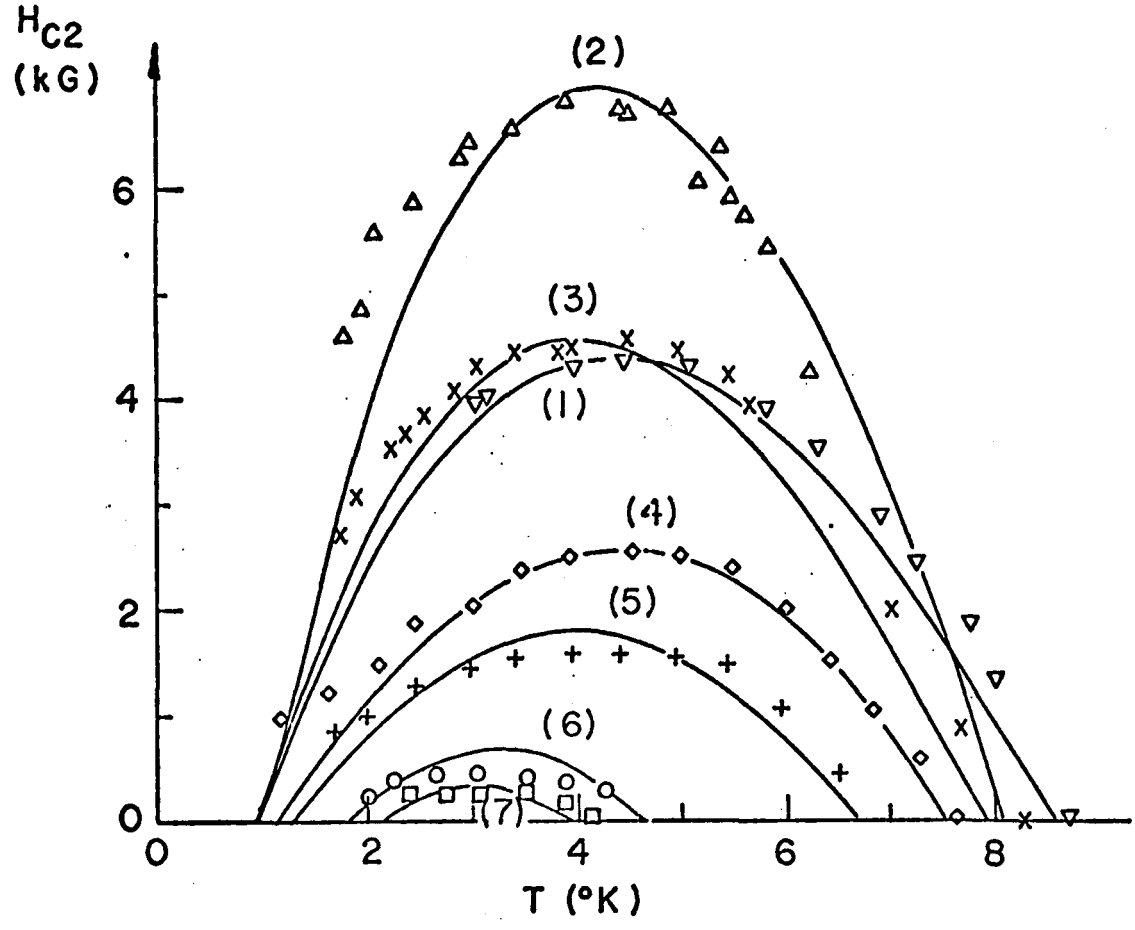

Figure 26. Upper critical field of $Er_{1-x}Gd_xRh_4B_4$ (51). x, D, and $1/(2\pi T_{c0}\tau_{so})$ are respectively: (1) 0.0, 1.35, 1,000.0; (2) 0.02, 0.8, 3,000.0; (3) 0.03, 1.3, 2,000.0; (4) 0.05, 1.4, 300.0; (5) 0.09, 2.0, 300.0; (6) 0.20, 2.0, 300.0; (7) 0.24, 2.0, 300.0

E. Inelastic Scattering

So far, we have considered only the effects of elastic electron-magnon-electron scattering on the superconducting properties of rare-earth compounds. We have neglected the inelastic scattering channel ($\omega \neq \omega'$) of the dynamical susceptibility defined in Eqs. (2.16), (2.24), and (2.27). In this section we consider how inelastic scattering (58) affects the superconducting state and the $H_{c2}(T)$ curve.

In order to calculate physical quantities dependent on the dynamical susceptibility, we must simplify its functional form without losing its characteristic features. The features we must retain are: (1) the dynamical susceptibility $\chi(q,\omega)$ has a singularity at $\omega = 0$ in the limit $q \to 0$ near the ferromagnetic transition temperature, and (2) in the region where $\Lambda q^2 >> |\omega|$, $\chi(q,\omega)$ is independent of ω. The following crude approximation for $\chi(q,\omega)$ retains these features:

$$\chi(q,\omega) = \chi(q)(\alpha + \beta\delta_{\omega,0}) \tag{2.61}$$

where $\chi(q)$ is given by Eq. (2.24c). We have introduced α and β as adjustable parameters. The case $\alpha = 0$, $\beta = 1$ corresponds to an AG (41) type theory. The case $\alpha = 1$, $\beta = 0$ corresponds to the Berk-Schrieffer (59) theory.

In sections B, C, and D we treated the case where the characteristic frequencies of the spin system were much smaller than T_c by neglecting the inelastic scattering channel in $\chi(q,\omega)$. In essence, we used Eq. (2.61) with $\alpha = 0$ and $\beta = 1$. If the characteristic frequencies of the spin system are much larger than T_c (e.g., $\Lambda q^2 >> |\omega|$), we may neglect

the frequency dependence in $\chi(q,\omega)$ by setting $\alpha = 1$ and $\beta = 0$. We then obtain

$$\Sigma(\omega) = \frac{1}{\tau(T)} \cdot \frac{-i\omega}{2\pi T} \tag{2.62}$$

and

$$\Gamma_{\uparrow\downarrow}(k\omega,k'\omega') = -\left(\frac{I}{2}\right)^2 \chi(k - k') \quad . \tag{2.63}$$

A Berk-Schrieffer (57) type of expression for T_c can be derived (see Appendix K):

$$\frac{1 + \rho_c}{gN(0) - \rho_c} = \sum_{\nu \geq 0}^{N} \frac{1}{\nu + \frac{1}{2}} \tag{2.64}$$

where $2\pi T(N + 1/2) = \omega_D$. In this expression the effective superconducting coupling, $gN(0)$, is shown to be weakened by the attractive, paramagnon mediated interaction. Furthermore, the inelastic paramagnon scattering causes the masses of the superconducting electrons to be renormalized. (Were there no mass renormalization, the numerator on the left would be replaced by unity.) This mass enhancement should have an effect on the electronic specific heat near T_M. If we neglect the mass enhancement factor, we obtain the same expression for T_c as Maekawa and Tachiki (42):

$$T_c = 1.14\ \omega_D \exp\left(\frac{-1}{gN(0) - \rho_c}\right) \tag{2.65}$$

where ω_D is the Debye frequency.

Equation (2.64) has two solutions, T_{c1} and T_{c2}. If $(T_{c0} - T_{c1})/T_{c0} \ll 1$, and $\rho_{c1} \ll 1$, the depression of T_c is given by

$$\frac{T_{c0} - T_{c1}}{T_{c0}} = \rho_{c1}\left(\frac{1}{[gN(0)]^2} + \frac{1}{gN(0)} \right) \quad . \tag{2.66}$$

Numerical solutions to Eq. (2.64) with and without mass renormalization are shown in Fig. 27.

If we leave α and β as free parameters, we can solve Eq. (2.12) using Eq. (2.61) to obtain (see Appendix K):

$$Q(T) = \frac{N(0)\Phi(T)}{1 + \alpha\rho\Phi(T)} \tag{2.67}$$

$$\Phi(T) = \sum_{\nu \geq 0} \frac{1}{(\nu + \frac{1}{2})(1 + \alpha\rho) + \beta\rho} \tag{2.68}$$

where convergence must be introduced in the ν sum as demonstrated in Appendix E. The superconducting transition temperatures are determined by $1 = gQ(T_c)$, which becomes

$$\frac{1 + \alpha\rho_c}{gN(0) - \alpha\rho_c} = \sum_{\nu \geq 0} \frac{1}{\nu + \frac{1}{2} + \frac{\beta\rho_c}{\alpha\rho_c + 1}} \quad . \tag{2.69}$$

This equation also has two solutions (T_{c1} and T_{c2}). If $(T_{c0} - T_{c1})/T_{c0} \ll 1$, and $\rho_{c1} \ll 1$, we obtain

$$\frac{T_{c0} - T_{c1}}{T_{c0}} = \rho_{c1}\left[\alpha\left\{ \frac{1}{[gN(0)]^2} + \frac{1}{gN(0)} \right\} + \beta \cdot 3\zeta(3) \right] \quad . \tag{2.70}$$

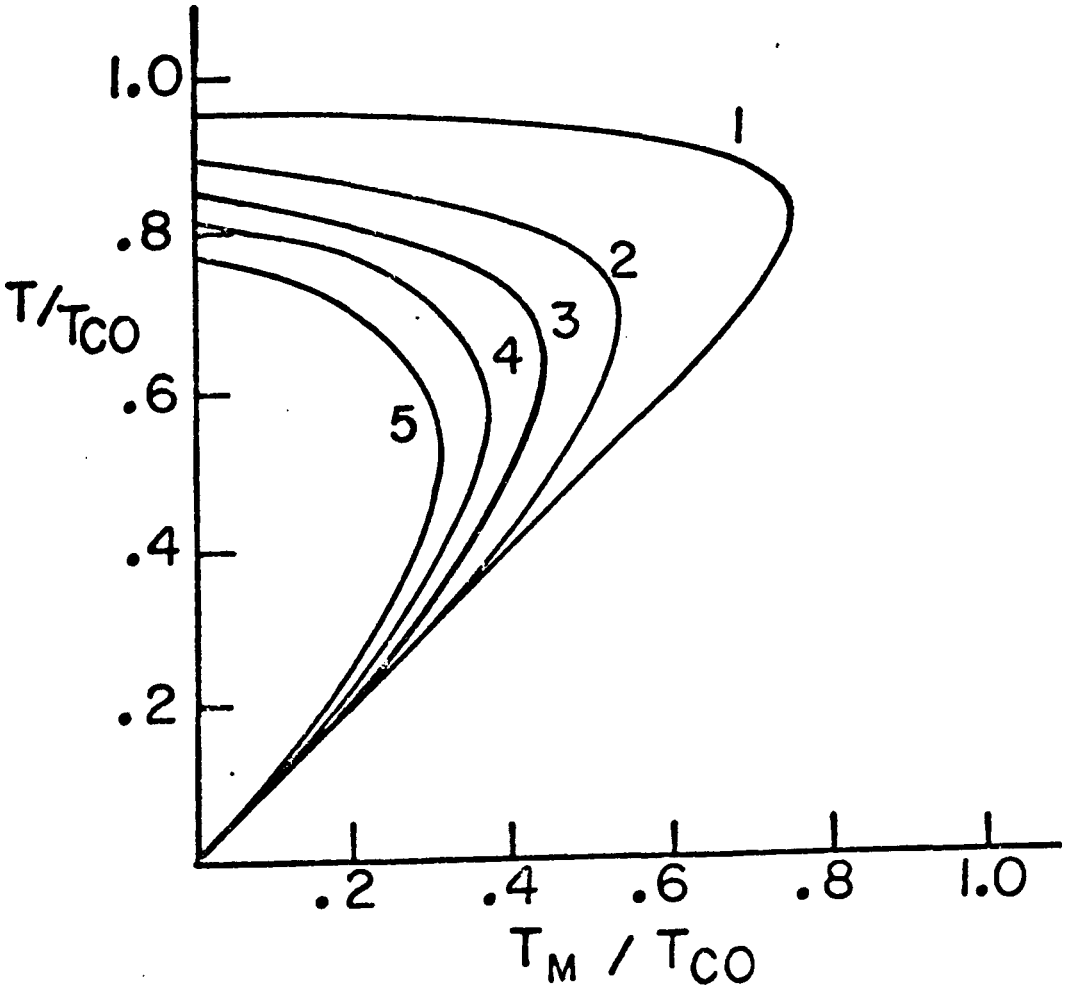

Figure 27. Comparison of the phase diagrams for several theories. $gN(0) = 0.25$, $(2ak_F)^2/T_{c0} = 0.5$, and $N(0)(\frac{I}{2})^2 \cdot S(S+1)/T_{c0} = 0.01$; (1) = 0, = 1 (Abrikosov-Gor'kov type theory); (2) $\alpha = 0.5$, $\beta = 0.5$; (3) $\alpha = 1$, $\beta = 0$ (Berk-Schrieffer type theory without mass renormalization); (4) $\alpha = 1$, $\beta = 0$ (Berk-Schrieffer type theory); (5) $\alpha = \beta = 1$

Numerical results for all temperatures and for several different values of α and β are shown in Fig. 27.

1. The upper critical field

It is straightforward to calculate the upper critical field, H_{c2}, if we confine our discussion to the dirty limit. Following standard procedures (34) leads us to an implicit equation for H_{c2}:

$$\frac{1}{gN(0) - \alpha\rho} = \Psi(T,H_{c2}) \tag{2.71}$$

$$\Psi(T,H_{c2}) = \mathrm{Re} \sum_{\nu \geq 0} \frac{1}{(\nu + \frac{1}{2})(1 + \alpha\rho) + \beta\rho + \frac{ih}{2\pi T} + \frac{DeB}{2\pi T}} \quad . \tag{2.72}$$

As before, h, the internal molecular field acting on the conduction electrons, is given by

$$h = g\mu_B \frac{IH_{c2}}{T - T_M} + \mu_B B \quad . \tag{2.73}$$

The diffusion constant, D is a measure of the dirtiness of samples. We depict numerical results in Fig. 28.

The results of this section show that as the inelastic scattering channel is "turned on", the BCS coupling weakens and the effective mass of the superconducting electrons increases. This causes an overall suppression of the superconducting state which manifests itself by lowering T_{c1}, raising T_{c2}, and reducing $H_{c2}(T)$.

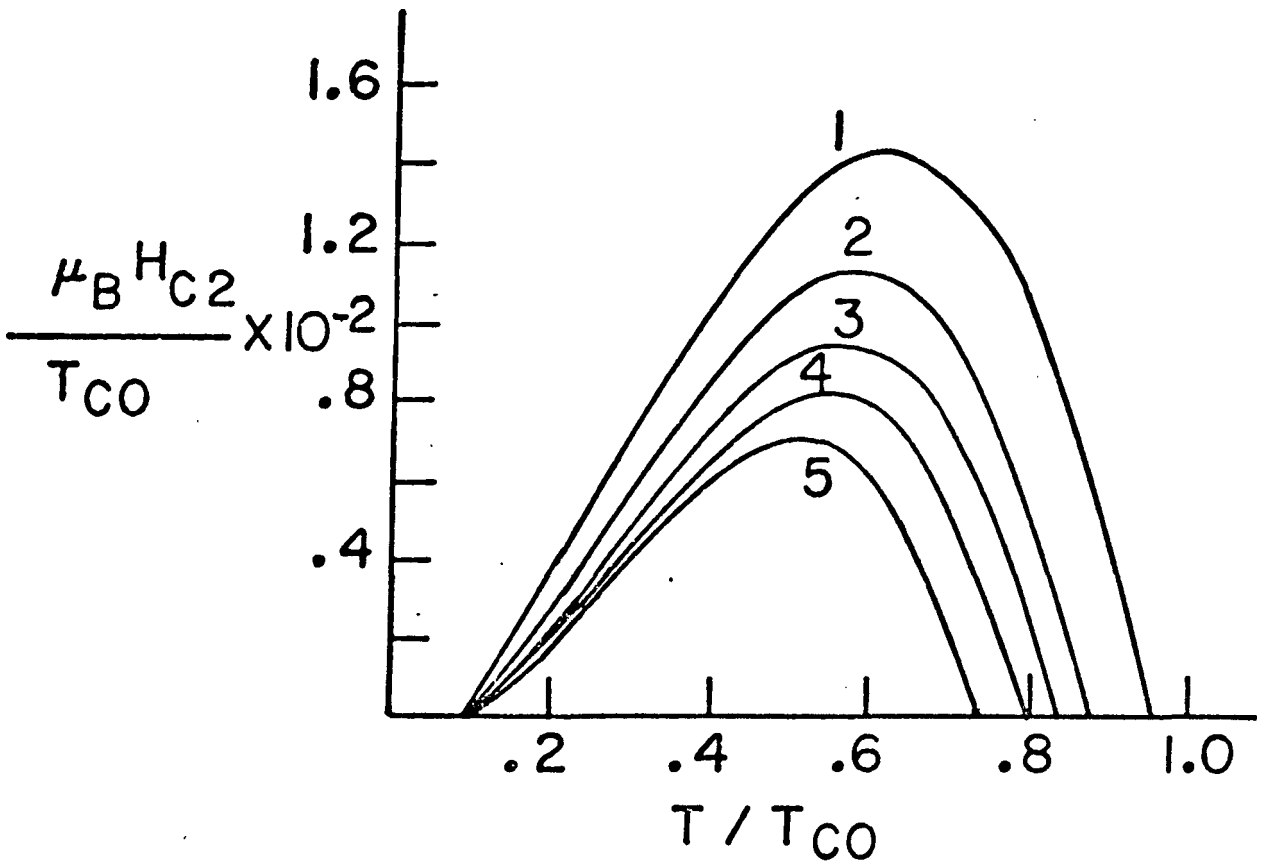

Figure 28. Upper critical field vs. temperature. The same parameters as in Fig. 27 are used here. Additional parameters used in all 5 curves are: $T_M/T_{c0} = 0.1$, $De/2\pi\mu_B = 2.0$, $N(0)\cdot T_{c0} = 8.6 \times 10^{-4}$, $4\pi N_0 J(J+1)(\mu_B g_J)^2/(3T_{c0} = 0.25$, $g_J J(J+1) I/T_{c0} = 82$. Note that as inelastic scattering increases, $H_{c2}(T)$ decreases

F. Discussion

In this chapter we have considered the effects of ferromagnetic fluctuations -- fluctuations for which the dominant wavenumber is zero -- on the properties of the superconducting state. There are, however, rare-earth alloys which like to order antiferromagnetically. Experimental evidence (60) indicates that superconductivity and long-range antiferromagnetic order coexist in some of these alloys. A theoretical investigation of this phenomenon has been published (61) by K. Machida.

Other theorists (62) have developed models in which long range ferromagnetic order weakens superconductivity but can coexist with it. Maekawa and Tachiki (42) have presented a model in which superconductivity is stabilized by ferromagnetic fluctuations. These latter two phenomena have not been observed experimentally.

The results of calculations done with the model we have presented in this chapter agree well with experimental data. In particular, the reentrant behavior and the "mole-hill" shaped upper critical field curves demonstrated by many ternary and pseudo-ternary rare-earth alloys can be explained using the theory.

III. ANISOTROPIC SUPERCONDUCTORS

A. Introduction

The upper critical fields of materials with anisotropic Fermi surfaces have been the subject of many recent experimental investigations (12-18). In some of the anisotropic materials, the $H_{c2}(T)$ curve displays positive curvature near T_{c0} and retains anomalously high values as T approaches zero. Recent experimental work by Orlando et al. (12), for example, shows upward curvature in the critical field curve of the A-15 material Nb_3Sn, and perpendicular field measurements made by Dalrymple and Prober (13) and others (14-15) on the hexagonally distorted material $NbSe_2$ show H_{c2} exceeding the predicted (24) value for spherically symmetric materials by $\sim$20% in the low temperature regime. Similar effects are seen in other (16-18) anisotropic materials.

Theoretical models describing these features should include nonlocality of the superconducting pair state as well as anisotropy in both the Fermi surface and the pair state. Several years ago, Helfand and Werthamer (24) showed how to treat nonlocality in isotropic materials exactly. A short time later, Hohenberg and Werthamer (25) did a quasi-local calculation demonstrating that Fermi surface anisotropy can cause upward curvature in $H_{c2}(T)$ near T_{c0}. Takanaka and Nagashima (26) (TN) extended the work of Hohenberg and Werthamer by retaining higher order terms in the nonlocality and by perturbatively introducting gap anisotropy. The applicability of their (TN) work is limited to the immediate vicinity of T_{c0}. Teichler (27), using a different formalism,

found expressions for the first few terms in a cubic harmonic series expansion of the contributions to $H_{c2}(T)$ from anisotropy in the Fermi velocity and the electron-electron coupling. He obtained results for all temperatures, but predicted that $H_{c2}(T)$ could deviate either above or below the Helfand and Werthamer (24) curve depending on the phases of the anisotropies of the Fermi velocity and the e-e coupling. (No anisotropy-induced reduction of the Helfand-Werthamer curve has ever been seen experimentally.)

In this chapter we extend the Hohenberg-Werthamer (25) theory of the upper critical field by summing to infinite order the effects of nonlocality, and by perturbatively including Fermi surface and pair state anisotropy. We will restrict our consideration to fields applied along crystal symmetry axes, and will concern ourselves primarily with clean materials since it is in them that the effects of anisotropy are most pronounced.

In section B we formulate the theory. In section C we describe the theory appropriate for materials with general Fermi surface anisotropy but unperturbed pair states. In section D we allow both the Fermi surface and the pair state to be anisotropic and fit experimental upper critical field data on $NbSe_2$ in the perpendicular field direction.

B. Description of the Theory

The foundations for our theory are described by Hohenberg and Werthamer (25) and references therein. The assumptions made were that the transition to the superconducting state is second order (only terms

linear in the gap in the Gor'kov equation are retained), the electron-electron coupling is isotropic and weak, the electron scattering centers are randomly located and nonmagnetic, and the effect of the magnetic field on the orbital motion of the electrons may be treated in the semiclassical approximation (63). The Fermi surface may contain only one band. Although Hohenberg and Werthamer considered only the case where the Fermi surface anisotropy was small and the pair state was isotropic, the formalism they developed is sufficiently general as to allow arbitrary shapes for both the Fermi surface and the pair state. A brief discussion of the Hohenberg-Werthamer theory is given in Chapter I.

We begin with Eqs. (5) and (11) from Ref. 25, the solution of which gives $H_{c2}(T)$:

$$1 = gN(0)T \sum_{\nu=-\infty}^{\infty} [S_{\omega}^{-1} - 1/2\tau]^{-1} \qquad (3.1)$$

where

$$S_{\omega} = \frac{\pi}{|\tilde{\omega}|} \int d\hat{q}\, N(\hat{q}) \sum_{n=0}^{\infty} (-1)^n \langle S| \left(\frac{\vec{v} \cdot \vec{\pi}}{2\tilde{\omega}} \right)^{2n} |S\rangle \quad . \qquad (3.2)$$

In Eqs. (3.1)-(3.2) g, N(0), $1/\tau$ ($\equiv n|u|^2$), $N(\hat{q})$, and $\vec{v}$ are respectively the BCS coupling constant, the average density of states at the Fermi surface, the electron scattering rate (or the product of the impurity concentration and the square of the impurity scattering amplitude), the density of states at the Fermi surface in direction $\hat{q}$, and the Fermi velocity. Furthermore, $\vec{\pi} \equiv -i\vec{\nabla} - 2e\vec{A}$ is the gauge-invariant momentum

operator acting on the pair state $|S\rangle$ (described more fully later), and $\tilde{\omega} \equiv \omega_\nu + \text{sgn}\ \omega_\nu/(2\tau)$ is the Matsubara frequency renormalized by impurities. As usual, τ is the impurity scattering time, $\omega_\nu = (2\nu + 1)\pi T$ (ν = integer), $e = |e|$, and $\vec{A}$ is the magnetic vector potential. We remark that S_ω is the nonlocal pair propagator in the ladder approximation for the scattering, and Eq. (3.1) includes the usual vertex renormalization. Anticipating isomorphism with the harmonic oscillator problem (24,64), we choose $\vec{H} = (0,0,-H)$, and $\vec{A} = (0,-Hx,0)$ where the $\hat{z}$ axis may be any one of the three crystal axes. As always, units are chosen such that $\hbar = k_B = c = 1$.

By inserting $\frac{1}{|2\nu + 1|} - \frac{1}{|2\nu + 1|}$ in the ν sum in Eq. (3.1) and introducing the Debye frequency cutoff in the first of these sums in the usual manner (see Appendix E), Eq. (3.1) becomes

$$\ln \frac{T}{T_{c0}} = \sum_{\nu=-\infty}^{\infty} \left\{ T\left[S_\omega^{-1} - \frac{1}{2\tau} \right]^{-1} - \frac{1}{|2\nu + 1|} \right\} \tag{3.3}$$

where $T_{c0} = 2\gamma\omega_D/\pi \exp\left(\frac{-1}{gN(0)}\right)$ is the zero-field transition temperature, $\gamma = 1.781$ is the exponential of Euler's constant, and ω_D is the Debye frequency.

The equations we have written so far are formally identical to those in Ref. 25. We will extend their scope by deriving expressions for S_ω which are valid for all temperatures and for arbitrarily shaped single-band Fermi surfaces (section D), and by considering the modifications to S_ω resulting from the inclusion of anisotropy in the superconducting pair state (section D).

C. Anisotropic Fermi Surface

The nonlocal contributions to S_ω for materials with distorted Fermi surfaces but undistorted pair states can be summed analytically to infinite order. Following Helfand and Werthamer (24) we initially take the pair state $|S\rangle$ to be the lowest eigenstate of the harmonic oscillator operator $\pi^2/2m$. We denote this lowest state by $|0\rangle$. In real space, the wavefunction of this state is $\Delta_0(\vec{r}) = \langle\vec{r}|0\rangle = \exp(-eH_{c2}x^2)$. The system is quantized by setting $\pi_-|0\rangle = 0$ where $\pi_\pm = \pi_x \pm i\pi_y$, and establishing the commutation relations $[\pi_+,\pi_z] = [\pi_-,\pi_z] = 0$, $[\pi_-,\pi_+] = 4eH_{c2} \equiv \varepsilon$. For fields applied along crystal symmetry axes we expect the pair state to have no momentum parallel to the field, so $\pi_z|0\rangle = 0$.

The expectation values from Eq. (3.2) of the form $\langle 0|(\vec{v}\cdot\vec{\pi})^{2n}|0\rangle$ can be determined by establishing a recursion relations. In Appendix G we show that

$$\langle 0\ (\vec{v}\cdot\vec{\pi})^2|0\rangle = v_+v_-\varepsilon \equiv v_\perp^2 eH_{c2} \tag{3.4}$$

($v_\pm = \frac{1}{2}(v_x \pm iv_y)$). Furthermore (see Appendix H),

$$\langle 0|(\vec{v}\cdot\vec{\pi})^{2n}|0\rangle = (2n+1)v_+v_-\varepsilon\langle 0|(\vec{v}\cdot\vec{\pi})^{2n}|0\rangle \tag{3.5}$$

so by induction,

$$\langle 0|(\vec{v}\cdot\vec{\pi})^{2n}|0\rangle = (v_+v_-)^n\varepsilon^n(2n-1)!! \tag{3.6a}$$

$$= (v_\perp^2 eH_{c2})^n(2n-1)!! \quad . \tag{3.6b}$$

The sum in Eq. (3.2) then becomes

$$\sum_{n=0}^{\infty} (-1)^n \langle 0 | \left(\frac{\vec{v} \cdot \vec{\pi}}{2\tilde{\omega}} \right)^{2n} | 0 \rangle = 1 + \sum_{n=1}^{\infty} (-1)^n a^n (2n-1)!! \qquad (3.7)$$

$$= \sqrt{\pi}\, z \exp(z^2) \mathrm{erfc}(z) \qquad (3.8)$$

where $z = (2a)^{-1/2}$, $a = v_\perp^2 eH_{c2}/4\tilde{\omega}^2$, and erfc(z) is the complementary error function.

Notice that the perturbation series (Eq. (3.7)) treating the effects of nonlocality is asymptotic. If one attempts to evaluate it by retaining increasingly higher order terms (65) he finds that his approximation to $H_{c2}(T)$ improves in an increasingly narrow neighborhood of T_{c0}, but diverges at increasingly higher temperatures. To obtain results valid over the entire temperature range, this series must be summed to infinite order (Eq. (3.8)).

When Eq. (3.8) is substituted into Eq. (3.2) we have an integral over the Fermi surface which must in general be evaluated numerically. This is done by picking a particular ν value and evaluating the exact form of the n sum [Eq. (3.8)] for each of a dense series of points on the Fermi surface. This procedure is repeated for enough ν values that the ν sum is evaluated reliably. When $\lambda \equiv 1/(2\pi T_{c0}\tau) \neq 0$, H_{c2} and T are first estimated then determined self-consistently. Numerical solutions to Eqs. (3.2) and (3.3) assuming a spherical Fermi surface and various values of λ are shown in Fig. 10. Here $t \equiv T/T_{c0}$, $h \equiv eH_{c2}v_F^2/(2\pi T_{c0})^2$, and $h^*(t) \equiv h(t)/(-dh/dt\big|_{t=1})$. These solutions are numerically identical to those in Ref. 24 and are included here for future comparisons. (In Appendix I we show analytically that when the Fermi surface is spherical

and $\lambda = 0$, our more general equations defining $H_{c2}(T)$ reduce to those of Helfand and Werthamer.) The slopes of all curves in Figs. 10, 30-34 have been fixed to be -1 at $t = 1$. Table 1 contains the actual slopes at $t = 1$ for each of these curves.

Fermi surface anisotropy enters the calculations through the quantities $N(\hat{q})$ and $v_{\perp}^{2n}(\hat{q})$. For materials with hexagonally symmetric distortions (such as the transition metal dichalcogenides with the field perpendicular to the layers) we model the Fermi surface by setting $|v_{\perp}(\hat{q})| = v_F(1 + b_6(6\phi)) \cdot \sin\theta$ and $N(\hat{q}) \sim 1/|v(\hat{q})|$, where θ and ϕ are the polar and azimuthal angles respectively. Figure 29 shows how cross sections of the Fermi surface would appear for $b_6 = 0.0$, 0.15, 0.3, and Fig. 30 shows the upper critical field curves for materials with hexagonally distorted Fermi surfaces. We observe that increasing Fermi surface anisotropy causes the $h^*(T)$ curve to lie increasingly above the Helfand-Werthamer curve; for $b_6 = 0.5$ the upper critical field is nearly linear in temperature. Although we have plotted results only for hexagonally symmetric Fermi surfaces, identical results are obtained with $v_{\perp}(\hat{q}) = v_F \sin\theta(1 + b \cos n\phi)$ for all n. We therefore conclude that it is the magnitude and not the shape of the Fermi surface anisotropy that determines the enhancement of $H_{c2}(T)$.

Since impurity scattering tends to smear out the Fermi surface, we expect that increasing impurity scattering should drive the $H_{c2}(T)$ curves towards the isotropic dirty limit curve of Helfand and Werthamer. Figure 31 shows the results of numerical calculations with $b = 0.4$ and $\lambda = 0.0$, 0.5, 5.0, and 50.0 $\approx \infty$. (When $\lambda = 1.0$, the electron scattering

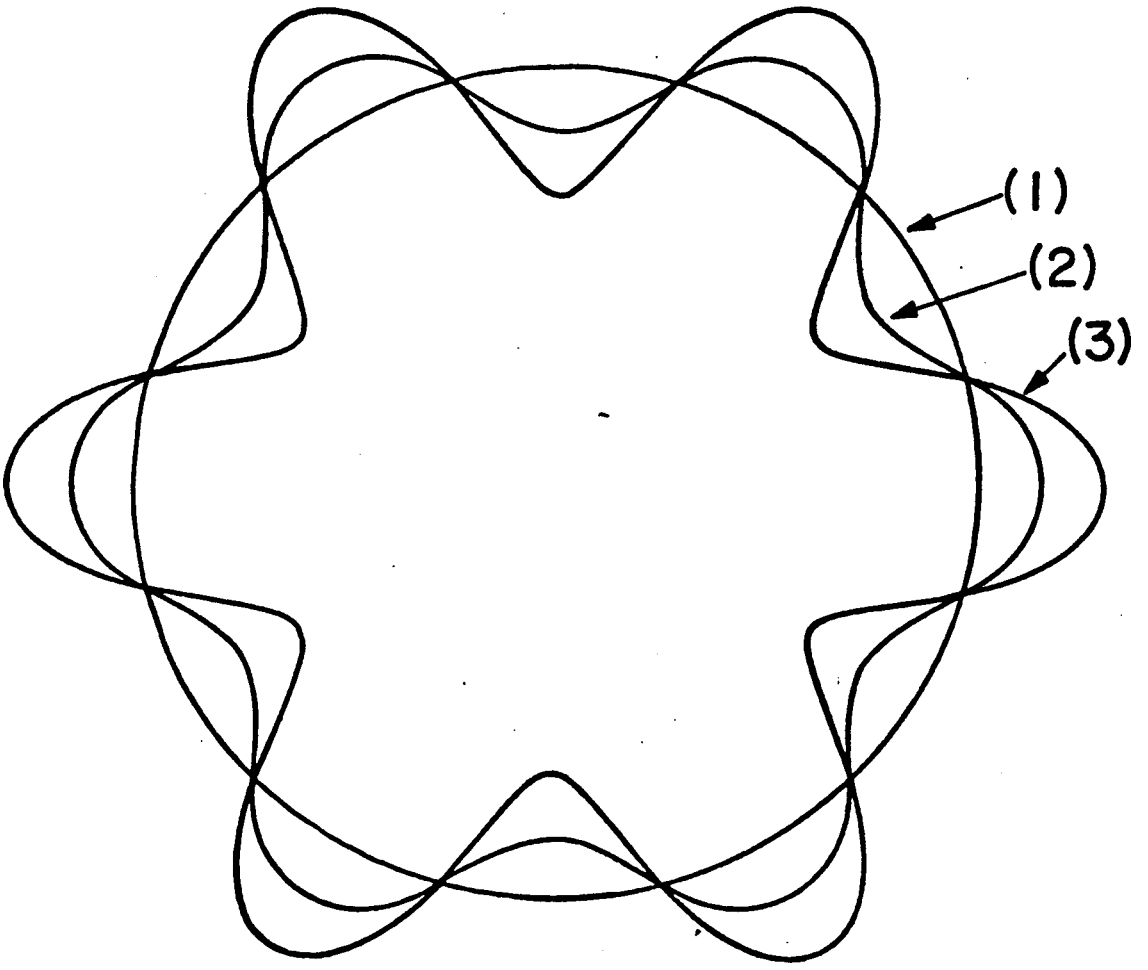

Figure 29. Cross sectional shapes of the Fermi surface. b_6 = (1) 0.0; (2) 0.15; (3) 0.3

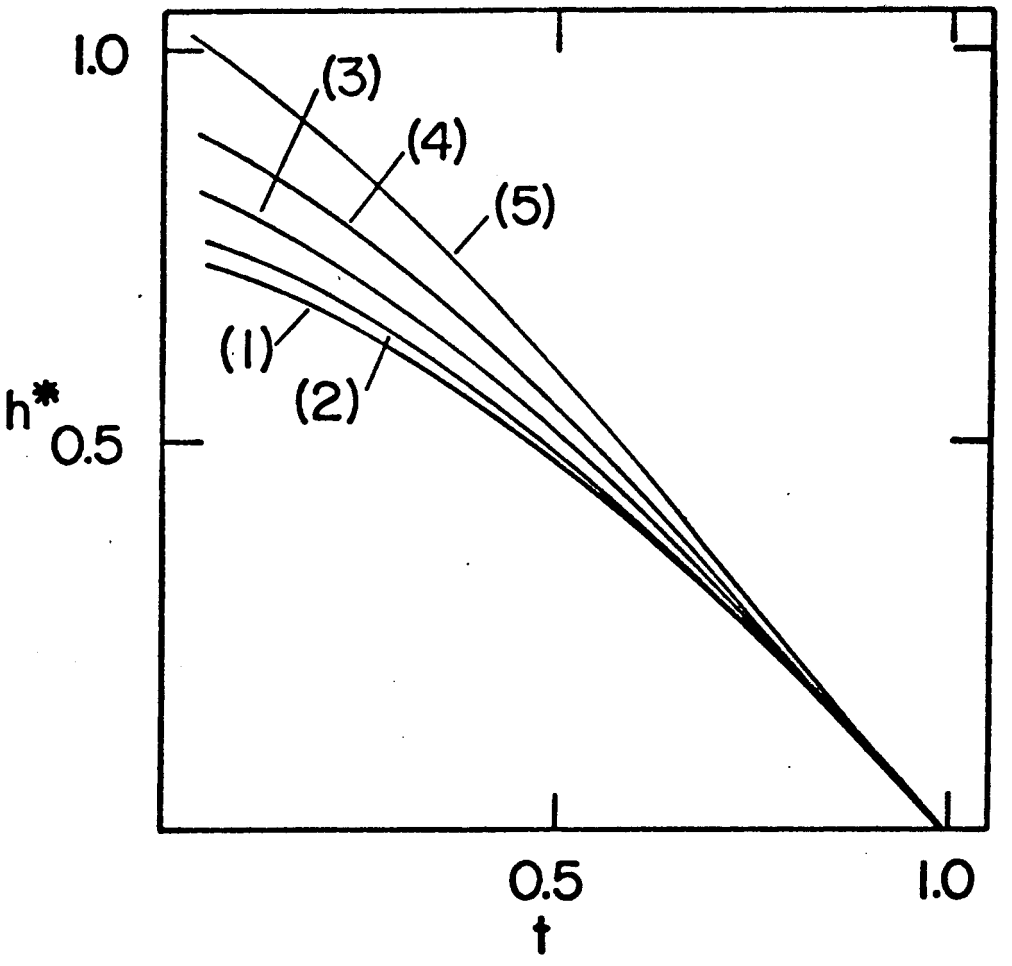

Figure 30. Upper critical fields for materials with distorted Fermi surfaces. $\lambda = 0.0$, b_6 = (1) 0.0; (2) 0.15); (3) 0.3; (4) 0.4; (5) 0.5

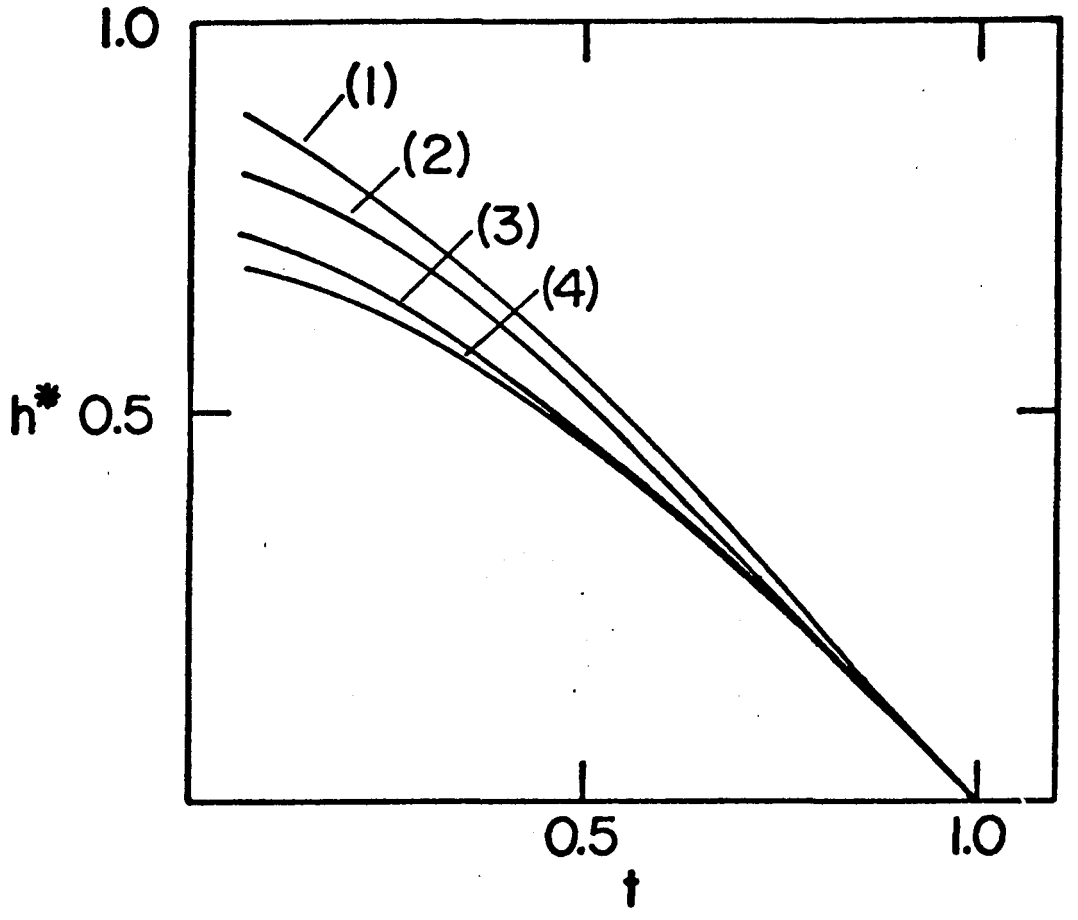

Figure 31. Upper critical fields for materials with distorted Fermi surfaces and impurity scattering. $b_6 = 0.4$, λ = (1) 0.0; (2) 0.5; (3) 5.0; (4) 50.0

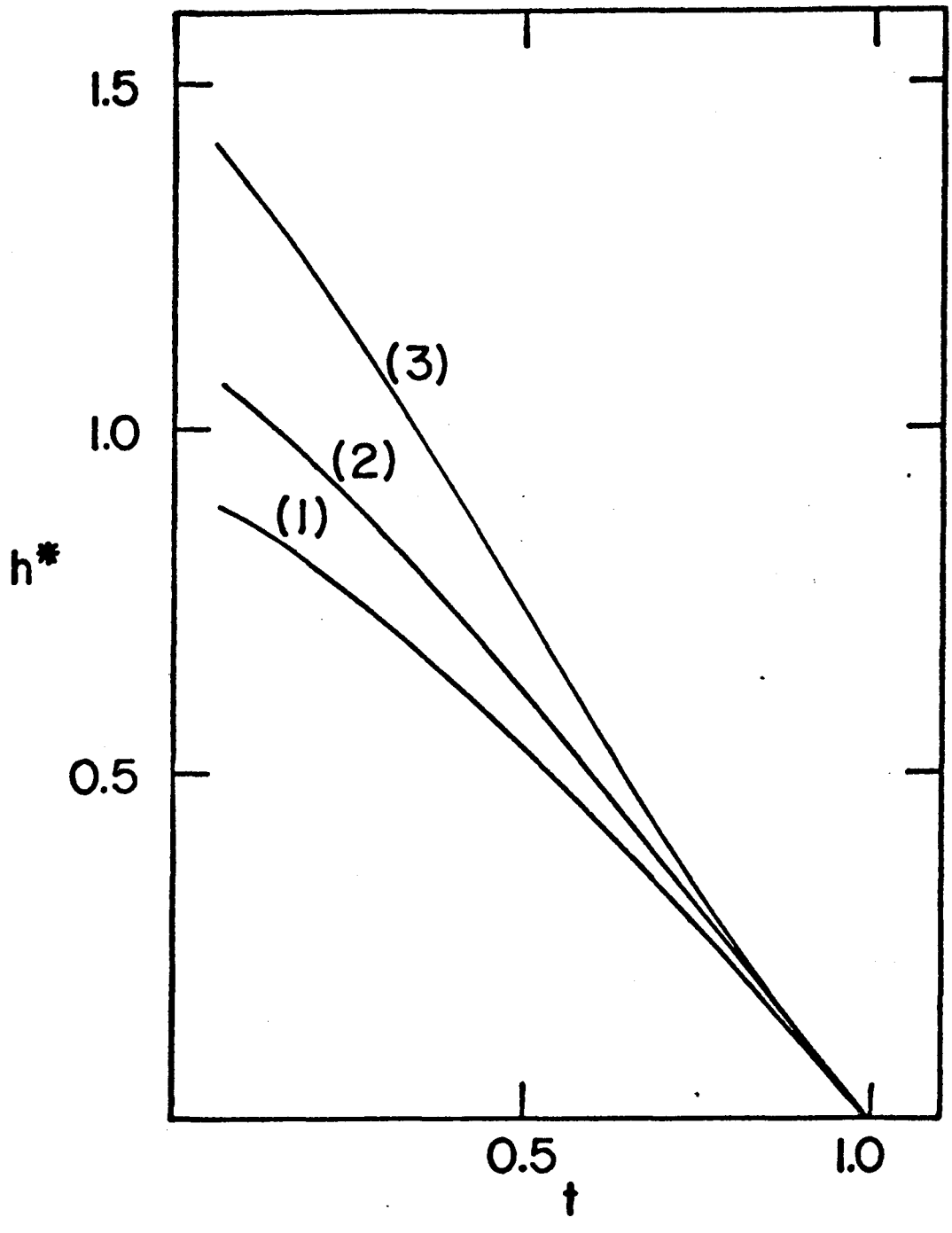

Figure 32. Upper critical fields for materials with distorted Fermi surfaces and distorted superconducting pair states. $\lambda = 0.0$, $b_6 = 0.4$, a_6 = (1) 0.0; (2) 0.15; (3) 0.3

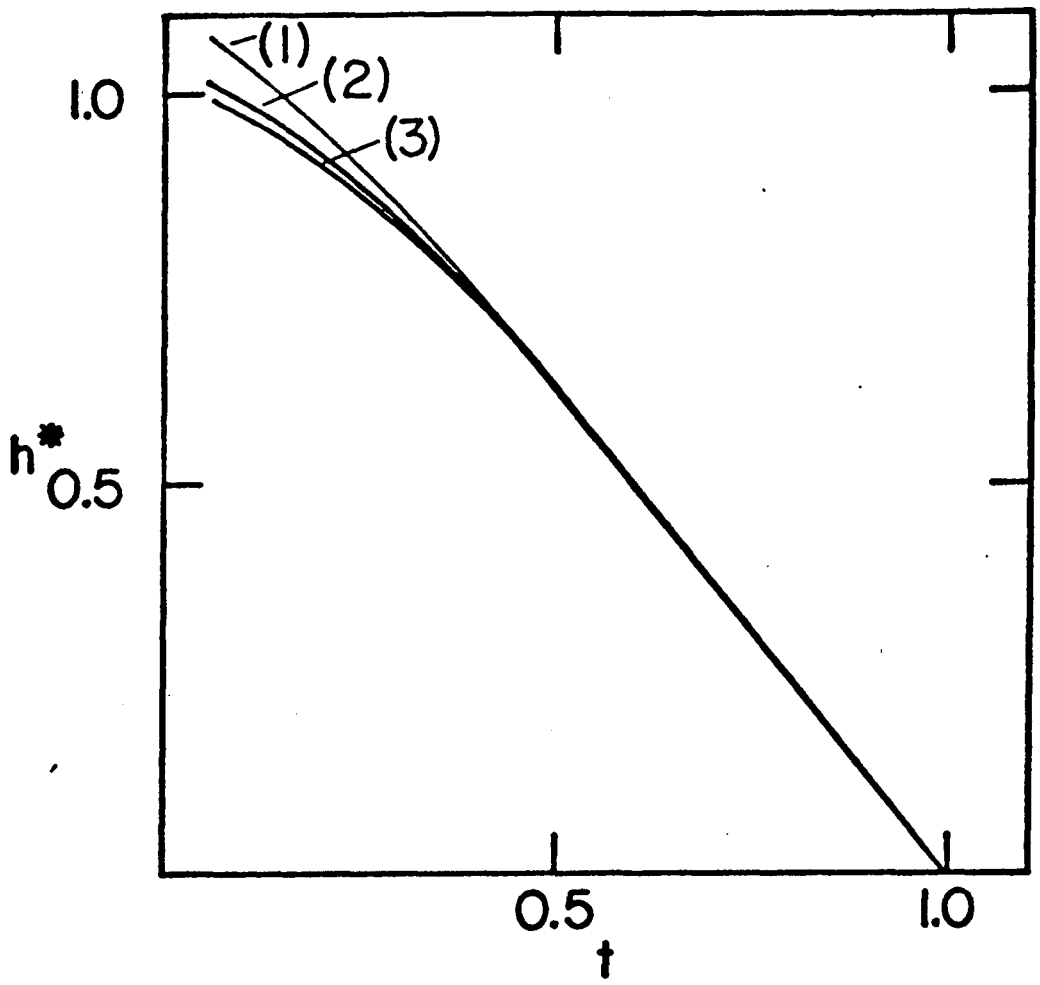

Figure 33. Upper critical fields. ϕ_6 measures the rotation of the pair state anisotropy relative to the Fermi surface anisotropy. $\lambda = 0.0$, $a_6 = 0.15$, $b_6 = 0.4$, ϕ_6 = (1) 0.0; (2) $\pi/2$; (3) π

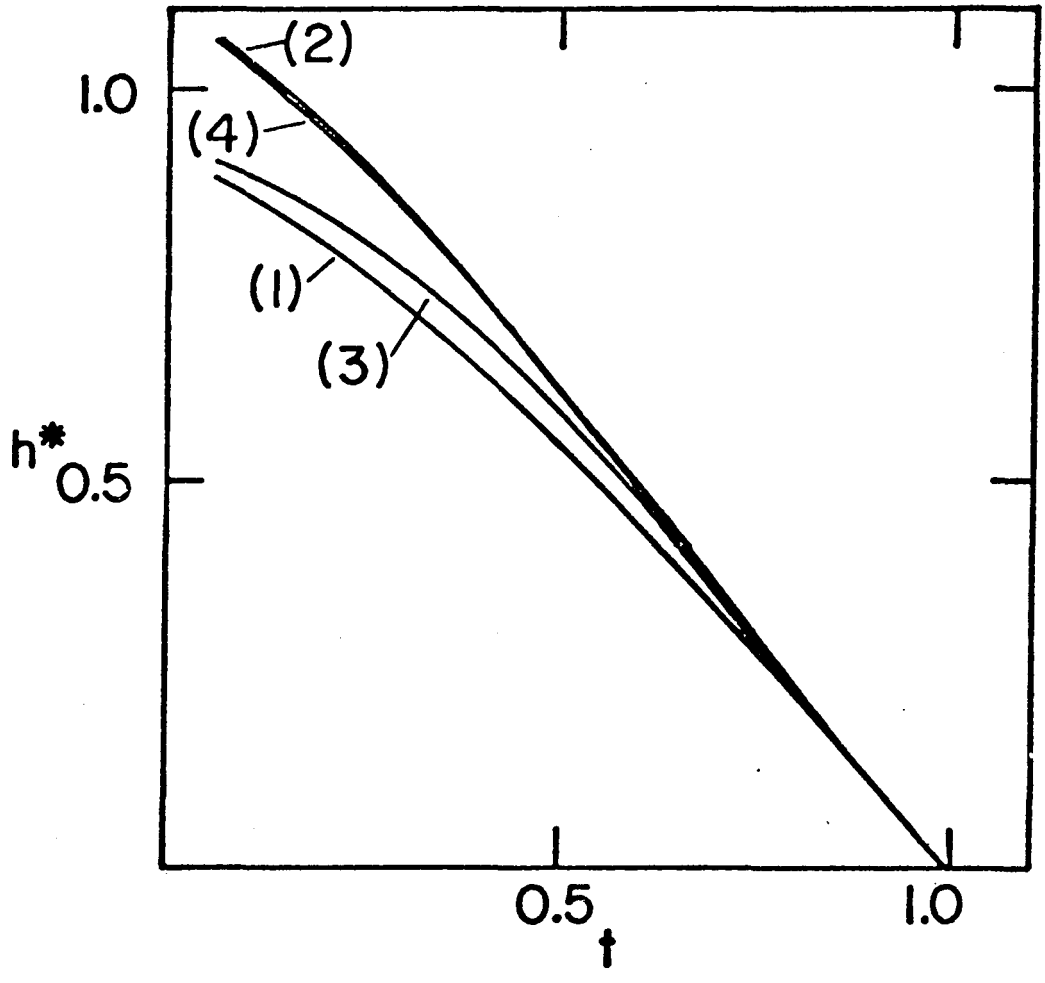

Figure 34. Upper critical fields for ellipsoidally, cubicly, and hexagonally distorted Fermi surfaces and pair states. $\lambda = 0.0$, $\phi_n = 0.0$, $a_n = b_n = 0.0$ except: (1) $b_n = 0.4$ (any n); (2) $a_2 = 0.15$, $b_2 = 0.4$; (3) $a_4 = 0.15$, $b_4 = 0.4$; (4) $a_6 = 0.15$, $b_6 = 0.4$

Table 1. Slopes (-dh/dt ± 0.2%) at t = 1 of the curves in Figs. 27, 30-34

Figure	Curve 1	2	3	4	5
27	0.711	1.055	3.70	31.8	
30	0.711	0.722	0.749	0.781	0.829
31	0.781	1.151	4.32	34.6	
32	0.781	0.627	0.405		
33	0.627	0.627	0.627		
34	0.781	0.669	0.672	0.627	

length is roughly equal to the pair coherence length.) We note that the $\lambda = 50.0$ curve is essentially identical to the isotropic dirty limit curve of Helfand and Werthamer. However, for $\lambda = 5$, which describes relatively dirty materials, $h^*(t)$ for $b = 0.4$ still lies above the isotropic clean limit curve. A material must be quite dirty before the effects of Fermi surface anisotropy vanish completely.

D. Anisotropic Pair States

It is expected that the anisotropy in the superconducting pair state will be strongly dependent on the anisotropy in the Fermi surface as well as on impurity scattering, temperature, and perhaps even the field. Takanaka and Nagashima (26) devised a scheme for relating the pair state anisotropy parameters a_{2n} to the Fermi surface parameters, but their scheme relied on the assumption that the upper critical field satisfied $\partial H_{c2}/\partial a_{2n}^* = 0$. (We know of no physical motivation for making this assumption. It does not necessarily imply that the free energy will be a minimum.) Their resulting expressions for a_2 and a_4 diverged at low temperatures and are therefore unacceptable. In our model the pair state anisotropy parameters are considered to be free and independent of the Fermi surface, but in practice are always taken to be smaller than the analogous Fermi surface anisotropy parameters.

In a manner similar to that proposed by Takanaka and Nagashima (26) we write the perturbed pair state as

$$|S\rangle = \left(1 + \sum_{m=1}^{\infty} |a_{2m}|^2 \right)^{-1/2} \left(1 + \sum_{m=1}^{\infty} \frac{a_{2m} \pi_+^{2m}}{\sqrt{2m!}\ \varepsilon^m} \right) |0\rangle \quad . \tag{3.9}$$

Here, a_6, for example, is a complex parameter which determines the magnitude and phase of the hexagonal distortion of the pair state. In much of this section we will consider only hexagonal distortions.

With $|S\rangle$ taken to be

$$|S\rangle = \left(1 + |a_6|^2\right)^{-1/2} \left(1 + \frac{a_6 \pi_+^6}{\sqrt{6!}\,\varepsilon^3}\right)|0\rangle \tag{3.10}$$

we find that the expectation value in Eq. (3.2) can be broken into three separate terms.

$$\langle S|\left(\frac{\vec{v}\cdot\vec{\pi}}{2\tilde{\omega}}\right)^{2n}|S\rangle = A + |a_6|B + |a_6|^2 C \tag{3.11}$$

where

$$A = \langle 0|\left(\frac{\vec{v}\cdot\vec{\pi}}{2\tilde{\omega}}\right)^{2n}|0\rangle = a^n(2n-1)!! \tag{3.12}$$

$$B = \frac{1}{\sqrt{6!}\,\varepsilon^3}\left\{\frac{a_6}{|a_6|}\langle 0|\left(\frac{\vec{v}\cdot\vec{\pi}}{2\tilde{\omega}}\right)^{2n}\pi_+^6|0\rangle + \text{h.c.}\right\}$$

$$= \frac{2\cos(6\phi + \phi_6)}{\sqrt{6!}}\, a^n P(n) \tag{3.13}$$

and

$$C = \frac{1}{6!\varepsilon^6}\langle 0|\pi_-^6\left(\frac{\vec{v}\cdot\vec{\pi}}{2\tilde{\omega}}\right)^{2n}\pi_+^6|0\rangle$$

$$= \frac{1}{6!}\, a^n Q(n) \quad . \tag{3.14}$$

Here, ϕ_6 is defined by $a_6 = |a_6|\exp(i\phi_6)$, and as before, $a = v_\perp^2 eH_{c2}/4\tilde{\omega}^2$. The functions P(n) and Q(n) are found by making repeated use of Eq. (3.6) and the commutation relation $[\pi_-,\pi_+] = \varepsilon$, and are given by

$$P(n) = (2n+5)!! - 15(2n+3)!! + 45(2n+1)!! - 15(2n-1)!! \qquad (3.15)$$

$$\text{for } n \geq 3$$

$$= 0 \quad \text{otherwise}$$

$$Q(n) = (2n+11)!! - 30(2n+9)!! + 315(2n+7)!! - 1380(2n+5)!!$$

$$+ 2475(2n+3)!! - 1350(2n+1)!! + 225(2n-1)!! \quad . \qquad (3.16)$$

The derivation of Eqs. (3.11)-(3.16) is given in Appendix J. Each of the sums over n of the terms in Eqs. (3.12)-(3.14) is essentially identical to the sum in Eqs. (3.7) and (3.8) and can therefore be evaluated exactly. Numerical solutions to Eq. (3.3) with $|S\rangle$ hexagonally distorted as given by Eq. (3.10) are shown in Fig. 32. We observe that even small amounts of pair state anisotropy cause positive curvature in $h^*(t)$ near $t = 1$, and increased values of $h^*(t)$ for lower temperatures. Further calculations indicate that as impurity scattering is increased, the effects of pair state anisotropy vanish in a manner nearly identical to that shown in Fig. 31.

Expression B [Eqs. (3.11) and (3.13)] is the coefficient on a term linear in the pair state anisotropy. By changing the phase of a_6 (i.e., by rotating the pair state anisotropy relative to the Fermi surface anisotropy) we can estimate the contribution of this linear term to $h^*(t)$. Numerical results are shown in Fig. 33.

Although the model used by Teichler (27) is quite unlike the model developed here and the approximations he made cannot easily be compared with ours, it is possible to contrast some of his results with ours. First, our $h^*(t)$ curve lies on or above Helfand and Werthamer's (24) curve for $h^*(t)$ in isotropic materials regardless of the relative phase of the Fermi surface anisotropy and the pair state anisotropy (Fig. 33). Teichler's $h^*(t)$ curves can fall below Helfand and Werthamer's curves for some reasonable values of his parameters. Secondly, we find that terms linear in the pair state anisotropy (term B, Eqs. (3.11) and (3.13)) contribute significantly to $h^*(t)$ at low temperatures. Teichler's formulism contains no such linear terms. Although parametrized differently, many of our other results are, however, qualitatively similar to Teichler's.

If the crystal symmetry perpendicular to the field is not hexagonal but either ellipsoidal or cubic, the pair state is described by

$$|S\rangle = (1 + |a_2|^2 + |a_4|^2)^{-1/2}\left(1 + \frac{a_2\pi_+^2}{\sqrt{2!}\ \varepsilon} + \frac{a_4\pi_+^4}{\sqrt{4!}\ \varepsilon^2} \right)|0\rangle \quad . \quad (3.17)$$

The sum over n from Eq. (3.2) can now be broken into six separate sums similar to those in Eqs. (3.12)-(3.14) (see Appendix J). Numerical results depicted in Fig. 34 show that ellipsoidal and hexagonal pair state perturbations cause significantly more enhancement of $h^*(t)$ than do cubic perturbations. The reason for this is not understood.

In Fig. 35 we fit our theory to experimental data (13) on 2H-$NbSe_2$, a material with hexagonal symmetry in the layers. Here $\alpha \equiv T_{c0}m^*/\varepsilon_F m$

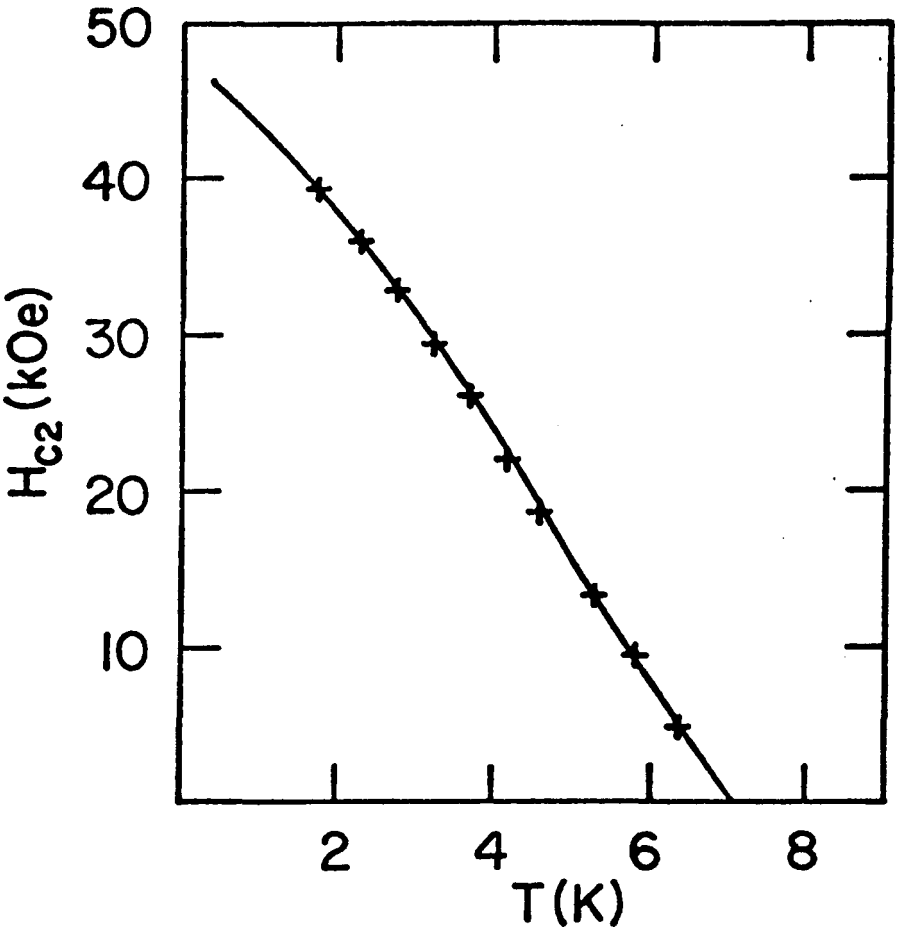

Figure 35. Fit to experimental H_{c2} data (13) (+) on 2H-$NbSe_2$. $\lambda = 0.0$, $a_6 = 0.12$, $b_6 = 0.34$, $\phi_6 = 0.0$, $T_{c0} = 7.06$ K, $\alpha = 0.071$

is a free parameter which sets the scale of H_{c2}, and m^* is an average effective mass of the conduction electrons. The choice of $b_6 = 0.34$ is consistent with Fermi surface calculations done by Wexler and Woolley (66). Prober et al. (67) estimate $\lambda \gtrsim \varepsilon_0/\ell = 0.15$ for $NbSe_2$. If we were to fit the data with $\lambda \neq 0$, b_6 and a_6 would be slightly larger and α would be slightly smaller.

E. Discussion

The model we have presented can be used to calculate the effects of Fermi surface anisotropy and pair state anisotropy on the upper critical fields of superconducting materials. It includes the effects of non-locality to all orders in perturbation theory giving results which are valid over the entire temperature range. We demonstrated that increasing Fermi surface anisotropy causes H_{c2} to become more nearly linear in temperature whereas even small amounts of gap anisotropy cause positive curvature in $H_{c2}(T)$ near T_{c0}. All effects of anisotropy are diminished by increasing the impurity scattering rate. The model successfully describes experimental upper critical field curves in many different anisotropic superconductors.

IV. CONCLUSIONS

We have presented discussions of two different models used to describe the upper critical field curves in three different types of superconductors. The models were essentially microscopic in nature, and incorporated most of the effects known to influence electrons in the superconducting state.

In Chapter II we focused our attention on the ternary and pseudo-ternary rare-earth superconductors which leave the superconducting state and reenter the normal state at low temperatures. The Hamiltonian we used in the model explaining this peculiar feature contained terms expressing the interaction of the rare-earth local magnetic moments with the superconducting electrons and with other local moments. The resulting equation which gave $H_{c2}(T)$ was formally identical to the equation normally encountered in theories describing type II superconductors, but contained a pair breaking term not found in the usual theories. This unusual pair breaking term diverged logarithmically as the temperature of the system approached the Curie temperature, T_M, and therefore forced the system back into the normal state at temperatures slightly above T_M.

In Chapter III we examined how Fermi surface and pair state anisotropy would affect the shape of the upper critical field curve. Both of the anisotropy effects were perturbatively inserted into a model which described $H_{c2}(T)$ in materials with spherically symmetric Fermi surfaces and unperturbed gaps. The results of our calculations showed that increasing Fermi surface anisotropy caused $H_{c2}(T)$ to become more nearly

linear in temperature whereas even small amounts of pair state anisotropy caused positive curvature in $H_{c2}(T)$ near T_{c0}. All effects of anisotropy were seen to be diminished by increasing the impurity scattering rate. The theory was fit to experimental data of $NbSe_2$.

We remark finally that in cases where experimental data existed, excellent agreement between theory and experiment could be obtained with very reasonable values of the theoretical fitting parameters.

V. REFERENCES

1. B. W. Roberts, J. Phys. Chem. Ref. Data 5, 581, (1976).

2. B. W. Roberts in Progress in Cryogenics, edited by K. Mendelssohn (Heywood, London, 1964), Vol. 4, p. 159.

3. C. Kittel, Introduction to Solid State Physics (John Wiley and Sons, Inc., New York, 1971), p. 404.

4. M. A. Janocko, J. R. Gavaler, J. K. Hulm, and C. K. Jones, J. Vacuum Sci. Technol 7, 127, (1970).

5. R. A. Ferrell, Phys. Rev. Letters 3, 262 (1959); P. W. Anderson, Phys. Rev. Letters 3, 325 (1959).

6. See, for example, ϕ. Fischer, M. Decroux, R. Chevrel, and M. Sergent in Proceedings of the Second Rochester Conference on Superconductivity in d- and f- Band Metals, D. H. Douglass, ed. (Plenum Press, New York, 1976), pp. 175-187.

7. R. W. McCallum, D. C. Johnston, R. N. Shelton, and M. B. Maple in Proceedings of the Second Rochester Conference on Superconductivity in d- and f- Band Metals, D. H. Douglas, ed. (Plenum Press, New York, 1976), pp. 625-634.

8. J. W. Lynn, D. E. Monton, W. Thomlinson, G. Shirane, and R. N. Shelton, Solid State Commun. 26, 493 (1978).

9. M. B. Maple, to be published in the Proceedings of the 13th Rare-Earth Research Conference.

10. W. A. Fertig, D. C. Johnston, L. E. DeLong, R. W. McCallum, M. B. Maple, and B. T. Matthias, Phys. Rev. Lett. 38, 987 (1977).

11. H. R. Ott, W. A. Fertig, D. C. Johnston, M. B. Maple, and B. T. Matthias, submitted to J. Low Temp. Phys.

12. T. P. Orlando, E. J. McNiff, Jr., S. Foner, and M. R. Beasley, Phys. Rev. B 19, 4545 (1979), and private communication.

13. B. J. Dalrymple and D. E. Prober, Bull. Am. Phys. Soc. 23, 230 (1978), and private communication.

14. N. Toyota, H. Nakatsuji, K. Nota, A. Hoshi, N. Kobayashi, and Y. Muto, J. Low Temp. Phys. 25, 483 (1976).

15. S. Foner and E. J. McNiff, Jr., Phys. Lett. 45A, 429 (1973).

16. J. A. Woollam, R. B. Somoano, and P. O'Connor, Phys. Rev. Lett. 32, 712 (1974).

17. H. W. Weber, E. Seidl, and G. Kirschenhofer, Sol. State Commun. 26, 795 (1978).

18-23. T. Ohtsuka, in Anisotropy Effects in Superconductors, ed. by H. W. Weber (Plenum Press, New York, 1977), pp. 27-41.

24. E. Helfand and N. R. Werthamer, Phys. Rev. 147, 288 (1966).

25. P. C. Hohenberg and N. R. Werthamer, Phys. Rev. 153, 493 (1967).

26. K. Takanaka and T. Nagashima, Progr. Theor. Phys. 43, 18 (1970).

27. H. Teichler, Phys. Stat. Sol. 72, 211 (1975).

28. V. L. Ginzburg and L. D. Landau, Zh. Eksperim. i Theor. Fiz. 20, 1064 (1950).

29. A. A. Abrikosov, L. P. Gor'kov, and I. E. Dzyaloshinski, in Methods of Quantum Field Theory in Statistical Physics (Dover Publications, Inc., New York, 1963).

30. N. R. Werthamer, in Superconductivity, R. D. Park, ed. (Marcel Dekker, New York, 1969), Vol. 1, and K. Maki, ibid, Vol. 2.

31. A. L. Fetter and J. D. Walecka, Quantum Theory of Many-Particle Systems (McGraw-Hill, Inc., New York, 1971).

32. D. Saint-James, E. J. Thomas, and G. Sarma, Type II Superconductivity (Pergamon Press, Oxford, 1969).

33. P. G. deGennes, Superconductivity of Metals and Alloys (W. A. Benjamin Inc., New York, 1966).

34. N. R. Werthamer, in Superconductivity, R. D. Park, ed. (Marcel Dekker, New York, 1969), Vol. 1.

35. A. I. Akhiezer and V. B. Berestetskii, Quantum Electrodynamics (Interscience, New York, 1965), p. 272.

36. N. R. Werthamer, E. Helfand, and P. C. Hohenberg, Phys. Rev. 147, 295 (1966).

37. G. Rickayzen, Phys. Rev. 138, A73 (1965).

38. B. T. Matthias, La Recherche 33, 319 (1973); and J. M. Vandenberg and B. T. Matthias, Proc. Natl. Acad. Sci. USA 74, 1336 (1977).

39. T. Jarlborg, A. J. Freeman, and T. J. Watson-Yang, Phys. Rev. Lett. 39, 1032 (1977).

40. R. W. McCallum, R. N. Shelton, M. B. Maple, and H. Adrian, Bull. Am. Phys. Soc. 21, 383 (1976).

41. A. A. Abrikosov and L. P. Gorkov, Zh. Eksp. Teor. Fiz. 39, 1781 (1961) [English transl., Sov. Phys.--JETP 12, 1243 (1961)]. Also see K. Maki, in Superconductivity, R. D. Park, ed. (Marcel Dekker, New York, 1969), Vol. 2.

42. S. Maekawa and M. Tachiki, Phys. Rev. B 18, 4688 (1978).

43. T. Matsuura, S. Ichinose, and Y. Nagaoka, Prog. Theor. Phys. 57, 713 (1977).

44. J. M. Ziman, Principles of the Theory of Solids (University Press, Cambridge, 1972), p. 334.

45. P. G. deGennes, in Magnetism, edited by G. T. Rado and H. Suhl (Academic Press, New York, 1963), Vol. 3, pp. 115-146.

46. P. G. deGennes, Phys. and Chem. Solids 4, 223 (1958).

47. H. Mori and K. Kawasiki, Prog. Theoret. Phys. (Kyoto) 27, 529 (1962).

48. K. Maki, in Superconductivity, edited by R. D. Parks (Dekker, Inc., New York, 1969), pp. 1035-1105.

49. V. Jaccarino and M. Peter, Phys. Rev. Lett. 9, 290 (1962).

50. M. B. Maple, H. C. Hamaker, D. C. Johnston, H. B. MacKay, and L. D. Woolf, J. Less Common Metals 62, 251 (1978).

51. R. H. Wang, R. J. Laskowski, C. Y. Huang, J. L. Smith, and C. W. Chu, in Proc. of 23rd Conference on Magnetism and Magnetic Materials (Nov. 8-11, 1977, Minneapolis), and private communication.

52. D. C. Johnston, W. A. Fertig, M. B. Maple, and B. T. Matthias, Solid State Commun. 26, 141 (1978).

53a. D. W. Youngner and K. Machida, J. Low Temp. Phys. 36, 617 (1979).

53b. R. J. Elliott, Magnetic Properties of Rare-Earth Metals (Plenum Press, London, 1972), p. 1.

54. B. D. Dunlap, G. K. Shenoy, F. Y. Fradin, and C. W. Kimball, in Proc. of LT 15, J. Phys. (Paris) Suppl. 39, C6-379 (1978).

55. D. E. Moncton, D. B. McWhan, J. Eckert, G. Shirane, and W. Thomlinson, Phys. Rev. Lett. 39, 1164 (1977).

56. $(Lu_{1-x}HO_x)RH_4B_4$ and $(Y_{1-x}Gd_x)Rh_4B_4$ have no observable magnetic transition for $x \lesssim 0.2$. We have extrapolated the linear curve for T_M vs. x, giving $T_M < 0$ K in this region. This does not significantly affect the suppression of T_c.

57. B. T. Matthias, E. Corenzwit, J. M. Vandenberg, and H. E. Barz, Proc. Nat. Acad. Sci. US 74, 1334 (1977).

58. D. Youngner and K. Machida, J. Low Temp. Phys. 35, 561 (1979).

59. N. F. Berk and J. R. Schrieffer, Phys. Rev. Letters 17, 433 (1966).

60, B. T. Matthias, A. L. Giorgi, V. O. Struebing, and J. L. Smith, Phys. Lett. 69A, 221 (1978).

61. K. Machida, J. Low Temp. Phys. 37, 485 (1979).

62. C. Balseiro and L. M. Falicov, submitted to Phys. Rev. B.

63. Landau quantization which becomes important when $eH_c2/m \approx \pi T+1/\tau$ is not considered in this thesis.

64. A. A. Maradudin, E. W. Montroll, and G. H. Weiss, Theory of Lattice Dynamics in the Harmonic Approximation (Academic Press, Inc., New York, 1963), Chap. VII. Sec. 2.

65. Hohenberg and Werthamer (Ref. 25) kept the first three terms in this series. Takanaka and Nagashima (Ref. 26) kept the first four terms.

66. G. Wexler and A. M. Woolley, J. Phys. C 9, 1185 (1976).

67. D. E. Prober, R. E. Schwall, and M. R. Beasley, preprint.

68. I. S. Gradshteyn and I. M. Ryzhik, Tables of Integrals, Series, and Products (Academic Press, New York, 1965), p. 3.

69. I. S. Gradshteyn and I. M. Ryhik, Tables of Integrals, Series, and Products (Academic Press, New York, 1965), p. 943.

70. E. Merzbacher, Quantum Mechanics (John Wiley and Sons, Inc. New York, 1970), pp. 53-61.

VI. ACKNOWLEDGEMENTS

I am deeply indebted to Professor Richard A. Klemm for the constant support, patient guidance, and knowledgeable tutelage he has given me during my stay at Iowa State University. I am also grateful to Dr. Kazushige Machida for the countless hours he spent discussing with me the details of many of the calculations included in this thesis. Finally, I would like to thank Mrs. Lesley Swope for her skillful preparation of this manuscript.

VII. APPENDIX A

There are several books (29,36) containing excellent descriptions of the effects of random impurity scattering on the single electron Green's function. The description given here is very similar to the description found in Ref. 29.

We begin by writing the integral equation satisfied by the Green's function when impurities are present:

$$G(\vec{p},\vec{p}',\omega) = \delta(\vec{p}-\vec{p}')G^0(p) + (2\pi)^{-3}\sum_a G^0(p)\int d\vec{p}''u(\vec{p}-\vec{p}'')\exp[i(\vec{p}-\vec{p}'')\cdot\vec{r}_a]$$
$$G(\vec{p}'',\vec{p}',\omega) \quad . \tag{A.1}$$

In Eq. (A.1) $\vec{r}_a$ is the position of the a-th impurity, and $\vec{q}$ is the momentum transferred to the lattice by the scattered electron. A factor

$$u(\vec{q})\exp(i\vec{q}\cdot\vec{r}_a)\delta(\omega-\omega') \tag{A.2}$$

is associated with each impurity vertex. The Feynman diagram corresponding to Eq. (A.1) is shown in Fig. 6a.

We aren't concerned with the exact solution of Eq. (A.1). Instead, we average over impurity locations to obtain

$$\overline{G(\vec{p},\vec{p}',\omega)} = G(p)\delta(\vec{p}-\vec{p}') \quad . \tag{A.3}$$

Three types of terms in the series shown in Fig. 6a need to be considered. (1) Averaging over the positions of individual scattering sites leads to

$$\overline{u(\vec{q})\exp(i\vec{q}\cdot\vec{r}_a)} = u(0)$$

which is constant and serves simply to renormalize μ. In the Born approximation we can therefore disregard all diagrams containing any scattering site only once. (2) Terms containing successive scattering from any particular site contribute a factor

$$\frac{1}{V} \int \frac{d\vec{p}''}{(2\pi)^3} |u(\vec{p} - \vec{p}'')|^2 G^0(p'') \tag{A.4}$$

to the self energy of the Green's function. Diagrams like 6b, 6c, and 6d must therefore be retained. (3) Other diagrams, such as those shown in Fig. 6e, contain crossed impurity scattering lines and can be shown (29) to be smaller than those of type (2) by a factor $(E_F\tau)^{-1} << 1$. AGD finds that by considering only diagrams of type (2), the main contribution to Σ can be written as

$$\sum = \frac{i \text{ sgn } \omega}{2\tau} \tag{A.5}$$

where

$$\frac{1}{\tau} = \frac{nmk_F}{(2\pi)^2} \int |u(\theta)|^2 d\theta \tag{A.6}$$

and θ is the angle between p and p'.

With the anzatz that Σ is purely imaginary we obtain

$$G(p) = \left[\omega - \xi(p) - \frac{i \text{ sgn } \omega}{2\tau} \right]^{-1} \tag{A.7}$$

for the real time Green's function, and

$$G(p) = \left[\omega_\nu - \xi(p) - \frac{\text{sgn } \omega}{2\tau} \right]^{-1} \tag{A.8}$$

for the temperature Green's function. Green's function of the form given by Eq. (A.8) are used frequently in the thesis.

VIII. APPENDIX B

Abrikosov, Gor'kov, and Dzyaloshinski (29) (AGD) show that in the absence of any scattering, the various equations of motion describing a superconducting system can be written as a single matrix equation:

$$\begin{pmatrix} -\frac{\partial}{\partial\tau} + \frac{\nabla^2}{2m} + \mu & \Delta \\ -\Delta^* & \frac{\partial}{\partial\tau} + \frac{\nabla^2}{2m} + \mu \end{pmatrix}$$

$$\times \begin{pmatrix} G(x-x') & F(x-x') \\ F^+(x-x') & -G(x'-x) \end{pmatrix} = \begin{pmatrix} 1 & 0 \\ 0 & 1 \end{pmatrix} \tag{B.1}$$

where

$$F(x,x') = \frac{\langle T_\tau(\psi(x,\tau)\psi(x',\tau')\mathcal{S})\rangle}{\langle\mathcal{S}\rangle} \tag{B.2}$$

$$F^+(x,x') = \frac{\langle T_\tau(\psi^+(x,\tau)\psi^+(x',\tau')\mathcal{S})\rangle}{\langle\mathcal{S}\rangle} \tag{B.3}$$

$$G(x,x') = \frac{-\langle T_\tau(\psi(x,\tau)\psi^+(x',\tau')\mathcal{S})\rangle}{\langle\mathcal{S}\rangle} \tag{B.4}$$

and

$$\Delta = gN(0)F(t = 0+) \quad , \quad \Delta^* = gN(0)F^+(t = 0+) \quad . \tag{B.5}$$

As always, g is the BCS coupling constant, ψ and ψ^+ are the Fermion field operators for the electrons, τ is the imaginary time, and $\mathcal{S}$ is given by

$$\mathcal{S} = T_\tau \exp\left[- \int_0^\tau d\tau' \int dr(\psi^+(\psi^+\psi)\psi) \right] \tag{B.6}$$

where ψ^+ and ψ are evaluated at $\vec{r}$ and τ'.

The superconducting transition temperature in such a system is described (36) by the scalar equation (see Appendix E)

$$-\ln\left(\frac{T}{T_{c0}}\right) = \sum_{\nu} \left[|2\nu + 1|^{-1} - s_{\omega}^{0}\right] \tag{B.7}$$

where s_{ω}^{0} is the lowest eigenvalue of the operator S_{ω}^{0} given by

$$S_{\omega}^{0} = T \int_{-\infty}^{\infty} d\varepsilon \; G_{\sigma}(p,\omega) G_{-\sigma}(-p,-\omega) \quad . \tag{B.8}$$

The potential describing normal and spin-orbit scattering has the form

$$V(\vec{r},\vec{r}') = \sum_{i} (2\pi)^{-6} \int d^3\vec{p}\; d^3\vec{q}\; \exp[i\vec{p}\cdot(\tfrac{1}{2}(\vec{r}+\vec{r}') - R_i) + iq\cdot(\vec{r}-\vec{r}')](u_1 + iu_2 \hat{p}\times\hat{q}\cdot\overleftrightarrow{\sigma}) \tag{B.9}$$

where u_1 and u_2 are the normal and spin-orbit scattering strengths respectively, R_i is the location of the i-th impurity and $\overleftrightarrow{\sigma}$ is the Pauli spin matrix. When the momentum of an electron changes from $\vec{p}(=\hat{p}k_F)$ to $\vec{q}(=\hat{q}k_F)$ it generates an orbital magnetic moment proportional to $\vec{p}\times\vec{q}$. The orbital moment couples to the electron's spin with a strength proportional to $\hat{p}\times\hat{q}\cdot\overleftrightarrow{\sigma}$.

The scattering potential described by Eq. (B.9) affects the different spin components of the Green's function in Eq. (B.1) differently. WHH (36) show that if one wishes to write the generalized version of Eq. (B.1) (i.e., including spin orbit effects), he must use 4 x 4 matrices. The additional matrix indices label the spins of the electrons.

The results of the calculations performed by WHH show that when spin-orbit scattering is considered, T_c is given by

$$- \ln \frac{T}{T_{c0}} = \sum_{\nu} \left[|2\nu + 1|^{-1} - \frac{1}{2} \text{tr} \int d\hat{p}\, S_{\omega}(\hat{p}) \right] \tag{B.10}$$

where

$$S_{\omega}(\hat{p}) = S_{\omega}^{0}[1 + hN(0)/T \int d\hat{p}'(u_1 + iu_2 \hat{p} \times \hat{p}' \cdot \vec{\sigma}) S_{\omega}(\hat{p}')(u_1 - iu_2 \hat{p} \times \hat{p}' \cdot \vec{\sigma}) \tag{B.11}$$

tr means the trace over spin indices and n is the number of impurities per unit volume.

In the limit $\tau_1 << \tau_{so}$ (a limit we expect most physical systems to satisfy), Eqs. (B.10) and (B.11) become

$$- \ln \frac{T}{T_{c0}} = \sum_{\nu} \left[|2\nu + 1|^{-1} - \frac{1}{2} \text{tr}\, s_{\omega} \right] \tag{B.12}$$

where

$$\frac{1}{2} \text{tr}\, s_{\omega} = \{[\text{Re}((s_{\omega}^{(0)})^{-1} - (\tau^{-1} - \frac{4}{3} \tau_{so}^{-1})/2\pi T)^{-1}]^{-1} - \frac{4}{3} (2\pi T \tau_{so})^{-1}\}^{-1} . \tag{B.13}$$

In cases where the Fermi surface is spherically symmetric, Eqs. (B.12) and (B.13) become Eqs. (1.28)-(1.31) in the text. In Chapter IV we use Eqs. (B.12) and (B.13) but with $s_{\omega}^{(0)}$ describing the pair state of a quasi zero-dimensional superconductor.

IX. APPENDIX C

Equation (2.13) can be written as

$$\sum(\vec{k},\omega) = \left(\frac{I}{2}\right)^2 T \sum_{\omega'} \frac{1}{(2\pi)^3} \int d^3k' \; G(k',\omega')\chi(\vec{k}-\vec{k}',\omega-\omega') \tag{C.1}$$

where

$$G(k,\omega) = \frac{1}{i\omega - \xi_k - \Sigma(\omega)} \quad . \tag{C.2}$$

Electron-hole symmetry requires that

$$\Sigma(\omega) = -\Sigma(-\omega) \quad . \tag{C.3}$$

If we concern ourselves only with the imaginary part of Σ (and, as is standard procedure (29), implicitly absorb the real part of Σ into μ), Eq. (C.1) becomes

$$\Sigma(\omega) = -i\left(\frac{I}{2}\right)^2 T \sum_{\omega'} \frac{1}{(2\pi)^3} \int d^3k' \; \frac{\text{sgn } \omega'(|\omega'| + |\Sigma(\omega')|)}{\xi_{k'}^2 + (|\omega'| + |\Sigma(\omega')|)^2}$$

$$\bar{\chi}(|k_F - k'|,\omega-\omega') \tag{C.4}$$

where we have defined $\bar{\chi}(|q|,\omega)$ by

$$\bar{\chi}(|q|,\omega) = \int \frac{d\Omega q}{4\pi} \chi(\vec{q},\omega) \quad . \tag{C.5}$$

Rewriting $1/(2\pi)^3 \int d^3k'$ as $N(0) \int_{-\infty}^{\infty} d\xi_k$ in Eq. (C.4) and performing the $d\xi_k$ integral leaves us with

$$\Sigma(\omega) = -i\pi\left(\frac{I}{2}\right)^2 TN(0) \sum_{\omega'=-\infty}^{\infty} \text{sgn } \omega' \; \bar{\chi}(|k_F - k'|,\omega-\omega') \tag{C.6}$$

Electron-hole symmetry requires that $\bar{\chi}(q,\omega)$ be an even function of ω. We can therefore rewrite Eq. (C.6) as

$$\Sigma(\omega) = -i\pi T\left(\frac{I}{2}\right)^2 N(0)\omega \sum_{\omega'} \frac{\theta(|\omega| - |\omega'|)}{|\omega|} \bar{\chi}(|k_F - k|,\omega') \quad . \qquad (C.7)$$

Equation (C.7) is identical to Eq. (2.14) in the text.

X. APPENDIX D

With $\chi(q,\omega) = \chi(q)\delta_{\omega,0}$, Eqs. (2.14), (2.24c), and (2.27) become

$$\sum = -iN(0)\left(\frac{I}{2}\right)^2 \pi T\, \bar{\chi}(q)\ \mathrm{sgn}\ \omega \tag{D.1}$$

or

$$\frac{1}{\tau(T)} \equiv 2i\ \Sigma\ \mathrm{sgn}\ \omega \tag{D.2}$$

$$= 2\pi T\ N(0)\left(\frac{I}{2}\right)^2 \bar{\chi}(q) \quad . \tag{D.3}$$

As before (Eqs. (C.5) and (2.15)),

$$\bar{\chi}(q) \equiv \frac{1}{4\pi} \int d\Omega q\ \chi(\vec{q}) \quad . \tag{D.4}$$

With $\chi(\vec{q})$ of the Orstein-Zernike form (Eq. (2.24c))

$$\chi(\vec{q}) = \frac{S(S+1)T}{T - T_M + a^2q^2} \quad , \tag{D.5}$$

and

$$q = |k-k'| = 2k_F \sin\left(\frac{\theta}{2}\right) \quad , \tag{D.6}$$

Eq. (D.3) becomes

$$\frac{1}{\tau(T)} = N(0)\left(\frac{I}{2}\right)^2 \frac{1}{4\pi} \int_{-1}^{1} 2\pi d\ \cos\theta\ \frac{S(S+1)T}{T - T_M + a^2(2k_F\hat{q}\ \sin\frac{\theta}{2})^2} \quad . \tag{D.7}$$

Equation (D.7) can be rewritten as

$$\frac{1}{\tau(T)} = \frac{\pi N(0)}{8a^2k_F^2} I^2 S(S+1)T \int_{-1}^{1} dt \frac{1}{1 - t + \frac{T - T_M}{2a^2k_F^2}} \tag{D.8}$$

or as

$$\frac{1}{\tau(T)} = 2\pi N(0)\left(\frac{I}{2}\right)^2 S(S+1) \frac{T}{(2ak_F)^2} \ln\left(\frac{T - T_M + (2ak_F)^2}{T - T_M}\right) . \tag{D.9}$$

Equations (D.2) and (D.9) are identical to Eqs. (2.28)-(2.31) in the text.

XI. APPENDIX E

Equation (2.33) is of a form frequently encountered in calculations involving superconductivity. Although the sum over ν is formally divergent, we can invoke the physical constraint that the particles under consideration (paired electrons) only interact as described by Eq. (2.33) when their energies are less than the Debye energy, and we can therefore terminate the ν sum at $\omega_\nu = \omega_D$. A mathematically-gentle method of terminating the sum, and the method which preserves the small, but functionally important logarithmic tail of the sum, involves adding and subtracting $1/(\nu+1/2)$ from the r.h.s. of Eq. (2.33), and introducing the Debye cutoff in only the first of these additional terms. We then have:

$$\frac{1}{gN(0)} = \sum_{\nu=0}^{N} \frac{1}{\nu + \frac{1}{2}} + \sum_{\nu=0}^{\infty} \left(\frac{1}{\nu + \frac{1}{2} + \rho_c} - \frac{1}{\nu + \frac{1}{2}} \right) \tag{E.1}$$

where

$$(2N + 1)\pi T = \omega_D \quad . \tag{E.2}$$

Using the relationships (68)

$$\sum_{k=1}^{n} \frac{1}{2k - 1} = \frac{1}{2} (C + \ln n) + \ln 2 \tag{E.3}$$

and (69)

$$\psi(x) = - C - \sum_{k=0}^{\infty} \left(\frac{1}{x + k} - \frac{1}{k + 1} \right) \tag{E.4}$$

C = Euler's constant = 0.577...

leads to

$$-\frac{1}{gN(0)} + C + 2\ln 2 + \ln\frac{\omega_D}{2\pi T} = \psi\left(\frac{1}{2}+\rho_c\right) - \psi\left(\frac{1}{2}\right) \tag{E.5}$$

or

$$\ln\frac{T_{c0}}{T} = \psi\left(\frac{1}{2}+\rho_c\right) - \psi\left(\frac{1}{2}\right) \tag{E.6}$$

where

$$T_{c0} = \frac{\exp(C + 2\ln 2)}{2\pi}\,\omega_D \exp\left(-\frac{1}{gN(0)}\right) \tag{E.7}$$

$$T_{c0} = 1.13\,\omega_D \exp\left(-\frac{1}{gN(0)}\right) \quad . \tag{E.8}$$

Equation (E.6) is the same as Eq. (2.34) in the text.

XII. APPENDIX F

The bare two particle propagator is given as the product of two unperturbed normal state Green's functions

$$Q^0_{-\sigma,\sigma}(\vec{r},\omega) = G^{n0}_{-\sigma,-\sigma}(\vec{r},-\omega_\nu)G^{n0}_{\sigma\sigma}(\vec{r},\omega_\nu) \tag{F.1}$$

where, as in Eq. (1.11), the normal state Green's functions are

$$G^{n0}_{\sigma\sigma}(\vec{r},\omega) = \frac{-m}{2\pi r}\exp\left(ik_{F\sigma}r(\text{sgn }\omega) - \frac{|\tilde{\omega}|r}{v_{F\sigma}}\right) \tag{F.2}$$

with

$$\tilde{\omega} = \omega + \frac{\text{sgn }\omega}{2\tau_1} \tag{F.3}$$

$$\frac{1}{\tau_1} = 2\pi N(0)n|u|^2 \tag{F.4}$$

$$k_{F\sigma} = k_F - \frac{\sigma h}{v_{F\sigma}} \quad . \tag{F.5}$$

Using the relation

$$\frac{m}{2\pi r} = \frac{\pi N(0)}{k_F r} \tag{F.6}$$

leads to

$$Q^0_{-\sigma,\sigma}(r,\omega) = \left(\frac{\pi N(0)}{k_F r}\right)^2 \exp\left\{\frac{-2i\sigma}{v_F}hr(\text{sgn }\omega)\,\frac{-2|\tilde{\omega}|r}{v_F}\right\} \quad . \tag{F.7}$$

In reciprocal space we have

$$Q^0_{-\sigma,\sigma}(q,\omega) = \int d^3\vec{r}\; Q^0_{\sigma,-\sigma}(r,\omega)\exp(-i\vec{q}\cdot\vec{r}) \tag{F.8}$$

$$= \left(\frac{\pi N(0)}{k_F}\right)^2 2\pi \int \frac{dr}{-iqr}\,(e^{-iqr} - e^{iqr}) \cdot \exp\left\{-\left(\frac{2i\sigma h\ \mathrm{sgn}\ \omega}{v_F} + \frac{2|\tilde{\omega}|}{v_F}\right)r\right\} \quad . \tag{F.9}$$

Performing the integration leads to

$$Q^0_{-\sigma,\sigma}(q,\omega) = \frac{4\pi^3 N(0)^2}{qk_F^2}\ \tan^{-1}\left(\frac{qv_F}{2|\tilde{\omega}| + 2i\sigma h(\mathrm{sgn}\ \omega)}\right) \quad . \tag{F.10}$$

Retaining the first two terms in a Taylor series expansion of $\tan^{-1}(x)$ gives us

$$[Q^0_{-\sigma,\sigma}(q,\omega)]^{-1} = \frac{1}{\pi N(0)}\,(|\tilde{\omega}| + i\sigma h\ \mathrm{sgn}\ \omega)\left\{1 + \frac{1}{12}\,\frac{q^2v_F^2}{(|\tilde{\omega}| + i\sigma h\ \mathrm{sgn}\ \omega)^2}\right\} \quad . \tag{F.11}$$

Although we have not written our formuli in an explicitly gauge-invariant manner, replacing q^2 by $(-i\vec{\nabla}_r - 2e\vec{A})^2$ will make the equations gauge-invariant (35). (The factor of 2 multiplying $e\vec{A}$ appears because q is the sum of the momenta of two electrons.)

Vertex renormalization in the "ladder approximation" is shown schematically in Fig. 8 and is given algebraically by

$$Q_{-\sigma,\sigma}(q,\omega) = \{Q^0_{-\sigma,\sigma}(q,\omega) - (2\pi\tau_1 N(0))^{-1}\}^{-1} \tag{F.12}$$

$$= \pi N(0)\left[\,|\omega| + i\sigma h\ \mathrm{sgn}\ \omega + \frac{1}{12}\,\frac{q^2v_F^2}{|\omega| + \frac{1}{2\tau_1} + i\sigma h\ \mathrm{sgn}\ \omega}\right]^{-1} \tag{F.13}$$

In the dirty limit, $1/\tau_1 >> T, h$, Eq. (F.13) becomes

$$Q_{-\sigma,\sigma}(q,\omega) = \frac{\pi N(0)}{|\omega| + i\sigma h \operatorname{sgn}\omega + \frac{1}{6}\tau_1 q^2 v_F^2} \quad . \tag{F.14}$$

We now want to replace q^2 by the lowest eigenvalue (i.e., most stable value) of its gauge-invariant replacement $\pi^2 = (-i\vec{\nabla}_r - 2e\vec{A})^2$ where $\vec{A} = (0,Hx,0)$. The lowest eigenstate of the harmonic oscillator operator π^2 is

$$\Delta(x) = \exp(-eHx^2) \quad , \tag{F.15}$$

and

$$\pi^2\Delta(x) = 2eH\,\Delta(x) \tag{F.16}$$

Because of impurity scattering, the true ground state of the system will be slightly different from $\exp(-eHx^2)$. To within the Born approximation, however, we may replace q^2 by $2eH$ in Eq. (F.14). The basic equation (e.g., Eqs. (1.15) and (1.18))

$$\left[1 - gT \sum_{\nu} Q_{-\sigma,\sigma}(q = \pi,\omega)\right]\Delta(x) = 0 \tag{F.17}$$

becomes

$$1 = gN(0)\pi T \sum_{\nu} \frac{1}{|\omega| + i\sigma h \operatorname{sgn}\omega + \frac{1}{6}(2eH)\tau_1 v_F^2} \quad . \tag{F.18}$$

As shown in Appendix E, Eq. (F.18) can be written as

$$\ln\frac{T}{T_{c0}} = \operatorname{Re}\left[\psi\left(\frac{1}{2}\right) - \psi\left(\frac{1}{2} + \frac{i\sigma h}{2\pi T} + \frac{e\tau_1 v_F^2 H}{6\pi T}\right)\right] \quad . \tag{F.19}$$

Equation (F.19) is formally identical to Eq. (2.44) in the text.

XIII. APPENDIX G

The wavefunction $\Delta_0(\vec{r})$ introduced in Chapter III is defined to be the lowest eigenfunction of the gauge-invariant free particle operator $q^2/2m$ where $\vec{q} = (-i\vec{\nabla}_r - 2e\vec{A})$. We use $\vec{H} = (0,0,-H)$, and choose the gauge where $\vec{A} = (0,-Hx,0)$. $\Delta_0(\vec{r})$ satisfies the Schroedinger equation.

$$\frac{1}{2m}(-i\vec{\nabla} - 2e\vec{A})^2\Delta_0(\vec{r}) = E_0\,\Delta_0(\vec{r}) \qquad (G.1)$$

or

$$\frac{-1}{2m}[\partial_x^2 - (2eHx)^2 + \partial_y^2 + \partial_z^2]\Delta_0(\vec{r}) = E_0\,\Delta_0(\vec{r}) \qquad .(G.2)$$

Eigenfunctions of this equation are of the form

$$\Delta_0(\vec{r}) = u(x)\exp(ik_y y + ik_z z) \qquad . \qquad (G.3)$$

The lowest eigenvalue occurs when $k_y = k_z = 0$. $\Delta_0(\vec{r})$ then satisfies the harmonic oscillator equation

$$\left[-\frac{1}{2m}\partial_x^2 + \frac{1}{2m}(2eHx)^2\right]\Delta_0(x) = E_0\,\Delta_0(x) \qquad . \qquad (G.4)$$

Solutions (70) to this equation are known to be hermite polynomials multiplied by exponentially decaying tails. The lowest eigenvalue is $E_0 = 2eH/m$. The eigenstate corresponding to this eigenvalue is

$$\Delta_0(\vec{r}) = \exp(-eHx^2) \qquad . \qquad (G.5)$$

We now establish some basic relationships involving q_x, q_y, q_z, and Δ_0. If we define

$$q_{\pm} = q_x \pm iq_y \quad , \tag{G.6}$$

then

$$q_- \Delta_0(\vec{r}) = (-i\partial_x - i2eHx)\Delta_0 \tag{G.7a}$$

$$= (i2eHx - i2eHx)\Delta_0 \tag{G.7b}$$

$$= 0 \quad . \tag{G.7c}$$

Furthermore,

$$[q_+,q_-] = [q_x + iq_y, q_x - iq_y] \tag{G.8a}$$

$$= -2i[q_x,q_y] \tag{G.8b}$$

$$= -4eH \equiv -\varepsilon \tag{G.8c}$$

It is obvious that

$$[q_+,q_z] = [q_-,q_z] = 0 \quad . \tag{G.9}$$

The equations we have written so far in this appendix have been in the language of first quantization. It will prove convenient to shift into the language of second quantization. We define the state vector whose projection in real space is $\psi_0(x)$ to be labeled by $|0\rangle$, so

$$\langle\vec{r}|0\rangle = \psi_0(x) = \exp(-eHx^2) \tag{G.10}$$

and define second quantized momentum operators as

$$\pi_{\pm} = \int d^3r \; \psi^+(\vec{r}) q_{\pm} \; \psi(\vec{r}) \quad . \tag{G.11}$$

Noting Eqs. (G.6)-(G.9), we write

$$\pi_{\pm} \equiv \pi_x \pm i\pi_y \tag{G.12}$$

$$\pi_-|0\rangle = \langle 0|\pi_+ = 0 \tag{G.13}$$

$$[\pi_+,\pi_-] = -4eH = -\varepsilon \tag{G.14}$$

$$[\pi_+,\pi_z] = [\pi_-,\pi_z] = 0 \quad . \tag{G.15}$$

It follows that

$$\langle 0|(\vec{v}\cdot\vec{\pi})^2|0\rangle = \langle 0|(v_z\pi_z + v_x\pi_x + v_y\pi_y)^2|0\rangle \tag{G.16a}$$

$$= \langle 0|(v_x\pi_x + v_y\pi_y)^2|0\rangle \tag{G.16b}$$

$$= \langle 0|(v_+\pi_- + v_-\pi_+)^2|0\rangle \tag{G.16c}$$

$$= \langle 0|v_+^2\pi_-^2 + v_+v_-(\pi_+\pi_- + \pi_-\pi_+) + v_-^2\pi_+^2|0\rangle \tag{G.16d}$$

$$= v_+v_-\langle 0|\pi_-\pi_+|0\rangle \tag{G.16e}$$

$$= v_+v_-\langle 0|\varepsilon + \pi_+\pi_-|0\rangle \tag{G.16f}$$

$$= v_+v_-\varepsilon = v_\perp^2 eH_{c2} \quad . \tag{G.16g}$$

In going from Eq. (G.16a) to (G.16b) we have imposed the constraint that $\pi_z|0\rangle = 0$, and in time Eq. (G.16c) we introduced

$$v_{\pm} = \frac{1}{2}(v_x \pm iv_y) \quad . \tag{G.17}$$

Equation (G.16g) is the desired result and is identical to Eq. (3.4) in the text.

XIV. APPENDIX H

In Chapter III we need to evaluate terms of the form

$$A_{2n} \equiv \langle 0|(\vec{v}\cdot\vec{\pi})^{2n}|0\rangle \tag{H.1}$$

Consider

$$A_{2n+2} = \langle 0|(\vec{v}\cdot\vec{\pi})^{2n+2}|0\rangle \tag{H.2a}$$

$$= \langle 0|(\vec{v}\cdot\vec{\pi})^{2n}(\vec{v}\cdot\vec{\pi})^{2}|0\rangle \quad . \tag{H.2b}$$

Since only terms with equal numbers of π_+ and π_- operators survive in the expectation value, Eq. (H.2b) can be written as

$$A_{2n+2} = (v_+v_-)^{n+1}\langle 0|(\pi_+ + \pi_-)^{2n}(\pi_+ + \pi_-)^{2}|0\rangle \tag{H.3a}$$

$$= (v_+v_-)^{n+1}\langle 0|(\pi_+ + \pi_-)^{2n}(\pi_+^2 + \pi_-\pi_+)|0\rangle \quad . \tag{H.3b}$$

From the commutation relation $[\pi_+,\pi_-] \equiv -\varepsilon$ it follows that

$$[(\pi_+ + \pi_-),\pi_+] = \varepsilon \quad . \tag{H.4}$$

Therefore,

$$\langle 0|(\pi_+ + \pi_-)^{2n}\pi_+^2|0\rangle = \langle 0|(\pi_+ + \pi_-)^{2n-1}\pi_+(\pi_+ + \pi_-)^{1}\pi_+|0\rangle$$

$$+ \varepsilon\langle 0|(\pi_+ + \pi_-)^{2n-1}\pi_+|0\rangle \tag{H.5a}$$

$$= \langle 0|(\pi_+ + \pi_-)^{2n-m}\pi_+(\pi_+ + \pi_-)^{m}\pi_+|0\rangle$$

$$+ m\varepsilon\langle 0|(\pi_+ + \pi_-)^{2n-1}\pi_+|0\rangle \tag{H.5b}$$

$$\langle 0|(\pi_+ + \pi_-)^{2n}\pi_+^2|0\rangle = \langle 0|\pi_+(\pi_+ + \pi_-)^{2n}\pi_+|0\rangle + 2n\varepsilon\langle 0|(\pi_+ + \pi_-)^{2n}|0\rangle \quad \text{(H.5c)}$$

$$= 2n\varepsilon\langle 0|(\pi_+ + \pi_-)^{2n}|0\rangle \quad . \quad \text{(H.5d)}$$

And

$$\langle 0|(\pi_+ + \pi_-)^{2n}\pi_-\pi_+|0\rangle = \varepsilon\langle 0|(\pi_+ + \pi_-)^{2n}|0\rangle \quad . \quad \text{(H.6)}$$

Combining Eqs. (H.2a), (H.3b), (H.5d), and (H.6) yields

$$\langle 0|(\vec{v}\cdot\vec{\pi})^{2n+2}|0\rangle = (2n+1)\varepsilon v_+ v_-\langle 0|(\vec{v}\cdot\vec{\pi})^{2n}|0\rangle \quad \text{(H.7)}$$

which is identical to Eq. (3.5)

XV. APPENDIX I

If $\lambda = 0$ and the Fermi surface is spherically symmetric so $N(\hat{q}) = 1/4\pi$ and

$$\int d\hat{q}\, N(\hat{q})\, v_{\perp}^{2n} = v_F^{2n} \frac{2^n n!}{(2n+1)!!} \quad , \tag{I.1}$$

Eqs. (3.3, (3.7), (3.8) become

$$\ln \frac{T}{T_{c0}} = \sum_{\nu=-\infty}^{\infty} \frac{2\pi T}{|\omega|} \sum_{n=1}^{\infty} (-1)^n \left(\frac{eH_{c2} v_F^2}{4\omega^2} \right)^n \frac{2^n n!}{(2n+1)!!} (2n-1)!! \tag{I.2}$$

or

$$\ln(t) = \sum_{\nu=-\infty}^{\infty} \left\{ \frac{1}{|2\nu+1|} - \frac{1}{|2\nu+1|} \sum_{n=0}^{\infty} (-1)^n \left[\frac{(2h)^{1/2}}{t(2\nu+1)} \right]^{2n} \frac{n!}{2n+1} \right\} \tag{I.3}$$

where t and h are defined in Chapter III. Equation (I.3) is identical to Eqs. (24) and (36) in Ref. 24.

XVI. APPENDIX J

We found in Appendix H and Chapter III that

$$\langle 0|(\pi_+ + \pi_-)^{2n}|0\rangle = (2n-1)!!\varepsilon^n \quad . \tag{J.1}$$

In this appendix we evaluate terms of the form

$$\langle S|\left(\frac{\vec{v}\cdot\vec{\pi}}{2\tilde{\omega}}\right)^{2n}|S\rangle \tag{J.2}$$

where

$$|S\rangle = \left(1 + \sum_{m=1}^{\infty}|a_{2m}|^2\right)^{-1/2}\left[1 + \sum_{m=1}^{\infty}\frac{a_{2m}\,\pi_+^{2m}}{\sqrt{2m!}\;\varepsilon^m}\right]|0\rangle \quad . \tag{J.3}$$

Typically, only a few of the a_{2m}'s will be nonzero.

For simplicity, we will set $v_+ = v_- = 2\tilde{\omega} = 1$ in this appendix. It is trivial to reinstate factors of v_+, v_-, and $2\tilde{\omega}$ at the end of the calculations. Furthermore, we will drop the state label $|0\rangle$. Unless otherwise specified, all expectation values will be taken in the ground state. We begin by considering diagonal terms of the form

$$DN = \langle\pi_-^N(\pi_+ + \pi_-)^{2n}\pi_+^N\rangle \quad . \tag{J.4}$$

From Eq. (J.1) we know that

$$DO \equiv \langle(\pi_+ + \pi_-)^{2n}\rangle = (2n-1)!!\varepsilon^n \quad . \tag{J.5}$$

Furthermore,

$$D1 \equiv \langle \pi_-(\pi_+ + \pi_-)^{2n}\pi_+ \rangle = \langle (\pi_+ + \pi_-)(\pi_+ + \pi_-)^{2n}(\pi_+ + \pi_-)\rangle \tag{J.6a}$$

$$= (2n + 1)!!\varepsilon^{n+1} \quad . \tag{J.6b}$$

Similarly,

$$D2 \equiv \langle \pi_-^2(\pi_+ + \pi_-)^{2n}\pi_+^2\rangle \quad . \tag{J.7}$$

A simple exercise reveals that

$$\pi_+^2\rangle = \pi_+(\pi_+ + \pi_-)\rangle \tag{J.8a}$$

$$= [(\pi_+ + \pi_-)^2 - \pi_-\pi_+]\rangle \tag{J.8b}$$

$$= [(\pi_+ + \pi_-)^2 - \varepsilon]\rangle \tag{J.8c}$$

Similarly,

$$\langle\pi_-^2 = \langle[(\pi_+ + \pi_-)^2 - \varepsilon] \quad . \tag{J.9}$$

Combining Eqs. (J.5) and (J.7)-(J.9) yields

$$D2 = \varepsilon^{n+2}[(2n + 3)!! - 2(2n + 1)!! + (2n - 1)!!] \quad . \tag{J.10}$$

It is conceptually simple, but computationally cumbersome to repeat this procedure indefinitely. We quote some of the intermediate results:

$$D3 \equiv \langle \pi_-^3(\pi_+ + \pi_-)^{2n}\pi_+^3\rangle$$

$$= \varepsilon^{n+3}[(2n + 5)!! - 6(2n + 3)!! + 9(2n + 1)!!] \tag{J.11}$$

$$D4 \equiv \langle \pi_-^4 (\pi_+ + \pi_-)^{2n} \pi_+^4 \rangle$$

$$= \varepsilon^{n+4}[(2n+7)!! - 12(2n+5)!! + 42(2n+3)!! - 36(2n+1)!! + 9(2n-1)!!] \quad (J.12)$$

$$D5 \equiv \langle \pi_-^5 (\pi_+ + \pi_-)^{2n} \pi_+^5 \rangle$$

$$= \varepsilon^{n+5}[(2n+9)!! - 20)2n+7)!! + 130(2n+5)!! - 300(2n+5)!! + 225(2n+1)!!] \quad . \quad (J.13)$$

The final diagonal term with which we will concern ourselves is

$$D6 \equiv \langle \pi_-^6 (\pi_+ + \pi_-)^{2n} \pi_+^6 \rangle$$

$$= \varepsilon^{n+6}[(2n+11)!! - 30(2n+9)!! + 315(2n+7)!! - 1380(2n+5)!! + 2475(2n+3)!! - 1350(2n+1)!! + 225(2n-1)!!] \quad . \quad (J.14)$$

It is also necessary to evaluate some of the off-diagonal terms. With $|S\rangle$ given as in Eq. (3.17) by

$$|S\rangle = (1 + |a_2|^2 + |a_4|^2)\left(1 + \frac{a_2 \pi_+^2}{\sqrt{2!}\,\varepsilon} + \frac{a_4 \pi_+^4}{\sqrt{4!}\,\varepsilon^2}\right)|0\rangle \quad (J.15)$$

we have to evaluate the three off-diagonal terms

$$F02 = \langle (\pi_+ + \pi_-)^{2n} \pi_+^2 \rangle = \langle \pi_-^2 (\pi_+ + \pi_-)^{2n} \rangle^* \quad (J.16)$$

$$F04 = \langle (\pi_+ + \pi_-)^{2n} \pi_+^4 \rangle = \langle \pi_-^4 (\pi_+ + \pi_-)^{2n} \rangle^* \quad (J.17)$$

and

$$F24 = \langle \pi_-^2 (\pi_+ + \pi_-)^{2n} \pi_+^4 \rangle = \langle \pi_-^4 (\pi_+ + \pi_-)^{2n} \pi_+^2 \rangle^* \quad . \tag{J.18}$$

We begin with F02:

$$F02 = \langle (\pi_+ + \pi_-)^{2n} (\pi_+ + \pi_-)^2 \rangle - \langle (\pi_+ + \pi_-)^{2n} \pi_- \pi_+ \rangle \tag{J.19a}$$

$$F02 = \varepsilon^{n+1} [(2n + 1)!! - (2n - 1)!!] \quad . \tag{J.19b}$$

Making use of Eq. (H.4) allows us to write F04 as

$$F04 = \varepsilon^4 (2n)(2n - 1)(2n - 2)(2n - 3) \langle (\pi_+ + \pi_-)^{2n-4} \rangle \tag{J.20}$$

or

$$F04 = \varepsilon^{n+2} [(2n + 3)!! - 6(2n + 1)!! + 3(2n - 1)!!] \quad . \tag{J.21}$$

Similarly,

$$F24 = \langle (\pi_+ + \pi_-)^2 (\pi_+ + \pi_-)^{2n} \pi_+^4 \rangle - \langle (\pi_- \pi_+)(\pi_+ + \pi_-)^{2n\ 4} \rangle \tag{J.22a}$$

$$= \varepsilon^{n+3} [(2n + 5)!! - 6(2n + 3)!! + 3(2n + 1)!!]$$

$$- \varepsilon^{n+3} [(2n + 3)!! - 6(2n + 1)!! + 3(2n - 1)!!] \tag{J.22b}$$

$$F24 = \varepsilon^{n+3} [(2n + 5)!! - 7(2n + 3)!! + 9(2n + 1)!! - 3(2n - 1)!!] \, . \tag{J.22c}$$

The final type of off-diagonal expectation value we will consider arises when $|S\rangle$ is defined by

$$|S\rangle = (1 + |a_b|^2)^{-1/2} \left(1 + \frac{a_b \pi_+^6}{\sqrt{6!}\ \varepsilon^3} \right) |0\rangle \quad . \tag{J.23}$$

We define

$$F06 = \langle(\pi_+ + \pi_-)^{2n}\pi_+^6\rangle = \langle\pi_-^6(\pi_+ + \pi_-)^{2n}\rangle^* \tag{J.24}$$

Making use of Eq. (H.4) again allows us to write F06 as

$$F06 = \varepsilon^6(2n)(2n-1)\ldots(2n-5)\langle(\pi_+ + \pi_-)^{2n-6}\rangle \tag{J.24a}$$

$$= \varepsilon^{n+3}(2n)(2n-2)(2n-4)(2n-1)!! \tag{J.24b}$$

$$= \varepsilon^{n+3}[(2n+5)!! - 15(2n+3)!! + 45(2n+1)!! - 15(2n-1)!!] \quad . \tag{J.24c}$$

Equations (J.24c) and (J.14) give Eqs. (3.15) and (3.16) in Chapter III. Equations (J.2), (J.15), (J.19), (J.10), (J.21), (J.22), and (J.12) can be combined to give

$$\langle S|\left(\frac{\vec{v}\cdot\vec{\pi}}{2\tilde{\omega}}\right)^{2n}|S\rangle = A + |a_2|D + |a_2|^2E + |a_4|F + |a_2||a_4|G + |a_4|^2H \tag{J.25}$$

where

$$A = \langle 0|\left(\frac{\vec{v}\cdot\vec{\pi}}{2\tilde{\omega}}\right)^{2n}|0\rangle = a^n(2n-1)!! \tag{J.26}$$

$$D = \frac{1}{\sqrt{2!}\,\varepsilon}\left\{\frac{a_2}{|a_2|}\langle 0|\left(\frac{\vec{v}\cdot\vec{\pi}}{2\tilde{\omega}}\right)^{2n}\pi_+^2|0\rangle + \text{h.c.}\right\}$$

$$= \frac{2\cos(2\phi+\phi_2)}{2!}a^n[(2n+1)!! - (2n-1)!!] \tag{J.27}$$

$$E = \frac{1}{2!\varepsilon^2}\langle 0|\pi_-^2\left(\frac{\vec{v}\cdot\vec{\pi}}{2\tilde{\omega}}\right)^{2n}\pi_+^2|0\rangle$$

$$= \frac{1}{2!}\, a^n[(2n+3)!! - 2(2n+1)!! + (2n-1)!!] \qquad (J.28)$$

$$F = \frac{1}{\sqrt{4!}\,\epsilon^2}\,\frac{a_4}{|a_4|}\,\langle 0|\left(\frac{\vec{v}\cdot\vec{\pi}}{2\tilde{\omega}}\right)^{2n}\pi_+^4|0\rangle + \text{h.c.}$$

$$= \frac{2\cos(4\phi+\phi_4)}{\sqrt{4!}}\, a^n[(2n+3)!! - 6(2n+1)!! + 3(2n-1)!!] \qquad (J.29)$$

$$G = \frac{1}{\sqrt{2!4!}\,\epsilon^3}\,\frac{a_2^* a_4}{|a_2||a_4|}\,\langle 0|\pi_-^2\left(\frac{\vec{v}\cdot\vec{\pi}}{2\tilde{\omega}}\right)^{2n}\pi_+^4|0\rangle + \text{h.c.}$$

$$= \frac{2\cos(2\phi+\phi_4-\phi_2)}{\sqrt{2!4!}}\, a^n[(2n+5)!! - 7(2n+3)!! + 9)2n+1)$$

$$- 3(2n-1)!!] \qquad (J.30)$$

$$H = \frac{1}{4!\epsilon^4}\,\langle 0|\pi_-^4\left(\frac{\vec{v}\cdot\vec{\pi}}{2\tilde{\omega}}\right)^{2n}\pi_+^4|0\rangle$$

$$= \frac{a^n}{4!}\,[(2n+7)!! - 12(2n+5)!! + 42(2n+3)!! - 36(2n+1)!!$$

$$+ 9(2n-1)!!2 \quad . \qquad (J.31)$$

Here, ϕ_2 and ϕ_4 are defined by $a_2 = |a_2|\exp(i\phi_2)$ and $a_4 = |a_4|\exp(i\phi_4)$, and

$$a = \frac{v_\perp^2 eH_{c2}}{4\tilde{\omega}^2} \quad .$$

XVII. APPENDIX K

In this appendix we will derive an expression for T_c when both elastic and inelastic magnon scattering are included. We will use Eqs. (2.10)-(2.13), (2.16), and (2.61).

Equations (2.16) and (2.61) combine to give

$$\Gamma_{\uparrow\downarrow}(k\omega,k'\omega') = -\left(\frac{I}{2}\right)^2 \chi(k-k')(\alpha+\beta\delta_{\omega,\omega'}) \quad . \tag{K.1}$$

Similarly, combining Eqs. (2.10) and (2.12) gives

$$\gamma(\omega) = 1 + T\sum_{\omega'}\sum_{k'} \Gamma_{\uparrow\downarrow}(k\omega,k'\omega')G_{k'}(\omega')G_{-k'}(-\omega')\gamma(\omega') \tag{K.2}$$

$$\gamma(\omega) = 1 + \pi N(0)T\sum_{\omega'} \bar{\Gamma}_{\uparrow\downarrow}(k\omega,k'\omega')\gamma(\omega')/[|\omega'| + |\Sigma(\omega')|] \tag{K.3}$$

where

$$\bar{\Gamma}_{\uparrow\downarrow}(k\omega,k'\omega') = \int \frac{d\Omega_{k-k'}}{4\pi} \Gamma_{\uparrow\downarrow}(k\omega,k'\omega') \tag{K.4}$$

$$= -\left(\frac{I}{2}\right)^2 (\alpha+\beta\delta_{\omega,\omega'}) \int \frac{d\Omega}{4\pi} \chi(k-k') \tag{K.5}$$

$$\equiv -\left(\frac{I}{2}\right)^2 (\alpha+\beta\delta_{\omega,\omega'})\,\bar{\chi} \quad . \tag{K.6}$$

An expression for $\bar{\chi}$ is derived in Appendix D. We can now write $\gamma(\omega)$ as

$$\gamma(\omega) = 1 - \pi N(0)T\left(\frac{I}{2}\right)^2 \bar{\chi}\sum_{\omega'} (\alpha+\beta\delta_{\omega,\omega'}) \frac{\gamma(\omega')}{|\omega'| + |\Sigma(\omega')|} \tag{K.7}$$

or as

$$\gamma(\omega) = \frac{|\omega| + |\Sigma(\omega)|}{|\omega| + |\Sigma(\omega)| + \beta\pi N(0)\left(\frac{I}{2}\right)^2 \bar{\chi} T}\left(1 - N(0)\left(\frac{I}{2}\right)^2 \bar{\chi}\pi T \sum_{\omega'} \frac{\alpha\gamma(\omega')}{|\omega'| + |\Sigma(\omega')|}\right) \tag{K.8}$$

Rearranging terms and summing over ω gives

$$\pi T \sum_{\omega} \frac{\gamma(\omega)}{|\omega| + |\Sigma(\omega)|} = \pi T \sum_{\omega} \frac{1}{\omega + |\Sigma(\omega)| + \beta\pi N(0)\left(\frac{I}{2}\right)^2 \bar{\chi} T} \cdot \left(1 - \alpha N(0)\left(\frac{I}{2}\right)^2 \bar{\chi}\pi T \sum_{\omega} \frac{\gamma(\omega)}{|\omega| + |\Sigma(\omega)|}\right) \tag{K.9}$$

or

$$\pi T \sum_{\omega} \frac{\gamma(\omega)}{|\omega| + |\Sigma(\omega)|} = \frac{\Phi}{1 + \alpha\Phi N(0)\left(\frac{I}{2}\right)^2 \bar{\chi}} \tag{K.10}$$

where

$$\Phi \equiv \pi T \sum_{\omega} \frac{1}{|\omega| + |\Sigma(\omega)| + \beta\pi N(0)\left(\frac{I}{2}\right)^2 \bar{\chi} T} \,. \tag{K.11}$$

We note that Eq. (2.11) can be written in terms of Φ.

$$Q(T) \equiv \pi N(0) T \sum_{\omega} \frac{\gamma(\omega)}{|\omega| + |\Sigma(\omega)|} \tag{K.12}$$

$$Q(T) = \frac{N(0)\Phi}{1 + \alpha\Phi N(0)\left(\frac{I}{2}\right)^2 \bar{\chi}} \tag{K.13}$$

or, using Eq. (D.3),

$$Q(T) = \frac{N(0)\Phi}{1 + \alpha\rho\Phi} \tag{K.14}$$

where

$$\rho = 1/(2\pi T\tau(T)) \quad . \tag{K.15}$$

Equation (K.14) will later prove to be very useful.

We return now to our investigation of Φ. Using Eq. (D.3) allows us to write Eq. (K.11) as

$$\Phi = \pi T \sum_{\omega} \frac{1}{|\omega| + |\Sigma(\omega)| + \frac{\beta}{2\tau(T)}} \tag{K.16}$$

where $\tau(T)$ is given by Eqs. (2.29)-(2.31). The derivation of an expression for $\Sigma(\omega)$ is very similar to the derivation given in Appendix D. We find that

$$\Sigma(\omega) = \frac{1}{2\tau}\left[\alpha \frac{\omega}{\pi T} + \beta \text{ sgn } \omega\right] \quad . \tag{K.17}$$

Equation (K.16) then becomes

$$\Phi = 2\pi T \sum_{\omega>0} \frac{1}{\omega(1 + \alpha\rho) + 2\pi T\rho\beta} \quad . \tag{K.18}$$

Our basic equation

$$\Delta = gQ(T)\Delta \tag{K.19}$$

becomes

$$\frac{1}{gN(0)} = \frac{\Phi}{1 + \alpha\rho\Phi} \tag{K.20}$$

or

$$\frac{1}{gN(0) - \alpha\rho} = \Phi \quad . \tag{K.21}$$

Using Eq. (K.18) gives

$$\frac{1 + \alpha\rho}{gN(0) - \alpha\rho} = \sum_{n\geq 0} \frac{1}{n + \frac{1}{2} + \frac{\beta\rho}{\alpha\rho + 1}} \quad . \tag{K.22}$$

Equation (K.22) is identical to Eq. (2.69). The technique discussed in Appendix E may be used to rewrite Eq. (K.22) in terms of digamma functions.